5-18-2007

Nano-filled Epoxy: Mechanical and Fire Behavior and Modeling of Nanocomposite Columns Under Fire

Stefano Bietto
University of New Orleans

Nano-filled Epoxy: Mechanical and Fire Behavior and Modeling of Nanocomposite Columns Under Fire

A Dissertation

Submitted to the Graduate Faculty of the
University of New Orleans
in partial fulfillment of the
requirements for the degree of

Doctor of Philosophy
in
Engineering and Applied Sciences

by

Stefano Bietto

"Laurea" degree Politecnico di Torino, 2002

May 2007

To Mamma, Papa' and Francesca

Acknowledgment

I would like to dedicate my work to my family, my father Gian Domenico, my mother Pina, my sister Francesca, my "nonne" Palmira and Gina, my uncle Lello, and my aunt Francesca that always supported me and encouraged me. Their love, tenderness, and understanding gave me the strength to keep going and overcome the many obstacles that I encountered.

I would like to thank my major professor Dr. David Hui, who supported me continuously for these years. I am grateful to Dr. Christopher Ibeh, who, in September 2005 after the hurricane Katrina, welcomed me in his Center for Nanocomposites and Multi-Functional Materials in Pittsburg State University, where most of the tests were run. This work would not be possible without the help and the precious scientific suggestions of Dr. Andrey Beyle. My true appreciation goes to Dr. Margherita Clerico, who supervised my Master thesis at Politecnico di Torino and established the connections with University of New Orleans. My sincere gratitude goes to Dr. Mircea Chipara, who hosts me during the summer 2003 at the Cyclotron Facility at Indiana University. I would like to thank Dr. Leo Daniel for the valuable advices. I am grateful to Manan Aggarwal for helping me with the testing. My thankfulness goes to the faculties at the Mechanical Engineering Department of University of New Orleans, especially to Dr. Kazim Akyuzlu and Dr. Salvadore Guccione for their help. I would like to thank also the faculties of the Engineering Technology Department of Pittsburg State University. This work was partially funded by the Office of Naval Research, Solid Mechanics division, monitored by Dr. Yapa D.S. Rajapakse, subcontract from Pittsburg State University, under Grant N00014-05-1-0532.

It was hard and sometimes very stressful to complete the research for my PhD. Without the support of my friends I would not have had the energy to finish. For this reason I would like to thank Javier, Michael, Antonis, Nicos, Nestoras, Dinos, Monika, Iannos, Prodromos, Anders, Lisa, Yasu, Jimbo, Wai, Eunice, Sofia, Faisal and all my friends from Italy, which I felt always close to me, even if thousands miles were separating us.

Most of my PhD studies were done in New Orleans, a warm, colorful, and unique city, which will be always in my heart. New Orleans is a beautiful place, where I had the most amazing time of my life. During this time in august 2005 New Orleans was hit by the infamous hurricane Katrina. To the “Big Easy” go my sincere wishes for a sudden recovery.

Purposely I left this paragraph at the end. Doing a PhD was the hardest thing I ever done. Sometimes I was frustrated and unmotivated, besides being tired. A beautiful person came to rescue me, and with her infinite love gave me the strength to continue and achieve this incredible goal. This person conquered my heart with her sweetness and beauty. To Ivana goes my deepest gratitude.

Table of contents

Chapter 4 - Tests results

Chapter 5 - Modeling of stability of nanocomposites columns under fire

Chapter 6 - Conclusions and future work

List of figures

Chapter 1 - Introduction: nanotechnology and nanocomposites

Chapter 3 - Experimental procedure

Chapter 4 - Tests results

Chapter 5 - Modeling of stability of nanocomposites columns under fire

List of tables

Chapter 1 - Introduction: nanotechnology and nanocomposites

Chapter 2 - Literature review

Chapter 3 - Experimental procedure

Chapter 5 - Modeling of stability of nanocomposites columns under fire

Abstract

In this work, fracture, mechanical, and flammability tests, along with a modeling of the stability of nanocomposite columns under fire are presented for nano-filled Diglycidyl Ether of Bisphenol A epoxy. The nanofillers used are montmorillonite nanoclays and carbon nanofibers. Three types of nanocomposites are manufactured: epoxy-clay, epoxy-carbon nanofiber, and epoxy-clay-carbon nanofiber nanocomposites. Fracture tests performed include Izod impact and fracture toughness, for the determination of the net Izod impact strength, the stress intensity factor, and the critical energy release rate. With static mechanical tests the tensile and flexural properties of the nanocomposites are measured. Flammability tests made by cone calorimetry are used to determine the Heat Release Rate, Mass Loss Rate, time to ignition, to Peak of heat Release rate and to flameout, and total smoke and heat released. A mathematical modeling of the stability of columns, made of the same nanocomposites tested, burning continuously in one side is performed. Three configurations are considered: uniform burning along the span, and burning spot at the center and at the corner of the column. The testing and the mathematical modeling reveal the higher mechanical strength and superior flammability properties produced by addition of nanofillers.

Chapter 1

Introduction: nanotechnology and nanocomposites

1.1 Nanotechnology and nanofillers

The word "nano" is often linked to other words, such as nanotechnology, nanoparticles or nano-engineering, and, as for the word "micro", it implies size. A nanometer is 10^{-9} m and, if we think that a human hair's diameter averages 70 micrometers ($70 \cdot 10^{-6}$ m) and a diamond carbon-carbon bond is about 1.54 Å ($1.54 \cdot 10^{-10}$ m), it is clear that a nanometer corresponds to a very small dimension to find in nature. The term nanotechnology was first used by Norio Taniguchi (University of Tokyo) in 1974, and it means the design, characterization, production and application of structures, devices and systems by controlling shape and size at nanometer scale[1].

The interest in nanotechnology is increasing exponentially with years passing by. The reduction of size of products in many engineering fields and the self assembly properties of biological and chemical systems converge to a new scientific area oriented towards the development and implementation of nanotechnology (Fig. 1.1). The need of smaller scale is found evidently in computer science and in electronics. However nanotechnology covers a wider spectrum of industrial and scientific applications in chemistry, material science, medicine and biology (Fig. 1.2).

Nanotechnology in materials science involves mainly the production and the use of nanoparticles (particles with size of few nanometers of magnitude). A major breakthrough in the field of nanotechnology in material science occurred in 1985 when Harry Kroto, Robert Curl and Richard Smalley invented a new form of carbon called fullerenes ('buckyballs'), a single

molecule of 60 carbon atoms arranged in the shape of a soccer ball. This led to a Nobel Prize in Chemistry in 1996[2].

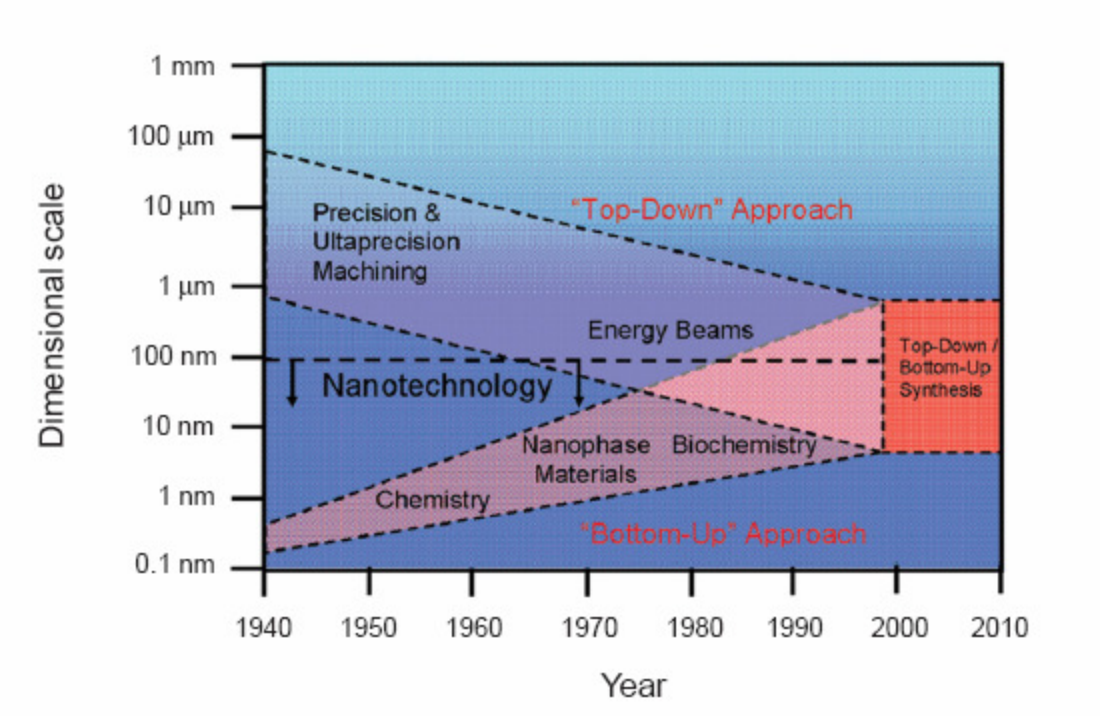

Figure 1.1: convergence of top-down and bottom-up nanotechnology[3]

Nanoparticles can be deposited to form layers or coating, or they can be combined to other materials to produce nanocomposites. It is believed and demonstrated that the effect of nano-size is beneficial for the resulting materials or structures, producing improvements in mechanical, chemical, optical, electrical and thermal properties. The most renowned nanoparticles produced today are layered silicate nanoparticles (known as nanoclay), carbon nanofibers, single- and multi-walled carbon nanotubes, and titanium dioxide. However many more nanoparticles are produced or under development, and the possibilities are virtually unlimited, opening a new frontier for material science (Fig. 1.3).

High costs and technological deficiencies still limit the mass production of nanomaterials: nevertheless few low cost nanoparticles (nanoclay) are currently produced and employed in many fields. Investment in nanotechnology has radically grown over the last years, with expenditure exceeding 8 billion of US dollars worldwide in 2005[4]. The trend seems to picture an increasing demand of nanomaterials products, with further increase in investments and consequently lower costs, prospect a bright future for this novel scientific niche.

This dissertation will deal with nanotechnology applied to materials science, specifically polymeric nanocomposites materials, with nanoclay particles as reinforcements.

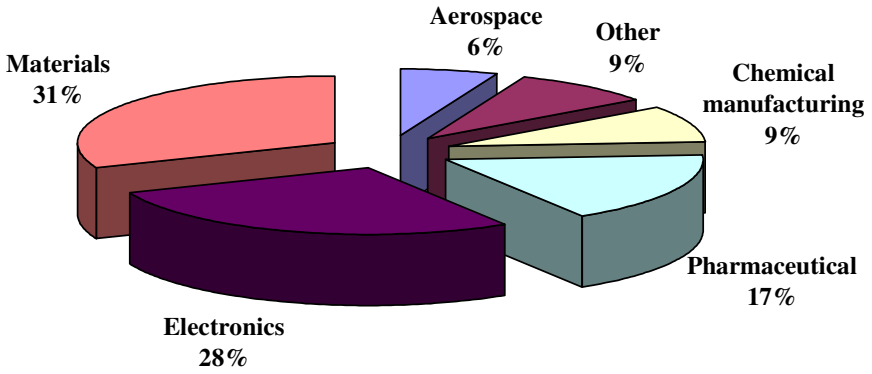

Figure 1.2: estimates of the nanotechnology market by 2010-2015[5]

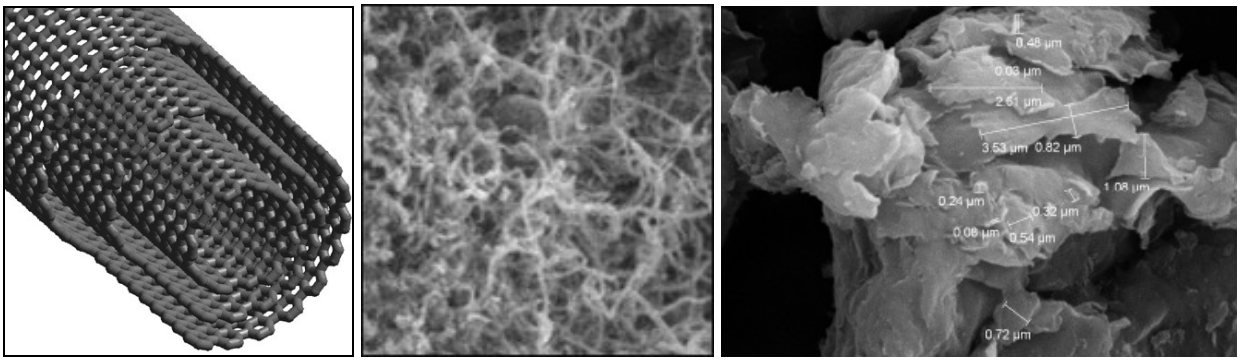

Figure 1.3: images representing (from right to left) multiwalled carbon nanotubes[6], carbon nanofibers[7], and nanoclay[8]

1.2 Layered silicate nanoparticles: montmorillonite nanoclay

Layered silicate nanoparticles are also known as nanoclay. Nanoclays are mainly blended with thermoplastics, such as polypropylene (PP), poly(ethylene-thereftalate) (PET), polyethylene (PE), polystyrene (PS), and nylon, to form nanocomposites. In recent times, the research activity is however directed mainly towards nanoclay nanocomposites with thermosets resins, such as epoxies, due to the employment of thermosets in naval and aerospace structures.

Nanoclay are the most widely utilized nanoparticles, for their low cost, and overall improvement of mechanical, thermal, electrical and optical properties compared with their macro- and micro- counterparts. The research on nanoclay nanocomposites produced thousands of papers and articles in the last decade and nanoclay have now a variety of commercial applications. The automotive industry was the first one to employ nanoclay in a vast scale, with the production of the step assist for the 2002 GMC Safari and the Chevrolet Astro van, the body side molding of the 2004 Chevrolet Impala, and the cargo bed for the 2005 Hummer H2 SUT. However nanoclay-hybrids were first developed by Toyota Inc. research laboratories and their development has motivated a number of studies today.

Layered silicate can be found easily (clay minerals) and they include both natural clays, for example montmorillonite, hectorite, and saponite, and synthesized clays for example fluorohectorite, laponite, and magadiite (Table 1.1). In this dissertation we will evaluate natural clays, specifically montmorrillonite (MMT).

The clay minerals can be classified in three groups: 2:1 type, 1:1 type and layered silicic acids. MMT belongs to the 2:1 type (smectite family) with the crystal structure consisting of nanometer thick layers (platelets) of aluminum octahedron sheet sandwiched in between two silicon tetrahedron sheets (Fig. 1.4 and 1.5). This structure is about 1 nm thick and 100–1000 nm

in diameter. Stacking of the layers leads to a van der Waals gap between the layers. Isomorphic substitution of Al with Mg, Fe, Li in the octahedron sheets and/or Si with Al in tetrahedron sheets gives each three-sheet layer and overall negative charge, which is counterbalanced by exchangeable metal cations residing in the interlayer space, such as Na, Ca, Mg, Fe, and Li[9]. The formula for montmorillonite is $M_y^+(Al_{2-y}Mg_y)(Si_4)O_{10}(OH)_2 \cdot nH_2O$, even if it is not found in nature, where substitutions always occur.

Type of clay	Formula	Origin	Substitution	Layer charge
2:1 type				
MMT	$M_x(Al_{2-x}Mg_x)Si_4O_{10}(OH)_2 \cdot nH_2O$	N	Octahedral	Negative
Hectorite	$M_x(Mg_{3-x}Li_x)Si_4O_{10}(OH)_2 \cdot nH_2O$	N	Octahedral	Negative
Saponite	$M_xMg_3(Si_{4-x}Al_x)O_{10}(OH)_2 \cdot nH_2O$	N	Tetrahedral	Negative
Fluorohectorite	$M_x(Mg_{3-x}Li_x)Si_4O_{10}F_2 \cdot nH_2O$	S	Octahedral	Negative
Laponite	$M_x(Mg_{3-x}Li_x)Si_4O_{10}(OH)_2 \cdot nH_2O$	S	Octahedral	Negative
Fluoromica (Somasif)	$NaMg_{2.5}Si_4O_{10}F_2$	S	Octahedral	Negative
1:1 type				
Kaolinite	$Al_2Si_2O_5(OH)_4$	N	—	Neutral
Halloysite	$Al_2Si_2O_5(OH)_4 \cdot 2H_2O$	N	—	Neutral
Layered silicic acid				
Kanemite	$Na_2Si_4O_9 \cdot 5H_2O$	N/S	Tetrahedral	Negative
Makatite	$NaHSi_2O_5 \cdot 7H_2O$	N/S	Tetrahedral	Negative
Octasilicate	$Na_2Si_8O_{17} \cdot 9H_2O$	S	Tetrahedral	Negative
Magadiite	$Na_2Si_{14}O_{29} \cdot 10H_2O$	N/S	Tetrahedral	Negative
Kenyaite	$Na_2Si_{20}O_4 \cdot 10H_2O$	S	Tetrahedral	Negative

M indicates exchangeable ions represented by monovalent ions. Symbols: N (nature) and S (synthetic).

Table 1.1: clay minerals used for polymer nanocomposites[9]

Naturally occurring montmorillonite is characterized by strong dipole moments, i.e. is hydrophilic (miscible in water) and it is immiscible in organic solvents. Since polymers are generally organophilic (miscible in organic solvents), unmodified nanoclay disperses in polymers with great difficulty. Through clay surface modification, montmorillonite can be made organophilic and, therefore, compatible with conventional organic polymers. This process of surface modification is known as compatibilization.

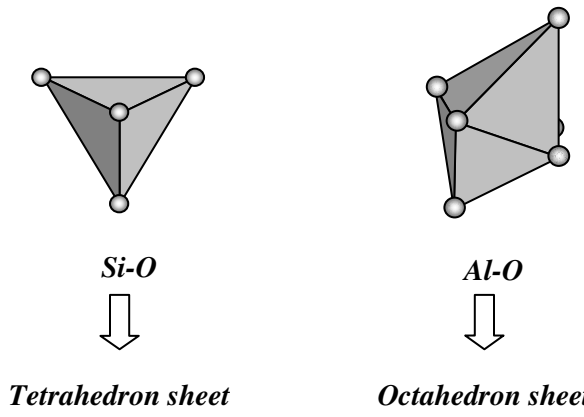

Figure 1.4: building block of the montmorillonite structure

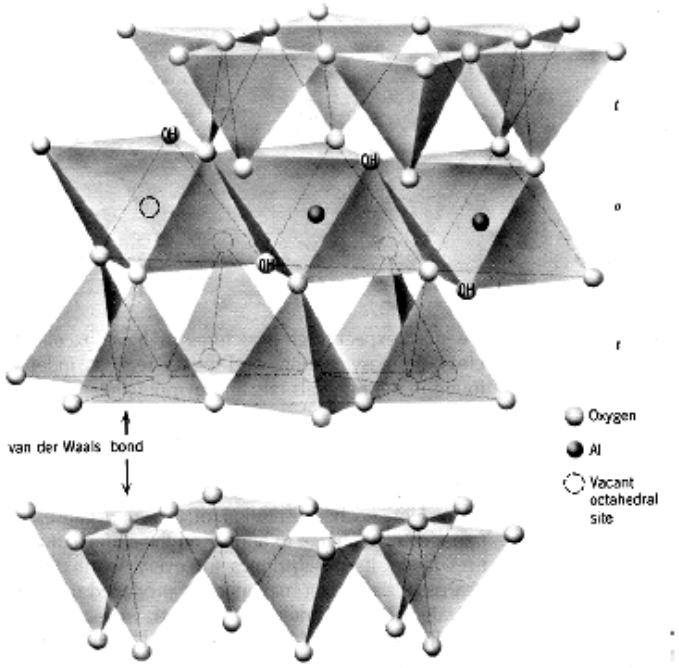

Figure 1.5: montmorillonite structure with two tetrahedron and octahedron layers[10]

The two most common compatibilization classes are onium ion modification and ion-dipole interaction. Onium ion modification is the formation of a clay-chemical complex using an intercalant (surface treatment) containing an ammonium or phosphonium functional group. The

groups modify a nanoclay surface by ionically bonding to it, converting the surface from a hydrophilic to an organophilic species. Ion dipole interaction is a type of chemical bond formed between a charged ion and a molecule that contains a dipole moment and a partial localized negative charge. A classic example is water of hydration in many compounds. The complex has a definite ratio of organic or polymer to clay[10].

The nanoclays employed for this dissertation have a compatibilization process that combines ion dipole interaction and onium ion modification and it is patented by Nanocor®. The resulting clay chemical complex has a determined gallery spacing between the platelets, which favors a good dispersion in the matrix system. Non-treated MMT nanoclays have spacing between the platelets of approximately 3.5 Å, while the treated nanoclays have spacing in of approximately 20 Å (Fig. 1.6). This higher spacing allows polymers chain to pass in between the platelets during the mixing process and thus producing a better dispersion of the nanoclays in the polymer matrix.

Nanoclays superior properties are due to their high aspect ratio between in-plane dimensions and thickness. In addition, nanoclay particles are so small that in a gram of materials you can have several millions particles. The properties enhancement occurs because nanometer-sized particles approach the scale of resin molecules. Consequently, a very close encounter can be made between the two materials when the mineral is properly surface modified. The particle-molecule interaction creates a constrained region at the particle surface, which immobilizes a portion of the resin matrix. With so many particles available for interactive association, the cumulative percent of constrained polymer can become large[10]. With small percentage of nanoparticles, the increase in properties can be substantial.

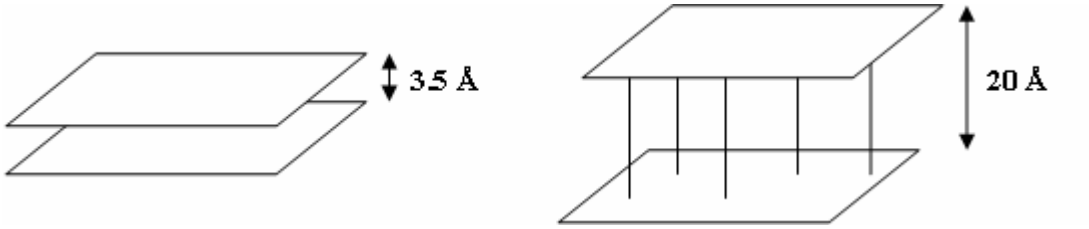

Figure 1.6: effect of surface modification (compatibilization) on nanoclay nanoparticles

There are few producers in the world of nanoclays. The most renowned are listed in table 1.2 with their products. However, there are more and more companies, especially in Japan, which are developing new nanoclay particles.

Product	Company	Country
Cloisite®	Southern Clay Products	USA
Nanomer®	Nanocor	USA
Bentone®	Elementis Specialties	USA
Nanofil®	Sud-Chemie	Germany
Planomers®	TNO	Holland
PlanoColors®	TNO	Holland
PlanoCoatings®	TNO	Holland
Somasif ME®	Co-Op Co.	Japan

Table 1.2: producing companies for the most common nanoclay

1.3 Carbon nanofibers

Carbon nanofibers are cylindrical nanostructures with graphene layers arranged as stacked cone, cups or plates. Carbon nanofibers with graphene layers wrapped into perfect cylinders are called carbon nanotubes. Carbon nanofibers are produced from the catalytic decomposition of hydrocarbon gases or carbon monoxide over selected metal particles that include iron, cobalt, nickel, and some of their alloys at temperatures over the range 400-1000°C. This process is termed Catalytic Chemical Vapor Deposition[11].

Graphene is an aromatic finite thickness flat sheet made of carbon atoms. Carbon nanotubes are graphene sheet rolled in a cylinder (Figure 1.3). The carbon atoms are bonded together forming hexagonal cells. Pentagonal and heptagonal cells may be present, creating distortion and curvature to the flat graphene sheet. This phenomenon, if controlled, allows shaping graphene in different forms.

Carbon nanofibers have diameter range of 3–100 nm and length range of 0.1–1000 μm, with very high surface area (300 - 700 m^2/g) and the totality of the surface area is chemically active. Carbon nanotubes have more regular cylindrical shape, while carbon nanofibers have more assorted conformations (Figure 1.7).

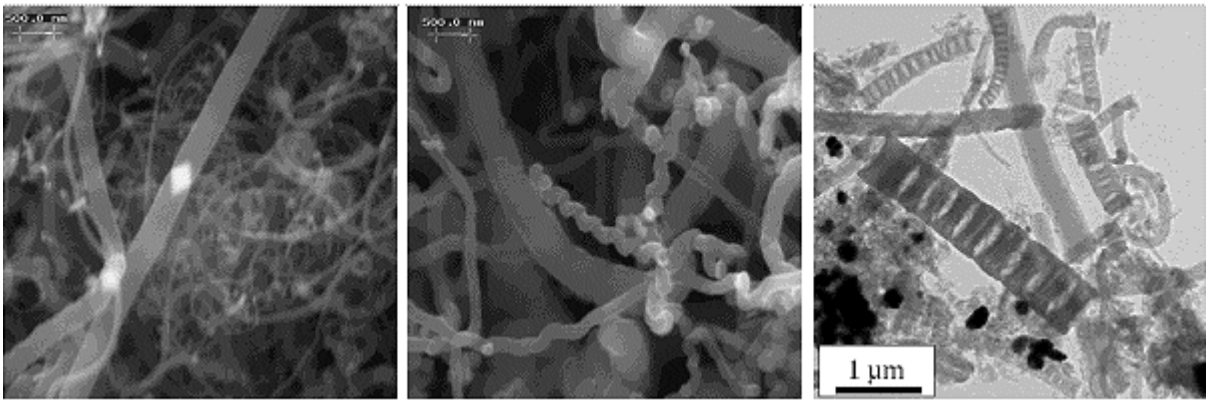

Figure 1.7: different fibers morphologies[12]

CNFs are grown from the decomposition of carbon-containing gases over metal or alloy surfaces which act as catalysts to the formation of the sheets. Certain nickel- and iron-based alloys are among the most effective catalysts for the reaction. During the reaction, the carbon containing gas molecules are adsorbed to certain faces of the catalyst's surface and are subsequently decomposed (Figure 1.8). Following this, the carbon atoms diffuse through the catalyst particle and precipitate and form successive sheets that stack on one another to form the carbon nanofibers[13]. By choice of the catalyst, the ratio of the hydrocarbon/hydrogen reactant mixture, and reaction conditions, it is possible to tailor the morphological characteristics, the degree of crystallinity, and the orientation of the precipitated graphite crystallites with regard to the fiber axis[14].

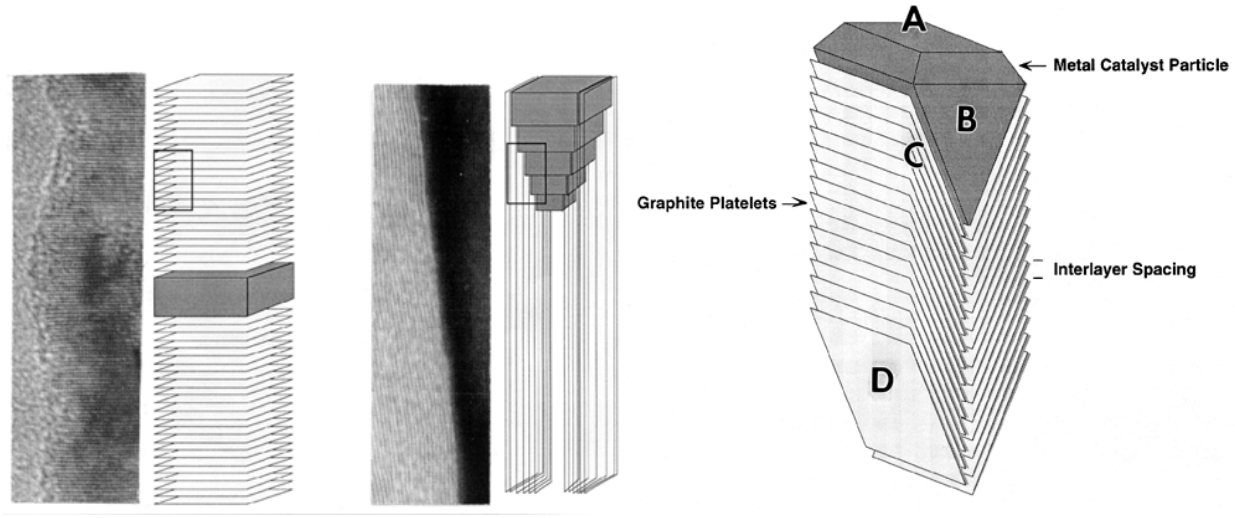

Figure 1.8: different deposition patterns for carbon nanofibers[14]

Carbon nanofibers used as additive in polymers produce positive effects, e.g. they induce electrical conductivity, improve mechanical properties, provide thermal conductivity, increase heat distortion temperature, lower the coefficient of thermal expansion, and render the polymer flame retardant.

Carbon nanofibers have still few commercial applications. One is the addition of a small amount of vapor growth carbon nanofibers (VGCF) to the electrodes of lithium-ion batteries with the effects of increasing the amount of battery current as a result of improved electrical conductivity of electrodes, enabling the use of lithium-ion batteries in electrical appliances requiring heavy-current discharges. Carbon nanofibers are used as reinforcements for plastics (nanocomposites). Investigations are studying the so called "whiskerization" of carbon fibers used for advanced composites, where nanofibers are grown on the surface of the larger carbon fibers to increase the adhesion of the latter to the polymer matrix. CNFs can be used for environmental purpose as decontaminant. They can remove toxic agents in the air and in the water, capitalizing on their high specific surface and their surface reactivity. Another important employment is the use of carbon nanofibers to make polymer conductive with consequent anti-static properties. This is very important for the aerospace industry, which is slowly substituting the traditional aluminum alloys with advanced polymer composites to build aircraft frame/parts. Electrical conductivity becomes important when facing electrostatic atmospheric charges.

Product	Company	Country
Pyrograph® III	Pyrograph Products Inc.	USA
Elicarb®	Thomas Swan & Co. Ltd	UK
Carbere®	GSI Creas Co.	Japan
VGCF-S	Showa Denko K.K.	Japan
ENF®	Electrovac AG	Austria

Table 1.3: producing companies of carbon nanofibers

1.4 Diglycidyl Ether of Bisphenol A epoxy

Epoxy is a thermoset polymer intensively used in composites for aerospace structures, although epoxy applications range from adhesives, composites for marine industry, electric devices, and molds for casting industrial tooling. Thermoset polymers are in liquid form before the polymerization and cross-linking process (called curing) bring them in solid form. The curing process happens when the polymer is mixed with a catalyst or when heat or irradiation is applied. Thermosetting plastics are cured into a solid form, which is stable at any temperature, while thermoplastics have melting or liquefying temperatures. Thermosetting plastics are also insoluble in their cured stated, while thermoplastics usually have several solvents.

Most common epoxy resins are produced from a reaction between epichlorohydrin and bisphenol-A. The first attempt to produce epoxy from epichlorohydrin occurred in 1927 in the United States. In 1936 bisphenol-A based epoxy were synthesized in Switzerland and United States, from two of the companies that later lead the epoxy production market (Ciba Ltd, now part of Huntsmann Co., and Devoe-Reynolds, now part of shell chemicals).

Epoxy curing, occurs when two parts called part A and part B, the latter called also hardener or catalyst, are mixed. The reaction is exothermic and gel time usually is between 20 minutes and 1 hour, according to the type of hardener used.

Epoxy resin begins with the reaction of two compounds, bisphenol A (or bisphenol F and/or Novolac used for superior temperature and chemical resistance) and epichlorohydrin. 98% of common epoxy uses bisphenol A. Epichlorohydrin (chemical formula C_3H_5ClO) is a reactive organic compound. It is an epoxide, a cyclic ether with only three ring atoms, and an organochloride, an organic compound containing at least one covalently bonded chlorine atom (Fig. 1.9). Bisphenol A (chemical formula $C_{15}H_{16}O_2$) is the chemical product of the combination

of one acetone unit with two phenol groups (Fig. 1.10). The reaction between bisphenol A and epichlorohydrin removes unreacted phenol and acetone and attaches two glycidyl groups to the ends of the bisphenol A, creating a diglycidyl ether of bisphenol A (DGEBA), which is standard epoxy resin (Fig. 1.11). The glycidyl group on both ends of the bisphenol A are also referred to as an oxirane or epoxy group. The size of the resulting molecule (and hence its molecular weight) depends upon the ratio of epichlorohydrin to bisphenol A[15].

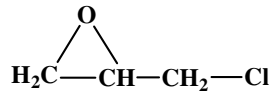

Figure 1.9: epichlorohydrin chemical structure

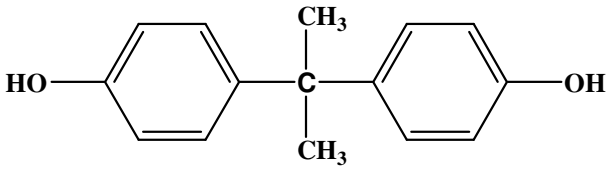

Figure 1.10: bisphenol A chemical structure

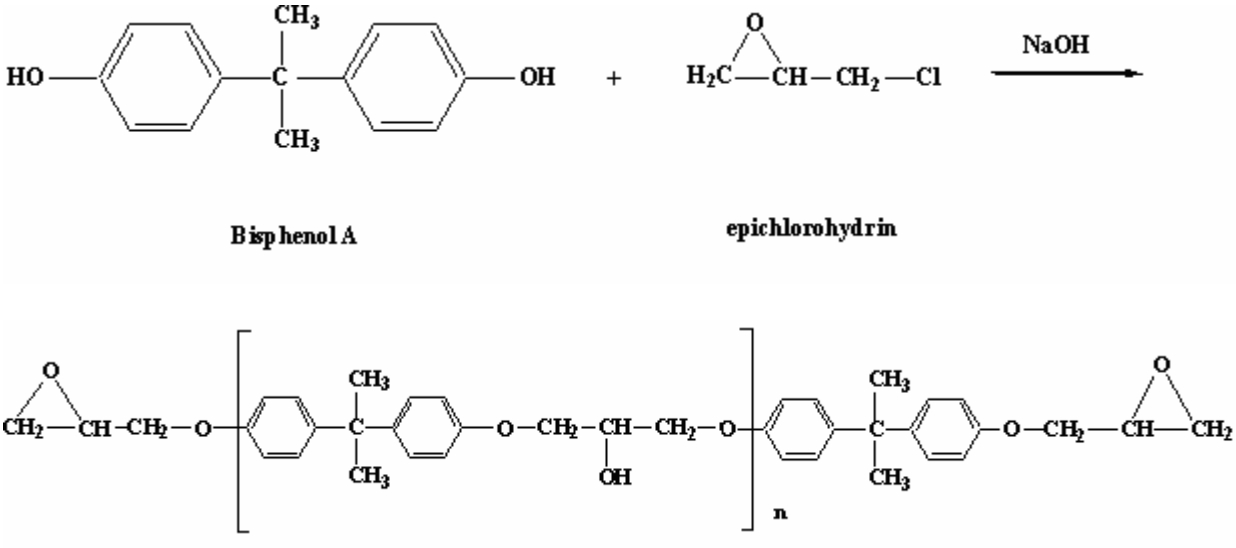

Figure 1.11: DGEBA reaction and chemical structure

The length of the DGEBA molecule depends on the grade of polymerization. When epoxy part A is in liquid form and before mixing with the part B, the molecule is not long, and *n* (see Fig. 1.11) is usually equal to 2. This molecule is sometimes called diepoxy. After the curing process (and thus the polymerization), *n* can be as high as 25.

The curing agent selection plays the major role in determining many of the properties of the final cured epoxy. These properties include pot life, dry time, penetration and wetting ability[15]. The curing agents can be amines or amides based. The most commons are:

- Aliphatic (carbon atoms forming open chains) and cycloaliphatic (ring structured aliphatics) amines and polyamines
- Amides and polyamides
- Cycloaliphatic curing agents.

Amines are ammonia with one or more hydrogen atoms replaced by organic groups, and amides are ammonia with a hydrogen atom replaced by a carbon/oxygen and organic group. Amine based curing agents are considered to more durable and chemical resistant than amide based curing agents. However, when humidity is high, the moisture in the air and the curing agent react, creating a white waxy surface layer (blushing). This layer becomes a white powder when dried. This reaction produces also a release of toxic agents. Amides don't react with moisture in the air, but they are less chemical resistant. Cycloaliphatic curing agents generally provide better water/moisture resistance, weatherability, low blush and water spotting, and better chemical resistance.

The polymerization and crosslinking process is described in Fig. 1.13 for diamine curing agent. The diamine (Fig. 1.12) reacts with the oxirane groups at the end of the DGEBA molecule

creating long molecules which are interlocked to each other and which give the chemical resistance, stability, and strength typical of epoxy.

Figure 1.12: diamine molecule

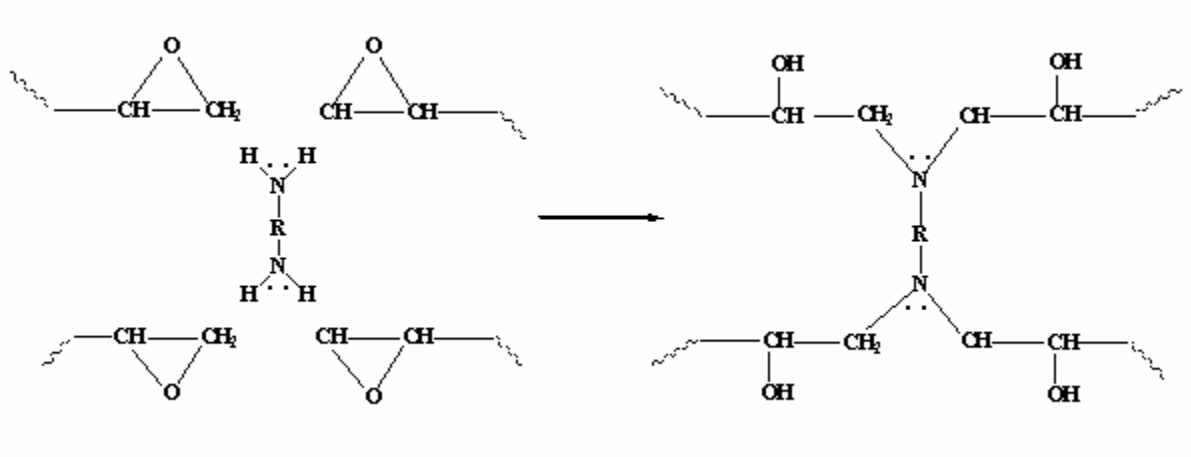

Figure 1.13: curing reaction between molecules of DGEBA and diamine curing agent[16]

1.5 Nanocomposites dispersion

Nanocomposites are prepared dispersing nanoparticles into a matrix system. Usually the matrix is a thermoset or a thermoplastics polymer. The dispersion procedure is performed using different mixing processes. The most widely used are mechanical mixing, sonication and high shear mixing by two or three mill rolls.

The mixing procedure is a very delicate part of the nanocomposite manufacturing. The properties of the final product in fact are highly dependent from the level of dispersion of the

nanoparticles in the matrix. According to the dispersion, three kinds of composites can be created: phase separated microcomposite, intercalated nanocomposite, and exfoliated nanocomposite (Fig. 1.14). The former is not considered a nanocomposite. The nanoparticles join together to form groups with size in the order of micrometers, and the properties are the ones of a microcomposite. In the exfoliated structure, nanoparticles form clusters, which are dispersed in the matrix system. Even if the polymer chains interact with single nanoparticles, the nanoparticles are not uniformly dispersed, but there are areas rich of nanoparticles assembled in clusters and areas of pure polymer. The exfoliated structure is the one that produce more improvements in the properties of the nanocomposites, when compared to the pure polymer. The nanoparticles are separated from each other and they are uniformly dispersed in the matrix system. Exfoliation is very difficult to achieve and it depends strongly on the mixing process, on the surface compatibilization, on the time of mixing and on other elements like temperature and viscosity of the polymer.

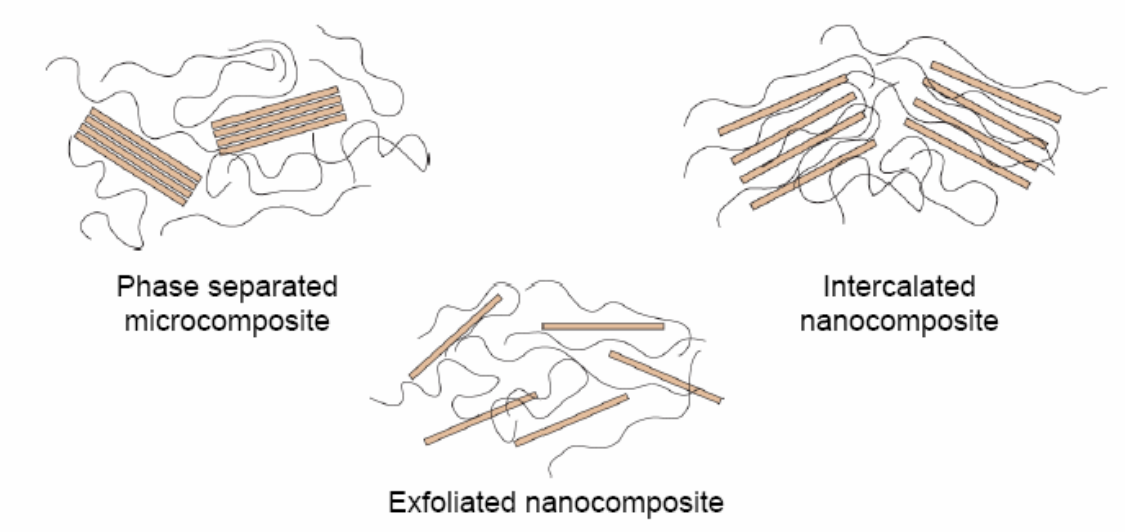

Figure 1.14: Dispersion of nanoparticles in the polymer chains[17]

[1] Lawrence H. Dubois, "Nanotechnology Today: the Reality and the Promise", IEEE Nanotech 5-05
[2] "Enabling technologies for Australian innovative industries", 11 March 2005
[3] Roger W. Whatmore, "Nanotechnology - should we be worried?"
[4] "Small wonders, a survey of nanotechnology", The Economist, 1 January 2005
[5] National Science Foundation
[6] www.msm.cam.ac.uk/polymer/index.html
[7] nanotechnology.e-spaces.com/carbon_nanofibers
[8] Daniel Beyene Ghile, "Effects of Nanoclay Modification on Rheology of Bitumen and on Performance of Asphalt Mixtures"
[9] Q. H. Zeng, A. B. Yu, G. Q. (Max) Lu, and D. R. Paul, "Clay-Based Polymer Nanocomposites: Research and Commercial Development", Journal of Nanoscience and Nanotechnology, Vol. 5, 1574-1592, 2005
[10] www.nanocor.com
[11] Wikipedia
[12] www.ep2.physik.uni-wuerzburg.de/ag_fricke
[13] www.eng.usf.edu
[14] R. Terry K. Baker, "Synthesis, Properties and Applications of Graphite Nanofibers" (1998)
[15] www.epoxyproducts.com
[16] www.pslc.ws/mactest/epoxy.htm
[17] Suraj C. Zunjarrao, Raman P. Singh, Ravi Sriraman, "Fabrication and Mechanical Properties Epoxy-Clay Nanocomposites", 2004 SEN X International congress and Exposition on Experimental and Applied Mechanics, California, USA

Chapter 2

Literature review

2.1 Literature review: nanoclay based nanocomposites

In this section, the properties of nanoclay-based nanocomposites will be reviewed from available literature. Several kinds of nanoclay particles will be considered. The matrix systems taken into consideration will be both thermoset and thermoplastic polymers. Impact, flammability and tensile properties will be analyzed and summarized in tables.

2.1.1 Impact properties of nanoclay nanocomposites

The impact properties of nanocomposites with nanoclay particles are still widely under investigation. The expectation is that the matrix with nanoclay reinforcements becomes more brittle and thus less resistant to impact. Anyway it is not uncommon in literature to find opposite results, with clay nanocomposites sensible increasing the impact toughness. This is due to the high sensitivity to the manufacturing process and to the addition of various impact resistant compounds.

Ratna et alii[1] manufactured and tested a nanocomposite made of epoxy resin, nanoclay particles and an epoxy functionalized hyperbranched polymer. The epoxy resin used is a liquid diglycidyl ether of bisphenol A (DGEBA), the nanoclay is the commercial treated I.30E, and the functional dendritic branched polymer (HBP) is a branched aliphatic polyester backbone with 11 reactive epoxy groups per molecule. The results show encouraging improvement of impact strength with respect to the pure epoxy. Both HBP (15% in weight) and nanoclay (5% in weight)

improve the impact strength, respectively of a factor of 3 and 1.5. The two compounds combined anyway show an intermediate result with only a factor of 2. This is due to the fact that the introduction of clay affects the uniformity of dispersion of HBP, lowering the impact strength with respect the epoxy + HBP.

Jong Hyun Park et alii[2] tested a nanocomposite made of a mixture of epoxy and polymethylmethacrylate (PMMA) and nanoclay as reinforcement. The manufacturing procedure uses melt blending technique where two epoxies (one aromatic and one aliphatic) were mixed with nanoclay (Cloisite® 30B). Izod impact tests were performed on notched samples at room temperature. For PMMA-nanoclay composites the impact toughness was reduced by the presence of clay, with values dropping up to 20% for clay content of 6%. The impact toughness also seemed to be linearly correlated with the clay content. A different behavior was observed for epoxy-clay nanocomposites, where the impact toughness was increased of 10% by addition of 15% of nanoclay. The blend produced by mixing 80 parts of PMMA and 20 parts of epoxy with various percentage of nanoclay showed increased of impact strength of 15% for 2% content of clay and then a drop in properties, until the value of the impact strength was the same of pure resin for a nanocomposite with 6% content of clay.

Yuan and Misra[3] studied the effect of different percentages of clay, 2% and 4%, of montmorillonite (MMT) I.44P, in a commercially available polypropylene. The Izod impact strength was studied at different temperatures, ranging from -40 to 70 Celsius degrees. The impact strength of nanocomposite with 4% of clay seemed not to differ in the range from -40 to 0 Celsius compared with the virgin polymer. The impact strength for the PP-clay nanocomposite became gradually better than the virgin polymer in the positive range of temperature, improving up to 30% improvement at 70 Celsius.

Poly hydroxy ether of bisphenol A (Ph) based polymer nanocomposites (PN) reinforced with a layered clay (montmorillonite) where studied by Gurmendi et alii[4] The clays used where three different kinds of organically modified montmorillonite (Cloisite 20A, 30B and Cloisite Na modified in laboratory). The impact strength increased only for Cloisite 20A used as nano-modifiers, while it was practically unchanged for the other two kinds of nanoclays. The improvement on impact strength of Cloisite 20A was outstanding, with value three times higher than pure resin.

The effect of nanoclay, modified with polyol, into an epoxy matrix system was studied by Isik et alii[5] The materials used were diglycdyl ether of bisphenol A as matrix system and montmorillonite Cloisite 30B modified with polyether polyol, which bond well with epoxy. The impact strength of the epoxy with no nanoclay increased with increasing content of polyol, up to 160% increase with 7% content of polyol. However the impact strength decreases with clay content. The optimal result was found with the combination of 1% nanoclay and 1% polyol, with 130% increase in impact strength.

The relationship between morphology and the mechanical properties of thermoplastic olefin (TPO) materials that are reinforced with organoclay fillers and prepared by melt processing was reported by Hyuk-Soo Lee et alii[6] The nanocomposites were prepared by melt compounding, mixing PP, an ethylene–octane based elastomer and a masterbatch material containing equal parts of maleated PP and an organically modified montmorillonite. The Izod impact strength diminished of about 25% for all percentage of nanoclay with respect to the virgin polymer. The relative content of elastomer had a beneficial effect on Izod impact strength, with an increase that reached 40 times the value for virgin polymer with 40% content of elastomer. In

this extent, the nanoclay contributed for half of the effect, with no difference between all percentages of nanoclay.

Meng and Hu evaluated the impact properties and the fracture morphology of bismaldeide-organoclay nanocomposites[7]. 4,4' bismaleilmidodiphenil-methane (BMPM) was used as matrix system and a reactive diluent (dyallibisphenol A) was used to help the intercalation of the organically modified clay (I.30TC and 30B).Sharpy tests were performed on the nanocomposites manufactured by melt intercalation, with impact strength increasing with increasing for 1% and 3% clay content, and remaining unchanged for 5% clay content. Bigger increased was observed for 30B nanoclay. Intercalated nanoclay showed instead a drop of impact strength with respect to the virgin polymer.

Rubber toughening of nylon 6 nanocomposite was investigated by Young-Cheol Ahn and D.R. Paul[8]. The samples were prepared by melt compounding the nylon 6 and the nanoclay (Cloisite 30B) and then melt compounding the rubber, an ethylene–propylene random copolymer grafted with maleic anhydride (EPR-g-MA). The rubber particles size and inter-distance played a key role in determining the impact strength. The impact strength was determined at different temperature, for different rubber content and clays content. Without rubber, the nanocomposite showed a brittle behavior under 50 Celsius degrees and a ductile behavior above 50 Celsius (corresponding to the glass transition temperature). The addition of clay increased the temperature of the brittle-ductile transition. The addition of rubber decreased the transition temperature to -5 Celsius, increasing the toughness of the material at room temperature. The nanoclay contribute increasing the transition temperature, but also decreasing the value of impact strength in the range of temperature 0-40 Celsius and increasing it for higher temperature compared with the polymer with only nylon and rubber.

Tanniru et alii[9] studied the impact properties of high-density polyethylene (HDPE) copolymer reinforced with a natural montmorillonite clay surface modified dimethyl dialkyl ammonium (Nanomer I.44P). The data for virgin polymer and polymer reinforced with 4% clay were compared. The Izod impact strength was evaluated for different temperatures. The impact strength of both the neat polymer and the nanocomposite increased with temperature increasing. The addition of nanoclay reduced the impact strength to an average of 1/3 the original value.

Wan et alii[10] studied three kinds of nanocomposites made of polyvinyl chloride (PVC) and three different nanoclays, Na-MMT and two surface modified MMT. The two organic MMTs were modified by trimethyloctadecyl ammonium and dimethyldioctadecyl ammonium, respectively, and they were denoted as MMT-C18 and MMT-2C18. Izod Impact tests were performed on percentage of clays between 0 and 5%. The impact strength was in general enhanced with the addition of clay for all three kinds of nanocomposites. The curve impact strength vs. nanoclay content seemed to have a maximum for 3% clay content.

A study on poly(ε-caprolactone) (PCL) -clay nanocomposites was made by Lepoittevin et alii[11] Commercially available PCL and MMT nanoclay were mixed by melt intercalation. Three different MMT were used: Na-MMT, and two surface modified MMT, MMT-Alk (Cloisite 25A) and MMT-$(OH)_2$ (Cloisite30B). Izod impact tests were performed on samples with 1, 3, 5, and 10% clay content. The impact strength decreased for all three nanocomposites continuously with increasing clay content. The reduction was around 50% for 10% clay content for all three nanocomposites.

The fabrication of syndiotactic polystyrene (sPS) organophilic clay was done by Park et alii[12] using melt intercalation. Various amorphous styrenic polymers were introduced to improve the dispersion and two different mixing methods (stepwise and continuous) were used. The

organophilic clay employed was Cloisite 15A in percentages 3, 6, 9%. The Izod impact tests showed slight decrease in impact strength with increasing clay content. The decrease in impact strength was contained within 20% for nanocomposites containing sPS and SMA (styrenic maleic anhydride random copolymer) and 9% of clay. Reduction up to 35% was observed for nanocomposites containing SEBS-MA (maleic anhydride grafted styrene-ethylene-butylene-styrene block copolymer), which have also sensible higher impact strength.

Ref.	Nanoclay	Nanoclay conten	Polymer Matrix	Impact strength variation*
1	Nanomer I.30E	5%	Epoxy	50% Increase
2	Cloisite 30B	6%	PMMA	20% decrease
2	Cloisite 30B	15%	Epoxy	10% increase
2	Cloisite 30B	2%	80% PMMA + 20% Epoxy	15% increase
2	Cloisite 30B	6%	80% PMMA + 20% Epoxy	no change
3	I.44P	4%	PP	30% increase
4	Closiste 20A	-	Epoxy PhEBA	300% increase
4	Closite 30B and Na	-	Epoxy PhEBA	no change
5	Cloisite 30B	-	Epoxy	decrease
6	MMT	-	PP	25% decrease
7	I.30TC and 30B	1% and 3%	BMPM	increase
7	I.30TC and 30B	5%	BMPM	no change
8	Cloisite 30B	-	Nylon 6	increase
9	Nanomer I.44P	4%	HDPE	33% decrease
10	MMT	1% - 5%	PVC	increase
11	MMT	10%	PCL	50% decrease
12	Cloisite 15A	9%	sPS + SMA	20% decrease
12	Cloisite 15A	-	sPS + SEBS MA	35% decrease

*** compared to the values of pure resin**

Table 2.1: impact properties for various nanoclay based nanocomposites

2.1.2 Flammability properties of nanoclays nanocomposites

Nanoclays show promising flame retardant characteristics when dispersed in a matrix system. Valera-Zaragoza et alii[13] studied the thermal stability and flammability behavior of polypropylene-(ethylene-propylene) copolymer (PP-EP)/poly(ethylene vinyl acetate)

(EVA)/montmorillonite nanocomposite. Nanoclays, according to concentration and dispersion, showed flame retardation properties. The nanoclay used was Cloisite 20A, an organically modified nanoclay with dimethyl di(hydrogenated tallow) quaternary ammonium chloride. The EVA/C20A and PP-EP/EVA/C20A showed flame retardation and thermal stability with absence of dripping in the burning phase with respect the non nano-modified copolymer.

Zhao et alii[14] prepared and tested a polyethylene/clay nanocomposite, using high density PE and Na-montmorrilonite (Na-MMT) clay, with two intercalating agents for the modification of Na-MMT. The peak of Heat Release Rate (HRR) was sensibly reduced with the addition of the nanoclays and intercalating agents (54% of reduction). Similarly the Mass Loss Rate (MLR) is reduced. This reduction increases with the increase of relative quantity of nanoclay. The time of burning increases, showing the effective flame retardation of nanoclay. The pure PE didn't leave any char residual, while in the PE/nanoclay black char was formed suggesting that a protective char, induced by the presence of nanoclay, contributes to the reduction of HRR.

Morgan et alii[15] studied the effect of organoclay Soxhlet extraction on the flammability properties of polypropylene nanocomposites. The typical synthesis of an organoclay can result in excess organic treatment which can hinder mechanical and flammability benefits. In the presence of excess of organic treatment the time of ignition was shortened, even if the peak of HRR was reduced. As Soxhlet time increases, the time of ignition increases as well, but the HRR oscillates. The total heat produced follows the trend of the HRR.

The thermal and flammability properties of polyamide 6/clay nanocomposites were measured by Kashwagi et alii[16]. The matrix system used was PA6 with 2 and 5% in weight of MMT. The addition of nanoclay slightly increases the ignition time and reduces the HRR. There is not evident change in the total heat released, indicating that the nanocomposites burn slowly,

but completely. The slow burning can be also seen in the MLR curve. The specific heat of combustion, obtained dividing the HRR with the MLR doesn't change for the pure resin and the nanocomposite, suggesting that reduction in HRR (and mass burning rate) tends to be due to chemical and physical processes mainly in the condensed phase instead of in the gas phase. In order to prove this conjecture, the samples were exposed to the same external flux as that in the cone calorimeter but in a nitrogen atmosphere to avoid any gas phase effects.

Poly(styrene-co-acrylonitrile) (SAN) nanocomposites were made by melt compounding and tested at flammability by Lih-Long Chu et alii[17], exhibiting reduced flammability. Cloisite 15A in 5% of weight and organic treatments were used in this research. The micro-cone calorimeter was used as test equipment, measuring the Heat Release Capacity (HRC) as most significant parameter. 20-45% of HRC reduction was observed.

Sodium MMT was modified with a polymeric surfactant by Jinguo Zhang et alii[18] the high molecular weight surfactant promote nanocomposite formation for polyethylene and polypropylene. Na-MMT (Cloisite) was used with PAE and Isotactic PP. PP and PE showed similar behavior in terms of peak of HRR (PHRR) reduction when modified with nanoclay. The total heat released and the time of ignition didn't change for the polymer and their corresponding nanocomposite. The smoke extinction area (SEA) increased with increasing amount of clay. The PHRR decreased of 20% with only 1% of clay, and it reached 50% reduction with 5% of clay.

Chigwanda et alii[19] prepared vinyl ester nanocomposites, using both clay and polyhedral oligosilsesquioxanes (POSS) as the nano-dimensional materialii From the cone calorimeter data it was observed that both clay and POSS helped to reduced the PHRR. To further improve the flame retardancy the nanocomposite was combined with phosphorous containing fire retardants (FRs). The organically modified clay used was Cloisite 15A. Three different vinyl ester,

bisphenol A/Novolac epoxy, bisphenol A epoxy, and brominated bisphenol A epoxy were used. A reduction of PHRR and no change in total heat released were observed. Time to ignition is lower for the nanocomposite with respect to the pure resin. The addition of phosphorous containing fire retardants didn't improve the time of ignition, but a significant reduction in the PHRR, the MLR and the total heat released was observed. The reduction of the total heat released showed that not the entire polymer is burned with the presence of phosphate.

Another research by Chigwanda et alii[20] examined nanocomposites containing MMT modified with pyridine and quinoline-containing salts. Polystyrene (PS) and Cloisite were used in this study. The time of ignition is shorter in presence of nanoclay, showing easier ignition for the nanocomposite compared with the virgin PS. The MLR and the PHRR decreased, and the total heat released remained the same as expected.

Zheng et alii[21] studied the flammability properties of nanocomposites made of nanoclay and high impact polystyrene, acrylonitrile–butadiene–styrene terpolymer, polypropylene, and polyethylene, prepared using a methyl methacrylate oligomerically-modified clay by melt blending. The different percentages mixed were 1, 3, and 5% of MMT in PS, HIPS, ABS, PE, and PP. For all kind of nanocomposites the ignition time seemed to diminish with clay content. The peak of HRR diminished for all nanocomposites, and the reduction was more visible as the clay content increase. For 5% clay content, the reduction was between 50% (ABS nanocomposites) and 71% (PS nanocomposites). The total heat released behaved similarly to the PHRR, with values decreasing with increasing clay content. The reduction was between 20-30% for 5% clay content. The Mass Loss Rate followed the trend of the HRR.

Ref.	Nanoclay	Nanoclay content	Polymer Matrix	Flammability behavior*
13	Cloisite 20A	-	PP-EP/EVA copolymer	Flame retardationand thermal stability
14	Na-MMT	-	HDPE	54% HRR reduction
15	organoclay FSM	-	PP	Peak of HRR reduction
16	MMT	2% and 5%	PA6	Ignition time increase reduction of HRR
17	Cloisite 15A	5%	SAN	20-45% reduction of HRC
18	Na-MMT	1%-5%	PP and PE	20%-50% decrease of PHRR no change in time of ignition
19	Cloisite 15A	-	various types of vinyl ester	Reduction of PHRR
20	Cloisite	-	PS	PHRR decrease and shorter time of ignition
21	MMT	1%,3%,5%	PS, HIPS, ABS, PE, and PP	Lower PHRR and THR

*** compared to the values of pure resin**

Table 2.2: flammability behavior for various nanoclay based nanocomposites

2.1.3 Mechanical properties of nanoclay nanocomposites

Jong Hyun Park et alii[2] tested a nanocomposite made of a mixture of epoxy and polymethylmethacrylate (PMMA) and nanoclay as reinforcement. The manufacturing procedure uses melt blending technique where two epoxies (one aromatic and one aliphatic) were mixed with nanoclay (Cloisite® 30B). Tensile tests were performed at room temperature. PMMA-nanoclay composites show a reduction of both maximum stress and strain at break of respectively 30 and 50% for 4% content of nanoclay. The Young's modulus increased of 33% for clay content of 4%. All results seemed to have linear correlation with the clay content. Epoxy-nanoclay composites behaved differently. The tensile strength increased up to 150% for 15% content of clay. Tensile strain at break decreased of 20% for 15% content of clay, and the Young's modulus almost doubled. The blend obtained by mixing PMMA, epoxy in 80-20 ratio,

and nanoclay showed no improvement of maximum tensile stress with the addition of nanoclay and a big increased (50%) of the tensile modulus with 6% of clay.

Poly hydroxy ether of bisphenol A (Ph) based polymer nanocomposites (PN) reinforced with a layered clay (montmorillonite) where studied by Gurmendi et alii[4] The clays used were three different kind of organically modified montmorillonite (Cloisite 20A, 30B and Cloisite Na modified in laboratory). The Young's modulus improved for each of the three clays, up to 40% increase for 4% of Cloisite 30B. A more modest improvement was found for the Yield stress (17% for 4% of Cloisite 30B). The elongation at break increased also, with 50% increase for 4% of Cloisite 20A, while Cloisite Na did not show any change.

The effect of nanoclay, modified with polyol, into an epoxy matrix system was studied by Isik et alii[5]. The materials used were diglycdyl ether of bisphenol A as matrix system and montmorillonite Cloisite 30B modified with polyether polyol, which bond well with epoxy. The tensile strength was decreasing with increasing amount of clay and constant content of polyol. The polyol instead seemed to have a beneficial effect on tensile strength with increase in polyol content. This is due to the higher level of crosslinking induced by the polyol. The Young's modulus increased with increasing amount of nanoclay and constant amount of polyol. The extension at break is smaller for the clay nanocomposite than for the virgin polymer.

The relationship between morphology and the mechanical properties of thermoplastic olefin (TPO) materials that are reinforced with organoclay fillers and prepared by melt processing was reported by Hyuk-Soo Lee et alii[6]. The nanocomposites were prepared by melt compounding, mixing PP, an ethylene–octane based elastomer and a masterbatch material containing equal parts of maleated PP and an organically modified montmorillonite. The Young's modulus increased with increasing clay content, up to 60% with 7% clay content. The

Yield strength increased initially with clay content up to 6% (7% increases) and then it dropped under the value of virgin polymer. The changes were however very contained. The elongation at break gradually diminished with presence of nanoclay, reaching about 66% decrease for 7% of clay content. The relative content of elastomer produced a decrease in Young's modulus and Yield Strength. The elongation at Yield and the elongation at break instead increased. In this extend, the clay content didn't have a comparable effect on Young's modulus and Yield stress, but they lowered sensibly the value of elongation at break and at yield.

Jinguo Zhang et alii[22] studied a styrenic polymer nanocomposite based on oligomerically modified nanoclay. The styrenic polymer was made with acrylonitrile-butadiene-styrene copolymer (ABS), high-impact polystyrene (HIPS), styrene-acrylonitrile copolymer (SAN), sodium montmorillonite, vinylbenzyl chloride (VBC), styrene (St), lauryl acrylate and 2,2' -azobisisobutyronitrile (AIBN). The tensile strength with various percentage of nanoclay increased for nanocomposites with ABS, and PS, while it doesn't change for HIPS. Data with SAN weren't reported. The effect of clay was very limited, with less than 20% increase for 10% of nanoclay. The Young's modulus increased for all the three kind of nanocomposite, with major effect on PS nanocomposite (40% increase for 10% clay content). The elongation at break slightly changed for PS nanocomposite (50% decrease), while a bigger effect was found for HIPS and ABS nanocomposites, with values that dropped from 36 and 39% elongation at break to 2-3%.

Rubber toughening of nylon 6 nanocomposite was investigated by Young-Cheol Ahn and D.R. Paul[8]. The samples were prepared by melt compounding the nylon 6 and the nanoclay (Cloisite 30B) and then melt compounding the rubber, an ethylene–propylene random copolymer grafted with maleic anhydride (EPR-g-MA). The presence of rubber decreased the Young's

modulus and the tensile strength of the virgin polymer, and increased the value of elongation at break. The opposite effect was found with the addition of the nanoclay, where the Young's modulus increased of 90% with 7% of nanoclay and absence of rubber, and more modest, but still significant increases with presence of rubber. The tensile strength increased in all cases of about 25% for 7% content of clay. The most significant effect was the decrease of elongation at break of about 90% for 7% clay content. The combination of rubber and clay seemed to have a positive effect in general, with increase in Young's modulus and tensile strength and more dimensional stability, with decrease of elongation at break.

Tanniru et alii[9] studied the tensile properties of high-density polyethylene (HDPE) copolymer reinforced with a natural montmorillonite clay surface modified dimethyl dialkyl ammonium (Nanomer I.44P). The data for virgin polymer and polymer reinforced with 4% clay were compared. The Young's modulus increased of about 26% with 4% clay, the yield stress remained practically unaffected, and the elongation at break sensibly reduced at half of the original value.

Wan et alii[10] studied three kinds of nanocomposites made of polyvinyl chloride (PVC) and three different nanoclays, Na-MMT and two surface modified MMT. The two organic MMTs were modified by trimethyloctadecyl ammonium and dimethyldioctadecyl ammonium, respectively, and they were denoted as MMT-C18 and MMT-2C18. The tensile strength of the nanocomposites produced was improved with the addition of clay. An average of 20% increased of tensile strength was found for 1-3% content of clay, followed by a reduction to level comparable to the virgin polymer for clay content close to 5% for the surface modified MMT nanocomposites. A 20% increase in tensile strength persisted at 5% clay content for Na-MMT nanocomposites.

A study on poly(ε-caprolactone) (PCL) -clay nanocomposites was made by Lepoittevin et alii[11]. Commercially available PCL and MMT nanoclay were mixed by melt intercalation. Three different MMT were used: Na-MMT, and two surface modified MMT, MMT-Alk (Cloisite 25A) and MMT-$(OH)_2$ (Cloisite30B). Tensile tests were performed for clay content that varied from 0 to 10%. The Young's modulus increased slightly for Na-MMT-PCL, with only 10% increase for 10% clay content. The increase in Young's modulus for the other two nanocomposites is more evident, with increase of 42% and 54% for 10% clay content of respectively MMT-Alk-PCL and MMT-$(OH)_2$-PCL. The elongation at break was reduced for all nanocomposites with addition of clay. Very evident reduction, with brittle fracture was observed for 10% of MMT-Alk-PCL and MM-$(OH)_2$-PCL. Tensile strength was almost unvaried for 1-5% clay content of Na-MMt, while reduction was observed for higher content. Tensile strength continuously reduced with increasing clay content for the other two nanocomposites, with reduction around 45-55% for 10% clay content.

The fabrication of syndiotactic polystyrene (sPS) organophilic clay was done by Park et alii[12] using melt intercalation. Various amorphous styrenic polymers were introduced to improve the dispersion and two different mixing methods (stepwise and continuous) were used. The organophilic clay employed was Cloisite 15A in percentages 3, 6, 9%. The tensile strength was increasing along with increasing content of nanoclay for nanocomposites with sPS and SMA (styrenic maleic anhydride random copolymer). Increases around 65-70% were recorded for 9% content of clay. Tensile strength was practically not altered for nanocomposites containing SEBS-MA (maleic anhydride grafted styrene-ethylene-butylene-styrene block copolymer).

Ref.	Nanoclay	Nanoclay content	Polymer Matrix	Mechanical behavior*
2	Cloisite 30B	4%	PMMA	30% reduction of stress at break 50% reduction of strain at break, 33%increase of Young's modulus
2	Cloisite 30B	15%	Epoxy	150% increase in tensile strength 20%decrease of strain at break 100% increase Young's modulus
2	Cloisite 30B	6%	80% PMMA + 20% Epoxy	50% increase Young's modulus
4	Cloisite 30B	4%	Epoxy PhEBA	40% increase Young's modulus
4	Cloisite 20A	4%	Epoxy PhEBA	50% increase elongation at break
4	Cloisite Na	-	Epoxy PhEBA	no change
5	Cloisite 30B	-	Epoxy	decreasing tensile strength increasing Young's modulus smaller extension at break
6	MMT	7%	PP	60% increase Young's modulus modest increase in tensile strength 66% decrease elongation at break
22	Na MMT	-	ABS	tensile strength increase increase Young's modulus big decrease of elongation at break
22	Na MMT	10%	PS	40% increase of tensile strength 40% increase Young's modudulus 50% decrease elongation at break
22	Na MMT	-	HIPS	no change in tensile strength increase Young's modulus big decrease of elongation at break
8	Cloisite 30B	7%	Nylon 6	90% increase of Young's modulus 25%increase tensile strength 90% decrease elongation at break
9	Nanomer I.44P	4%	HDPE	26% increase Young's modulus no change in tensile strength 50% reduction elongation at break
10	MMT	1% - 3%	PVC	20% increase tensile strength
10	Na MMT	5%	PVC	20% increase tensile strength
11	Na MMT	10%	PCL	10% increase Young's modulus no change in tensile strength decrease elongation at break
11	Cloisite 25A	10%	PCL	42% increase Young's modulus 50% decrease in tensile strength decrease elongation at break
11	Cloisite 30B	10%	PCL	54% increase Young's modulus 50% decrease in tensile strength decrease elongation at break
12	Cloisite 15A	9%	sPS	70% increase tensile strength

*** compared to the values of pure resin**

Table 2.3: mechanical properties of nanoclay based nanocomposites

2.2 Literature review: carbon nanofibers based nanocomposites

In this section, the properties of carbon nanofibers (CNF) based nanocomposites will be reviewed from available literature. The matrix systems taken into consideration will be both thermoset and thermoplastic polymers. Impact, flammability and tensile properties will be analyzed and summarized in tables. Unlike for nanoclay based nanocomposites, the research on carbon nanofibers is somehow limited, due to the high cost of the nanoparticles and the more problematic dispersion procedure.

2.2.1 Impact properties of carbon nanofibers nanocomposites

Impact strength of carbon nanofibers nanocomposites was investigated by Miyagawa and Drzal[23]. Two commercial grades of carbon nanofibers were used, Pyrograf III PR-19-PS and Pyrograf III PR-19-HHT. The matrix system was a bisphenol F based epoxy. An increase of 20% in Izod impact strength was observed for volume fractions of 1% and 2%.

Vapor-grown graphite nanofibers (GNFs) were modified by plasma treatment and Seo, Park and Lee[24]. The carbon nanofibers were obtained from Shova Denko Co. and mixed with DGEBA epoxy. The Izod impact strength increased for all percentages in weight, with a pick for 2% (32% increase). For higher nanofibers content, the improvement in impact strength was more contained (20% increase for 5% weight fraction).

Ref.	CNF	CNF content	Polymer Matrix	Impact strength variation*
23	Pyrograf III	1% - 2% volume fraction	Epoxy	20% Increase
24	from Shova Denko Co.	2%	Epoxy	32% increase
25	from Shova Denko Co.	5%	Epoxy	20% increase

*** compared to the values of pure resin**

Table 2.4: impact properties of carbon nanofibers based nanocomposites

2.2.2 Flammability behavior of carbon nanofibers nanocomposites

Flammability properties for carbon nanofibers nanocomposites were not investigated so consistently like for nanoclay nanocomposites. Recent articles however report improvement in flame retardation with the addition of carbon nanofibers.

Improvement in flammability properties of carbon nanofibers-PMMA nanocomposites was observed in the National Institute of Standards and Technology and the University of Pennsylvania[25], by Takashi Kashiwagi et alii. When the researchers heated polymethyl methacrylate (PMMA) dispersed with carbon nanofibers, the material behaved like a gel. The carbon nanofibers created a stable network, which produced a transition from liquid to solid. This shift enhanced the flame resistance of the polymer.

Arobindo Chatterjee, B. L. Deopura[26] studied the thermal stability of polypropylene-carbon nanofibers nanocomposites. The flame behavior of the nanocomposites suggested the beneficial effect of the addition of the nanofibers in the thermoplastic matrix.

2.2.3 Mechanical properties carbon nanofibers nanocomposites

Jijun Zeng et alii[27] evaluated poly(methyl methacrylate) (PMMA) nanocomposites, processed by melt blending, containing two different grades (PR-21-PS and PR-24-PS) of Pyrograf III CNF. The amount of nano fibers used was 5 and 10 wt%, respectively. At 5 wt% CNF, composite rods as well as fibers showed over 50% improvement in axial tensile modulus as compared to the control PMMA rod and fibers, respectively. For 10% content in weight the tensile modulus was approximately the same that the pure polymer. Tensile strength and elongation at break were both lower than the values for the virgin PMMA.

Yutaka Iwahori et alii[28] investigated the effect of carbon fibers reinforced plastics, with epoxy nanomodified with carbon nanofibers. Two CNF aspect ratios of 10 and 50 were employed (AR10 and AR50). The CNF was dispersed to epoxy resin in two values of CNF weight ratios, 5 and 10% to the resin. The static strength tests led to the conclusion that the dispersion of CNF into epoxy improves mechanical properties of the tow-phase composites. The tensile modulus increased for both 5% and 10% content in weight, showing increase up to 46% for 10% weight content of CNF. Tensile strength increase too, up to 21% increase for 10% wt content of AR50. Elongation at break reduces for all percentages, up to 40% for 10% weight content of AR50.

A work made by Kuriger et alii[29] investigates the processing and the properties of vapor growth CNF in a thermoplastic polymer. The CNF used were two kinds of Pyrograf III in polypropylene homopolymer. The samples were produced molding the polymer, which was previously extruded with a twin screw extruder. The tensile strength gradually increases for all fiber volume fractions, with double value for 0.1 volume fraction. The Young's modulus increased almost linearly with increasing volume fraction, with triple value for 0.125 volume fraction.

Vapor growth CNF properties were determined in a work by Hasan et alii[30]. Pyrograf III PR24 was used together with PP powder. Dry mixing and extrusion was then performed. Tensile modulus and tensile strength have increased by 154% and 69.5%, respectively. 75 % of reduction of strain at break was also observed.

Characterization of polycarbonate CNF nanocomposites sheet was carried out by Choi et alii[31]. The carbon nanofibers used were VGCF supplied by Shova Denko Co., and they were mixed by high shear with a twin extruder. Rolling and casting where used to produce the sheets.

25% increase in tensile strength was observed for rolled nanocomposites sheet for 10% weight content. For higher percentages the tensile strength dropped. Young's modulus instead increase linearly with increasing content of CNF, up to 100% increase for 26% weight content of CNF.

Another work by Choi et alii[32] evaluated the properties of epoxy CNF nanocomposites. Vapor growth carbon nanofibers VGCF were supplied by Shova Denko Co. and mixed with bisphenol A based epoxy. The maximum improvement in mechanical properties was modest (15%) and was found for 5% percentage in weight. The Young's modulus for 5% weight percentage instead almost double.

Ref.	CNF	CNF content	Polymer Matrix	Mechanical behavior*
27	Pyrograf III	5%	PMMA	50% increase in Young's modulus Lower tensile strength Lower elongation at break
27	Pyrograf III	10%	PMMA	Inferior overall mechanicalproperties
28	Carbere AR10	10%	Epoxy	46% increase in young's modulus 17% increase in tensile strength 38% decrease strain at break
28	Carbere AR50	10%	Epoxy	46% increase in young's modulus 21% increase in tensile strength 40% decrease strain at break
29	Pyrograf III	0.1 (volume fraction)	PP	100% increase in tensile strength
29	Pyrograf III	0.125 (volume fraction)	PP	300% increase in Young's modulus
30	Pyrograf III	0.50%	PP	154% increase in Young's modulus 70% increase in tesile strength 75% decrease of strain at break
31	VGCF	10%	PC	25% tensile strength increase 33% young's modulus increase
31	VGCF	26%	PC	10% tensile strength increase 100% increase in Young's modulus
32	VGCF	5%	Epoxy	15% increase in tensile strength 100% increase in Young's modulus

*** compared to the values of pure resin**

Table 2.5: mechanical properties of carbon nanofibers nanocomposites with various matrix system

2.3 Literature review: stability of burning structural elements

One of the chapters of this dissertation will deal with a mathematical modeling of stability of structural elements under the process of burning. The use of composites structural elements in civil, aerospace and naval structures is a very current topic, since composites are employed extensively due to their superior mechanical, corrosion and fatigue resistance. One of the issues associated to the use of polymer composites is the low resistance to flammability, with consequent degradation of properties and premature failure. Moreover the burning process ablate the polymer matrix with resulting reduction of resistant section.

A study by Gu and Asaro[33] analyzed the structural safety ofpolymer matrix composites, subject to compressive loading and thermal gradient along the out-of-plane direction caused by fire. The model considers uniform burning in one side of the structural element and the reduction of mechanical properties due to the thermal gradient produced by the fire. The model is quasi-static, with two time frames, one with the structure integer and the other with part of it ablated by burning. The study is extended to sandwich structures. The properties change due to thermal lading is modeled considering three check points for the temperature, which were previously found by experimental evaluation.

Dao et alii[34] performed a combined experimental; and theoretical study of the compressive failure of polymer composites under fire degradation. Panels were subjected to time-temperature history with applied multi-axial loading. The Young's modulus variation with temperature gradient was modeled as a second-degree polynomial. The experimental results were then compared to analytical model. A design criterion was finally proposed.

Another paper by Gu and Asaro[35] discuss the distortion of panels made of fiber reinforced polymer matrix composites. The formulation makes use of thermal distortion and

functionally graded materials theory associated with internal forces. The temperature distribution was again modeled using the temperature at the face exposed to fire, the center face and the back face. The Young's modulus was supposed having a parabolic distribution in relation with the temperature variation along the thickness.

Ramroth et alii[36] proposed a thermal model for fiber reinforced polymer sandwich structures, using finite elements analysis. The theory fully accounts for arbitrary reorientations of the laminate and anisotropic material response, as well as for finite strains. The model takes also into account local failure, besides global failure. the total deformation as prescribed is decomposed into a process of interlaminar shear followed by an elastic deformation of the orthotropic framework. The model was experimentally validated.

An experimental evaluation completed with analytical modeling of fire-damaged polymer sandwich composites was proposed by Mouritz and Gardiner[37]. The sandwich structure was tested using a cone calorimeter and the residual properties were evaluated at room temperature. Core-shear failure and global buckling were both considered in the model. The fire degradation in relation with heat flux applied and time of burning was evaluated and modeled.

A work from Usmani et alii[38] presents theoretical descriptions of the key phenomena that govern the behavior of composite framed structures in fire. The model shows a comprehensive picture of the combined effect of thermal loading, due to material axial thermal expansion, and mechanical loading, with different constrains at the extremes of the beam. Another effect, called thermal bowing, was considered. Thermal bowing describes the behavior of a beam subjected to thermal loading where surfaces along the thickness expand differently due to severe thermal gradients. The models, completed with numerical evaluation, provide an estimation of deflection for various types of thermal loading.

[1] D. Ratna, O. Becker, R. Krishnamurthy, G.P. Simon, R.J. Varley, "Nanocomposites based on a combination of epoxy resin, hyperbranched epoxy and a layered silicate", *Polymer 44 (2003) 7449-7457*

[2] Jong Hyun Park, Sadhan C. Jana, "The relationship between nano- and micro-structures and mechanical Properties in PMMA-epoxy-nanoclay composites", *Polymer 44 (2003) 2091-2100*

[3] Q. Yuan and R.D.K. Misra, "Impact fracture behavior of clay–reinforced polypropylene nanocomposites", *Polymer, Volume 47, Issue 12, 31 May 2006, Pages 4421-4433*

[4] U. Gurmendi, J.I. Eguiazabal and J. Nazabal, "Structure and properties of a new polymer nanocomposite based on a poly(hydroxy ether of bisphenol A) matrix", *Composites Science and Technology, Volume 66, Issue 10, August 2006, Pages 1221-1228*

[5] Isil Isik, Ulku Yilmazer and Goknur Bayram, "Impact modified epoxy/montmorillonite nanocomposites: synthesis and characterization", *Polymer, Volume 44, Issue 20, September 2003, Pages 6371-6377*

[6] Hyuk-soo Lee, Paula D. Fasulo, William R. Rodgers and D.R. Paul, "TPO based nanocomposites. Part 1. Morphology and mechanical properties", *Polymer, Volume 46, Issue 25, 28 November 2005, Pages 11673-11689*

[7] Jiru Meng and Xiao Hu, "Synthesis and exfoliation of bismaleimide–organoclay nanocomposites", *Polymer, Volume 45, Issue 26, December 2004, Pages 9011-9018*

[8] Young-Cheol Ahn and D.R. Paul, "Rubber toughening of nylon 6 nanocomposites", *Polymer, Volume 47, Issue 8, 5 April 2006, Pages 2830-2838*

[9] M. Tanniru, Q. Yuan and R.D.K Misra, "On significant retention of impact strength in clay–reinforced high-density polyethylene (HDPE) nanocomposites", *Polymer, Volume 47, Issue 6, 8 March 2006, Pages 2133-2146*

[10] Chaoying Wan, Xiuying Qiao, Yong Zhang and Yinxi Zhang, "Effect of different clay treatment on morphology and mechanical properties of PVC-clay nanocomposites", *Polymer Testing, Volume 22, Issue 4, June 2003, Pages 453-461*

[11] Bénédicte Lepoittevin, Myriam Devalckenaere, Nadège Pantoustier, Michaël Alexandre, Dana Kubies, Cédric Calberg, Robert Jérôme and Philippe Dubois, "Poly(ε-caprolactone)/clay nanocomposites prepared by melt intercalation: mechanical, thermal and rheological properties", *Polymer, Volume 43, Issue 14, June 2002, Pages 4017-402*

[12] Cheon Il Park, O Ok Park, Jae Gon Lim and Hyun Joon Kim, "The fabrication of syndiotactic polystyrene/organophilic clay nanocomposites and their properties", *Polymer, Volume 42, Issue 17, August 2001, Pages 7465-7475*

[13] M. Valera-Zaragoza, E. Ramírez-Vargas, F.J. Medellín-Rodríguez and B.M. Huerta-Martínez, "Thermal stability and flammability properties of heterophasic PP–EP/EVA/organoclay nanocomposites", *Polymer Degradation and Stability, Volume 91, Issue 6, June 2006, Pages 1319-1325*

[14] Chungui Zhao, Huaili Qin, Fangling Gong, Meng Feng, Shimin Zhang and Mingshu Yang, "Mechanical, thermal and flammability properties of polyethylene/clay nanocomposites", *Polymer Degradation and Stability, Volume 87, Issue 1, January 2005, Pages 183-189*

[15] Alexander B. Morgan and Joseph D. Harris, "Effects of organoclay Soxhlet extraction on mechanical properties, flammability properties and organoclay dispersion of polypropylene nanocomposites", *Polymer, Volume 44, Issue 8, April 2003, Pages 2313-2320*

[16] Takashi Kashiwagi, Richard H. Harris, Jr , Xin Zhang, R. M. Briber, Bani H. Cipriano, Srinivasa R. Raghavan, Walid H. Awad and John R. Shields, "Flame retardant mechanism of polyamide 6–clay nanocomposites", *Polymer, Volume 45, Issue 3, February 2004, Pages 881-891*

[17] Lih-Long Chu, Stephanie K. Anderson, Joseph D. Harris, Mark W. Beach and Alexander B. Morgan," Styrene-acrylonitrile (SAN) layered silicate nanocomposites prepared by melt compounding", *Polymer, Volume 45, Issue 12, May 2004, Pages 4051-4061*

[18] Jinguo Zhang and Charles A. Wilkie, "Polyethylene and polypropylene nanocomposites based on polymerically-modified clay containing alkylstyrene units", *Polymer, Volume 47, Issue 16, 26 July 2006, Pages 5736-5743*

[19] Grace Chigwada, Panchatapa Jash, David D. Jiang and Charles A. Wilkie, "Fire retardancy of vinyl ester nanocomposites: Synergy with phosphorus-based fire retardants", *Polymer Degradation and Stability, Volume 89, Issue 1, July 2005, Pages 85-100*

[20] Grace Chigwada, Dongyan Wang and Charles A. Wilkie, "Polystyrene nanocomposites based on quinolinium and pyridinium surfactants", *Polymer Degradation and Stability, Volume 91, Issue 4, April 2006, Pages 848-855*

[21] Xiaoxia Zheng, David D. Jiang, Dongyan Wang and Charles A. Wilkie, "Flammability of styrenic polymer clay nanocomposites based on a methyl methacrylate oligomerically-modified clay**",** *Polymer Degradation and Stability, Volume 91, Issue 2, February 2006, Pages 289-297*

[22] Jinguo Zhang, David D. Jiang, Dongyan Wang and Charles A. Wilkie, "Styrenic polymer nanocomposites based on an oligomerically-modified clay with high inorganic content", *Polymer Degradation and Stability, Volume 91, Issue 11, November 2006, Pages 2665-2674*

[23] Hiroaki Miyagawa and Lawrence T. Drzal, "Effect of oxygen plasma treatment on mechanical properties of vapor grown carbon fiber nanocomposites", *Composites Part A: Applied Science and Manufacturing*, *Volume 36, Issue 10*, *October 2005*, *Pages 1440-1448*

[24] Min-Kang Seo, Soo-Jin Park and Sang-Kwan Lee, "Influence of atmospheric plasma on physicochemical properties of vapor-grown graphite nanofibers", *Journal of Colloid and Interface Science*, *Volume 285, Issue 1*, *1 May 2005*, *Pages 306-313*

[25] www.azonano.com

[26] Arobindo Chatterjee, B. L. Deopura, "Thermal stability of polypropylene/carbon nanofiber composite", Journal of Applied Polymer Science Volume 100, Issue 5 , Pages 3574 - 3578

[27] Jijun Zeng, Bethany Saltysiak, W.S. Johnson, David A. Schiraldi, Satish Kumar, "Processing and properties of poly(methyl methacrylate)/carbon nano fiber composites", *Composites: Part B 35 (2004) 173–178*

[28] Yutaka Iwahori, Shin Ishiwata, Tomoji Sumizawa, Takashi Ishikawa, "Mechanical properties improvements in two-phase and three-phase composites using carbon nano-fiber dispersed resin", *Composites: Part A 36 (2005) 1430–1439*

[29] Rex J. Kuriger, M. Khairul Alam, David P. Anderson and Ronald L. Jacobsen, **"**Processing and characterization of aligned vapor grown carbon fiber reinforced polypropylene**",** *Composites Part A: Applied Science and Manufacturing*, *Volume 33, Issue 1*, *January 2002*, *Pages 53-62*

[30] Mohammad M. Hasan, Yuanxin Zhou and Shaik Jeelani, "Thermal and tensile properties of aligned carbon nanofiber reinforced polypropylene**",** *Materials Letters*, *Volume 61, Issues 4-5*, *February 2007*, *Pages 1134-1136*

[31] Young-Kuk Choi, Koh-ichi Sugimoto, Sung-Moo Song and Morinobu Endo, "Production and characterization of polycarbonate composite sheets reinforced with vapor grown carbon fiber", *Composites Part A: Applied Science and Manufacturing*, *Volume 37, Issue 11*, *November 2006*, *Pages 1944-1951*

[32] Young-Kuk Choi, Koh-ichi Sugimoto, Sung-Moo Song, Yasuo Gotoh, Yutaka Ohkoshi and Morinobu Endo, **"**Mechanical and physical properties of epoxy composites reinforced by vapor grown carbon nanofibers", *Carbon*, *Volume 43, Issue 10*, *August 2005*, *Pages 2199-2208*

[33] Pei Gu, R. J. Asaro, "Structural buckling of polymer matrix composites due to reduced stiffness from fire damage", *Composites Structures 69 (2005) 65-75*

[34] Ming Dao, Robert J. asaro, "A study of failure prediction and design criteria for fiber composites under fire degradation*", Composites: Part A 30 (1999) 123-131*

[35] Pei Gu, R. J Asaro, " Distortion of Polymer Matrix Composite Panels under Transverse Thermal Gradients", *accepted manuscript Composite Structures (2007)*

[36] W.T. Ramroth, R**.**J**.** Asaro, B. Zhu and P. Krysl, "Finite element modelling of fire degraded FRP composite panels using a rate dependent constitutive model", *Composites Part A: Applied Science and Manufacturing*, *Volume 37, Issue 7*, *July 2006*, *Pages 1015-1023*

[37] A. P. Mouritz and C. P. Gardiner, "Compression properties of fire-damaged polymer sandwich composites", *Composites Part A: Applied Science and Manufacturing*, *Volume 33, Issue 5*, *May 2002*, *Pages 609-620*

[38] A. S. Usmani, J. M. Rotter, S. Lamont, A. M. Sanad and M. Gillie, "Fundamental principles of structural behaviour under thermal effects", *Fire Safety Journal*, *Volume 36, Issue 8*, *November 2001*, *Pages 721-744*

Chapter 3

Experimental procedure

3.1 Nanocomposites manufacturing

Epoxy-clay nanocomposites, epoxy-carbon nanofibers (CNFs) nanocomposites, and nanocomposites made with both types of reinforcements together were manufactured and tested for this work. The manufacturing parameters were kept constant for all nanocomposites produced, since it was revealed by preliminary tests that the properties of a nanocomposite are strongly dependent by the mixing procedure. A combination of mechanical mixing and ultra-sonication mixing was used.

3.1.1 Materials

All nanocomposites produced are made with marine epoxy resin as matrix system. The two nanoparticles used as reinforcements were montmorillonite layered silicates and carbon nanofibers. The epoxy is a viscous liquid made of two parts, resin and hardener, the nanoclays are a white powder, and carbon nanofibers are a black powder with some agglomerate (figure 3.1).

A


B


C

Figure 3.1: ***(A)*** **epoxy part B and part A,** ***(B)*** **nanoclays[1],** ***(C)*** **carbon nanofibers**

3.1.1.1 Epoxy

The marine epoxy employed was diglycdyl ether of bisphenol A (DGEBA) marine epoxy, commercially denominated Silvertip® from System Three Resins, Inc. The epoxy was a two part system, with part A and part B mixed with a ratio of 2:1 in volume and 100:43 in weight. The composition is in table 3.1 and the physical properties are reported in table 3.2. The gel time at 25ºC occurs after about 60 minutes, and the tack free time after 6 hours. To obtain full curing, post curing is required in oven for 2 hours.

Part A	Diglycidyl Ether of Bisphenol A (70-80% weight) Benzyl Alcohol (10-15% weight) Alkylglycidyl Ether (10-15% weight)
Part B	Aliphatic Amines (60 – 70 % weight, mixture is a trade secret) Alkyl Phenols (15 – 20 % weight, mixture is a trade secret) Benzyl Alcohol (15 – 20 % weight) Aromatic Amines (5 – 10 % weight)

Table 3.1: composition of the epoxy used

	Viscosity (cps)	**Specific gravity**	**Color**
Part A	700	1.135	Colorless
Part B	620	0.961	Pale yellow

Table 3.2: physical properties of the epoxy used

3.1.1.2 Nanoclays

The nanoclays used for this work are montmorillonite nanoclays, commercially known as Nanomer I.30 E. Nanomer® I.30E nanoclay is a surface modified montmorillonite mineral which will disperse to nanoscale in epoxy resin systems. I.30E is supplied as a white powder

which disperses to particles so thin they are nearly transparent in the resin matrix. The physical properties are reported in table 3.3.

Appearance	white powder
Mean Dry Particle Size (micron)	8-10
+ 325 Mesh Residue (%)	0.1
Specific Gravity	1.71
Bulk density (g/cc)	0.41
Moisture (%)	3 max
Mineral purity (% min)	98.5

Table 3.3: physical properties of Nanomer I.30E nanoclays

3.1.1.3 Carbon nanofibers

The carbon nanofibers used are commercially available with the trade name Pyrograf®-III, from Pyrograf Products Inc., part of Applied Sciences Inc. Pyrograf®-III is a very fine, highly graphitic, low cost, carbon nanofiber. It is available in diameters ranging from 70 and 200 nanometers and a length estimated to be 50-100 microns. Therefore, nanofibers are much smaller than conventional continuous or milled carbon fibers (5-10 microns), but significantly larger than carbon nanotubes (1-10 nanometers). It comes in different grades, and the grades used is HT (Heat Treated), heated to temperatures up to 3,000°C. The treatment graphitizes chemically vapor deposited carbon present on the surface of Pyrograf®, creates a highly electrically conductive carbon nanofiber, and removes iron catalyst from carbon nanofiber. The physical properties are reported in table 3.4.

Appearance and odor	fluffy agglomerates with no odor
Moisture content (%)	< 5
Diameter (nm)	100-200
Length (microns)	30-100
Water solubility	NO
Specific gravity	2.0
Apparent density (kg/l)	0.032-0.32

Table 3.4: physical properties of the carbon nanofibers used

3.1.2 Manufacturing process

To produce the nanocomposites the nano-reinforcements are mixed directly in epoxy part A. After mixing the right amount of part B is added and the curing process starts. The procedure to manufacture them is listed below:

1. Drying nanoparticles in oven at 80˚C for 24 hours
2. Calculating amount of nanoparticles, epoxy part A and epoxy part B
3. Pre-mix nanoparticles with epoxy part A: mechanical mixing for 3 minutes
4. Mixing nanoparticles with epoxy part A: sonication directly in epoxy part A (30 min at 85˚C). Parameters for sonication:
    - Amplitude = 35%
    - Time = 30 min
    - Pulse = 2 sec ON, 2 sec OFF
    - Energy = 600,000
    - Temperature = 85˚C
5. Degassing the mixture in the beaker in vacuum oven (3 hours) at 70˚C
6. Removing DEGASSED samples from oven

7. Cooling mixture
8. Mechanical mixing of epoxy Part B (2-3 minutes), under lamp until the mixture has uniform appearance
9. Pouring into the mold and curing at room temperature in the mold for 24 hours
10. Removing the samples from the molds
11. Post curing the samples in oven at 100˚C (4 hours)
12. Removing POST-CURED samples from oven
13. Test samples after 7 days

The mixing process is carried out by pre-mixing mechanically and then using a 500 W ultra-sonicator Vibra-Cell® VCX-500, from Sonics & Materials Inc.(figure 3.2).The amount of nanoclays mixed is in weight percentage, and it takes into account the amount of nanoparticles added, so that the weight percentage is the effective weight percentage of all the mixture. To do so, weight factors are calculated in relation to the part A weight (1% → 0.01454, 2% → 0.02939, 3% → 0.04454, 4% → 0.06, 6% → 0.09192). First a quantity of part A is poured in the beaker and weighted, then the weight factor is multiplied by the weight of part A to obtain the quantity of nanoparticles to be added. This reduces the measurement error and it makes the process easier. After sonicating, a degassing cycle in vacuum oven is run and then part B is added and stirred mechanically, before casting in metal molds (figure 3.3). A post curing cycle is then performed and the samples will be left aging for a week before testing.

Figure 3.2: ultrasonicator Vibra-Cell® VCX-500

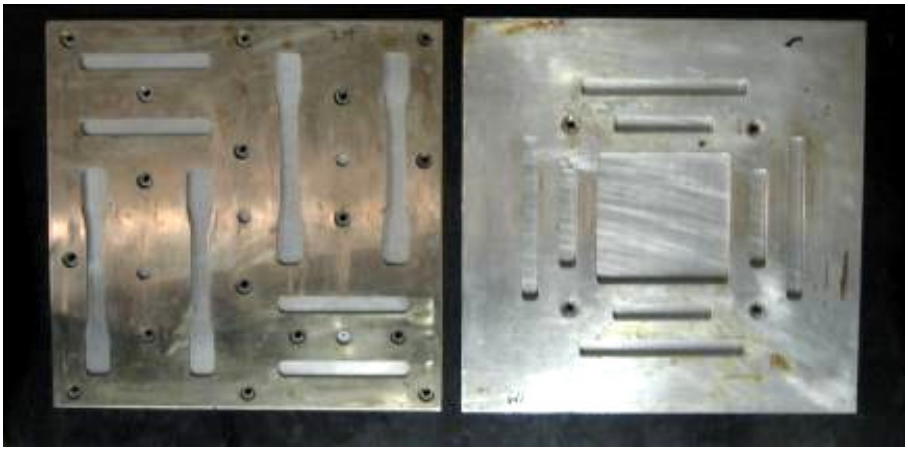

Figure 3.3: metal molds for casting the nanocomposites samples

The samples obtained are clear in color for pristine epoxy, golden-clear for nanocomposites with nanoclays, with color becoming darker with increasing amount of nanoclays. The nanocomposites that contain carbon nanofibers and carbon nanofibers plus nanoclays are black (figure 3.4)

Figure 3.4: pristine epoxy, epoxy-clay nanocomposites (2%, 4%, 6%), and epoxy-CNF nanocomposite (3%)

3.2 Fracture tests

Two kinds of tests were performed to evaluate the fracture properties of the nanocomposites produced: Izod impact tests and fracture toughness tests.

3.2.1 Impact tests

Izod impact tests were carried out in a Monitor Impact Tester from Testing Machines Inc. (figure 3.5) on samples previously notched with a notching machine (see figure 3.5 on the left). The tests are made following the ASTM D 256 – 06 standard test methods for determining the Izod pendulum impact resistance of plastics. The test cover the determination of the resistance of plastics to standardized pendulum type hammers, mounted in standardized machines, in breaking standard specimens with one pendulum swing[2]. The results are reported in terms of energy absorbed per unit of cross-sectional area.

The specimen is held as a vertical cantilever beam and it is broken by a single swing of the pendulum. The line of initial contact is at a fixed distance from the specimen clamp and from the centerline of the notch and on the same face as the notch[2]. The energy expended in tossing the broken part of the sample is subtracted from the value obtained during the test. To determine this energy, the broken part of the sample is repositioned on the clamped portion, and a second strike is performed in this condition. The value obtained by this subtraction is called the "net Izod impact resistance".

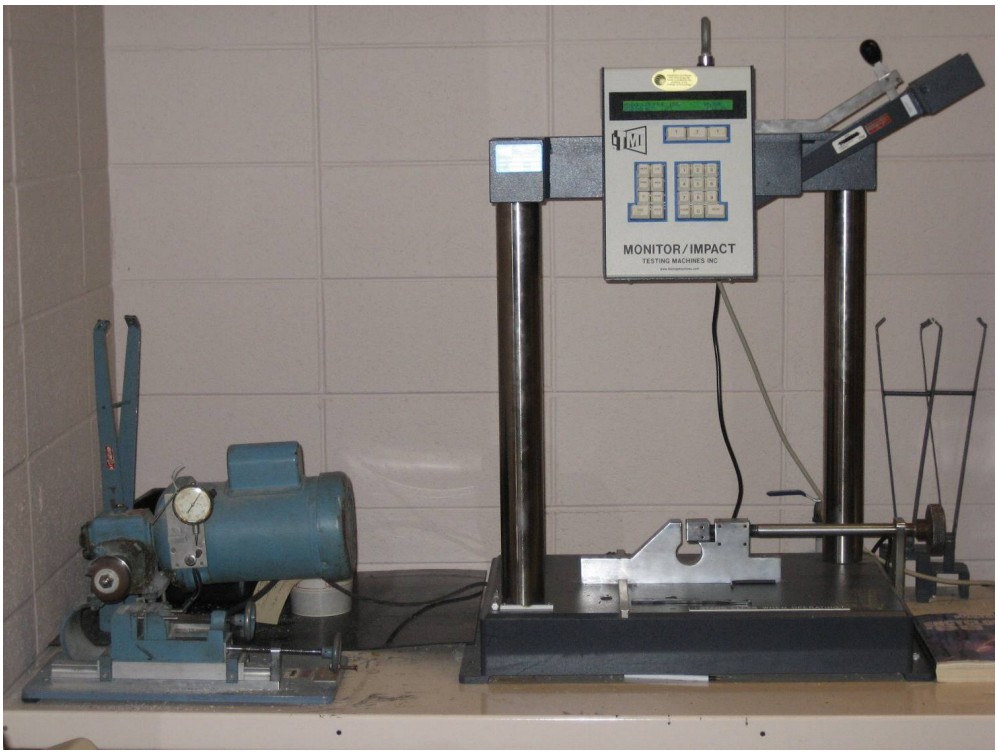

Figure 3.5: monitor impact tester

The energy lost by the pendulum during the breakage is the sun of the energy to initiate fracture, the energy to propagate the fracture, the energy to throw the free end (subtracted from the initial value), the energy to bend the specimen, the energy to produce vibration in the

pendulum arm, the energy to overcome friction at various components, and the energy to indent or deform plastically the specimen at the line of impact. For brittle samples the dominant portions are the energy required to initiate the crack and the energy to toss the sample (then subtracted to obtain the net value). The value obtained is expressed in J/m^2.

The specimen shall have the same nominal width. In our case it is 12.7 mm. The thickness was measured time by time, but it was approximately 9.525 mm (3/8 inches), which is the thickness of the mold (figure 3.6).

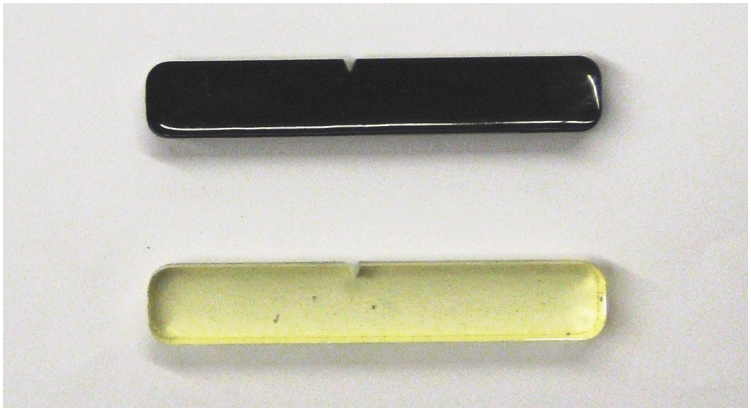

Figure 3.6: notched specimens for Izod impact tests

3.2.2 Fracture toughness tests

Fracture toughness tests where carried out on a universal testing machine Instron 4467 (figure 3.7) following the ASTM D 5045 – 99 standard tests method for plane-strain fracture toughness and strain energy release rate of plastic materials. These tests are designed to characterize the toughness of plastics in terms of the critical stress intensity factor K_{IC}, and critical strain energy release rate G_{IC}, at fracture initiation. The stress intensity factor K_{IC} is a toughness parameter indicative of the *resistance* of a material to fracture, the strain energy release rate G_{IC} is a toughness parameter based on *energy* required to fracture. The properties determined characterizes the resistance and the energy of a material to fracture in a neutral

environment in the presence of a sharp crack under severe tensile constraint, such that the state of stress near the crack-tip plastic region is small compared with the crack size and specimen dimensions in the constraint direction[3].

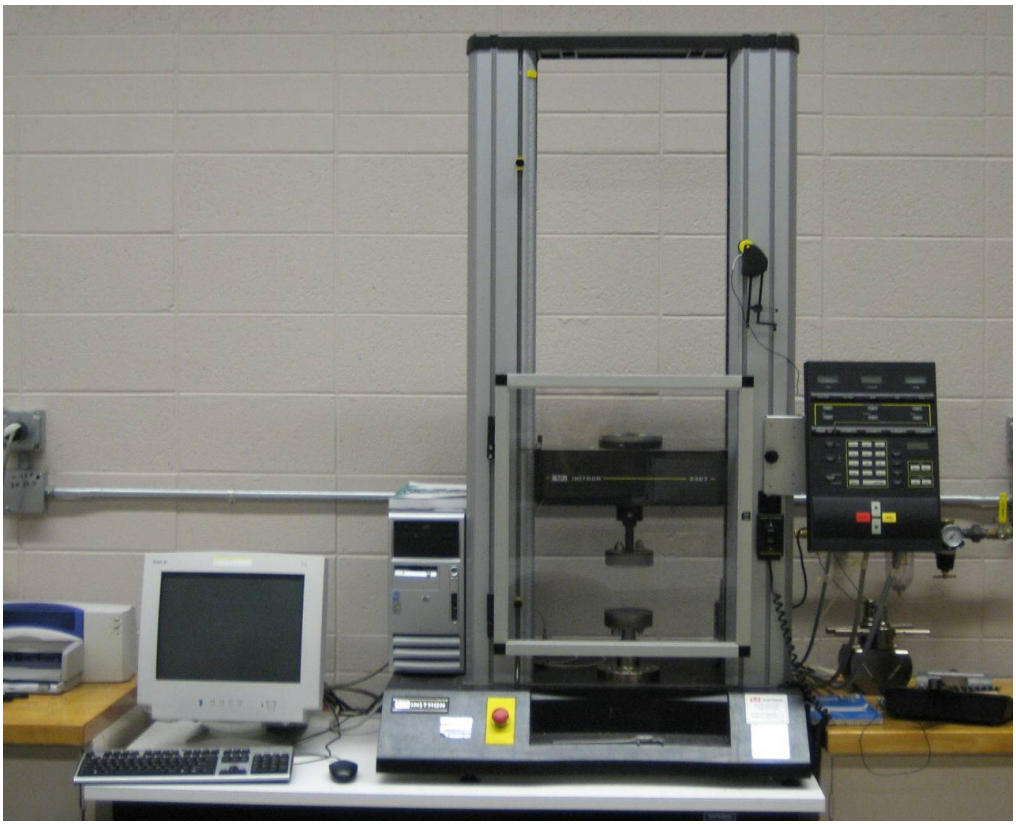

Figure 3.7: universal testing machine Instron 4467

The fracture toughness specimens used are single-edge-notch bending (SENB) samples (figure 3.8). The sample is before machine notched with a saw and then a crack is created with a razor blade (figure 3.9). To respect plain strain conditions, and to be able to consider the results valid, the following size criteria must be satisfied:

$$B, a, (W - a) > 2.5 \cdot \left(K_Q / \sigma_y\right)^2$$

where K_Q is the trial value for the stress intensity factor, B, a, W-a are dimensions of the specimen (figure 3.10), and σ_y is the yield stress of the material.

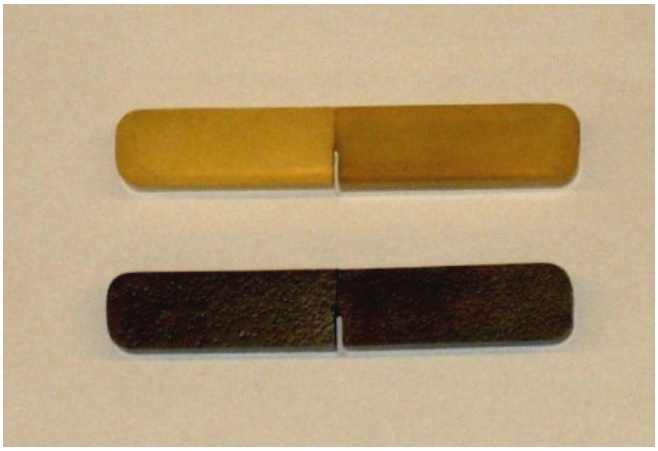

Figure 3.8: SENB samples for fracture toughness tests

A

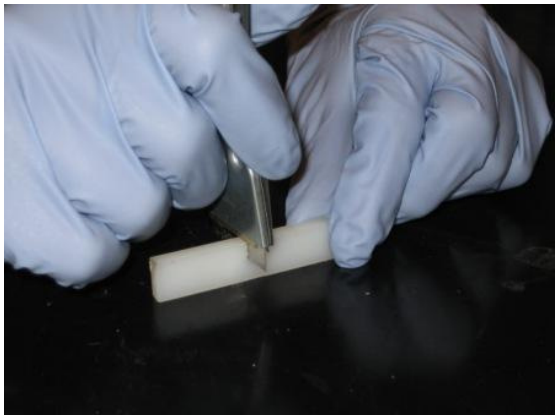

B

Figure 3.9: creation of the notch *(A)* and of the crack *(B)* for SENB samples

The fracture toughness test performed in this work, involves loading a notched specimen that has been pre-cracked in three-point bending (figure 3.10), with 10 mm/min loading rate. To calculate K_{IC}, a load-displacement curve needs to be obtained and a load P_Q needs to be computed. If the material is brittle and the load-displacement curve has a shape similar to a

triangle, P_Q is the maximum load. At this point it is possible to compute K_Q (trial value for K_{IC}) with the following equation:

$$K_Q = \left(\frac{P_Q}{BW^{1/2}} \right) f(x)$$

where *f(x)* is a geometrical parameter depending on the ratio *a/W* and it is tabulated in the ASTM standard. G_{IC} can be obtained either integrating the load-displacement curve or using the following formula, which is valid only for linear fracture behavior:

$$G_{IC} = \frac{(1-\upsilon^2)K_{IC}^2}{E}$$

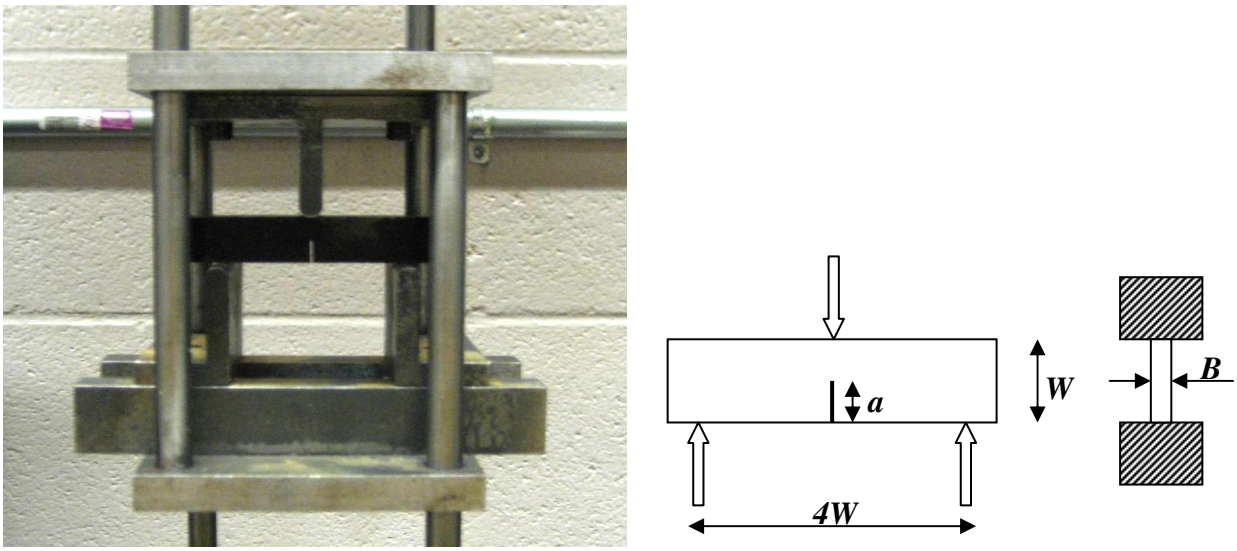

Figure 3.10: fracture toughness specimen loaded in three point bending

3.3 Static mechanical tests

Two types of static mechanical tests where performed on the nanocomposites manufactured: tensile tests and flexural tests.

3.3.1 Tensile tests

Tensile tests were performed with a universal testing machine Instron 4467 (figure 3.7) following the ASTM D 638 – 03 standard test method for tensile properties of plastics. This test method covers the determination of the tensile properties, such as strain at break, tensile strength, and Young's modulus, of plastics.

The specimens produced are dog-bone shape (figure 3.11). The thickness is 3.175 mm (1/8 inch, which is the thickness of the casting mold), and the width of the narrow section is 12.7 mm (0.5 inch). To facilitate the removal from the casting mold, a draft of 2º angle is present. The specimen are placed in tensile clamps (figure 3.12), and was pulled with a rate of 5 mm/min.

Load extension data are collected and the strain at break (mm/mm), tensile strength (MPa), yield point (MPa), and the Young's modulus (MPa) are calculated.

Figure 3.11: dog-bone specimens for tensile tests

Figure 3.12: clamps with dog-bone specimen for tensile tests

3.3.2 Flexural tests

Flexural tests were carried out in a universal testing machine Instron 4467 following the ASTM D 790 – 03 standard test methods for flexural properties of unreinforced and reinforced plastics. This test method utilizes a three point bending system (figure 3.13) applied to a simply supported beam. The procedure used provides the measurement of the flexural modulus of plastic materials.

The test specimens are rectangular bars 3.175 mm (1/8 inch) thick and 12.7 mm (0.5 inch) wide (figure 3.14). The specimens are casted in a metal mold. To facilitate the removal from the casting mold, a draft of 2º angle is present. The loading rate is calculated accordingly to the dimension of the specimen (the thickness slightly varies from specimen to specimen), with the following formulae:

$$R = 0.01 L^2 / 6d$$

where R is the rate in mm/min, L is the span (mm), and d is the depth (thickness) of the beam (mm).

With these tests it is possible to calculate Tangent flexural modulus of elasticity, flexural strength and strain at the maximum load, after plotting load versus displacement. The tangent flexural modulus of elasticity E_B is the ratio, within the elastic limit, of stress to corresponding strain. The modulus of elasticity calculated with flexural tests, differs from the one calculated by tensile testing, since in bending a portion of the sample is compressed and one is stretched. The modulus of elasticity so calculated takes into consideration both phenomena of compression and elongation. The flexural strength is the stress corresponding to the point at which the load stress does not increase with an increase of strain. The strain at this condition is calculated in this dissertation and it is called "flexural strain at peak load". To compute these properties the following formulae are used:

$$\sigma_f = \frac{3PL}{2bd^2}$$

$$\varepsilon_f = \frac{6Dd}{L^2}$$

$$E_B = \frac{L^3 m}{4bd^3}$$

where σ_f is the flexural stress, P the load, b the width, d the depth (thickness), ε_f the flexural strain, D the maximum deflection at the center of the beam, L the supporting span, E_B the modulus of elasticity in bending (flexural modulus of elasticity), and m is the slope of the elastic portion of the load-deflection curve.

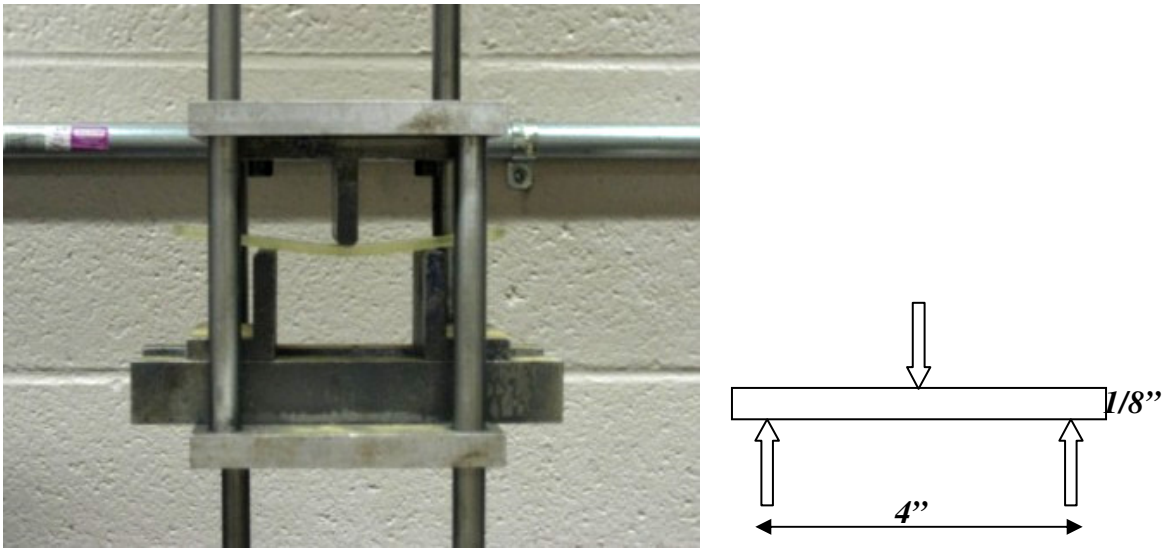

Figure 3.13: three point bending fixture with specimen for flexural tests

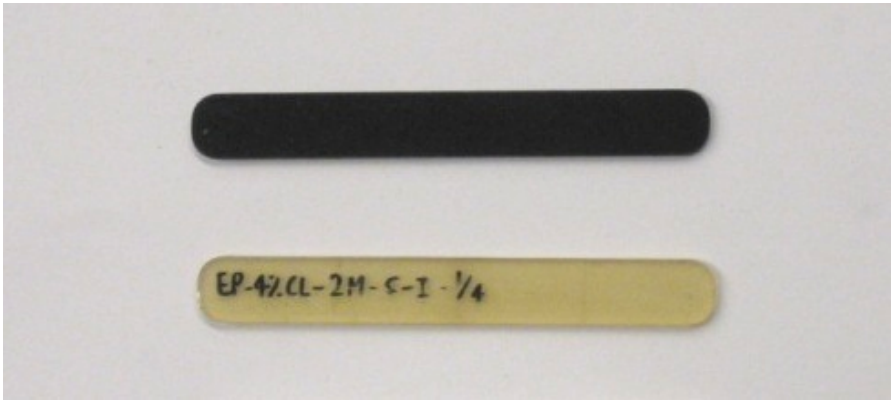

Figure 3.14: rectangular bar shaped specimens for flexural tests

3.4 Flammability tests

Flammability tests were carried out in a cone calorimeter from Fire Testing Technology (figure 3.15). The cone calorimeter tests allow determining the Heat Release Rate (HRR) and other fire-test-response characteristics. The samples used were squared tiles of 100 mm of sides and 5 mm of thickness (figure 3.4).

The cone calorimeter is a fire test instrument based on the principle of oxygen consumption calorimetry. This empirical principle is based on the observation that, generally, the net heat of combustion of any organic material is directly related to the amount of oxygen required for combustion. Approximately 13.1 MJ of heat are released per kilogram of oxygen consumed[4].

The cone calorimeter is a very sophisticated machine as depicted in figure 3.16. The sample is placed under a cone heater (figure 3.17), which heats the sample up at a constant heat flux (for the experiments made equal to 50 kW/m^2), before a spark igniter placed 13 mm above the sample, produce ignition. Different sensors calculate temperature, pressure, heat released, smoke produced, and, through a load cell, mass loss. The gas stream containing the combined combustion products is captured through an exhaust duct system. The air flow rate used is 24 l/s. Oxygen concentration in the exhaust stream is measured with an oxygen analyzer, and the heat release rate is determined by comparing the oxygen concentration with the value obtained when no sample is burning. Smoke obscuration measurements are made in the exhaust duct by a helium-neon laser, with silicon photodiodes as main beam and reference detectors. All data are collected with a PC, which records data continuously at fixed intervals of a few seconds while a test is being conducted[4]. The cone calorimeter can measure the Peak and Mean of HRR, the Peak and Mean of Mass Loss Rate (MLR), the Total Smoke Production, the Total Heat Released, the

time of ignition, the time to flameout, and the time were the Peak of HRR and MLR occurs, as well as many other interesting properties.

The calibration of the cone calorimeter is a very delicate and long process and consist in setting the duct flow to 24 l/s, calibrating the smoke (laser) system, calibrating the gas analyzer, imposing the value of oxygen at normal condition to 20.95%, and zeroing the oxygen using a flow of pure nitrogen, setting the heat flux to 50 kW/m^2 using a heat flux meter, and calibrating the load cell. Moreover, a factor called C-factor is calculated burning methane. The C-factor gives information about the correct functioning of the machine and if there are gas leaks along the lines.

Figure 3.15: cone calorimeter from FTT

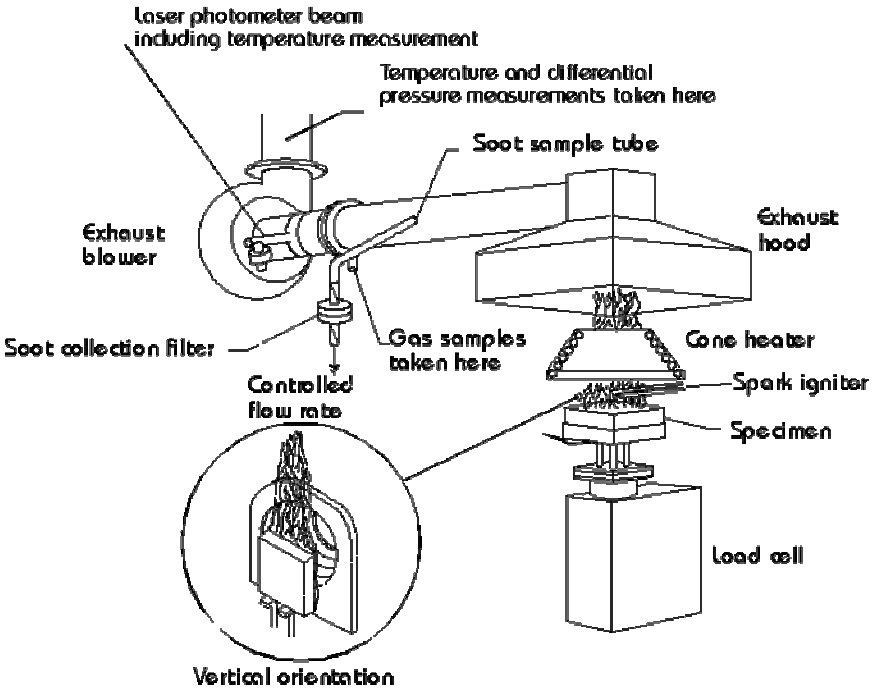

Figure 3.16: schematic of the various components constituting a cone calorimeter[5]

Figure 3.17: cone heater of the FTT cone calorimeter used

[1] www.nanocor.com
[2] ASTM D 256 – 06
[3] ASTME D 5045 – 99
[4] Fire Protection Engineering - Worcester Polytechnic Institute
[5] www.doctorfire.com/cone

Chapter 4

Tests results

4.1 Introduction

Tests on nanoclay-epoxy, carbon nanofibers-epoxy, and nanocomposites produced with both nanoclay and carbon nanofibers mixed together in epoxy are discussed here. Several tests were performed: tensile, impact, three point bending, fracture toughness and flammability. With these tests it was possible to evaluate the following properties:

- Mechanical static properties: Young's modulus, strain at break and at peak load, tensile strength, yield stress, flexural modulus, flexural strength and flexural strain at peak or break
- Fracture properties: impact strength and fracture toughness properties (stress intensity factor and critical energy release rate)
- Flammability properties: peak and mean of Heat Release Rate, time of ignition, time at peak of heat release rate, time to flameout, total smoke produced, peak and mean of mass loss rate, and total heat released

It is shown that the properties do not depend only on the type and quantity of the reinforcement. Tests ran previously on the same materials and with the same overall procedure of the ones presented here, which are not reported for sake of brevity, demonstrated that thermal cycling (such as post curing), degassing and type of mixing procedure affect greatly the properties of the polymer nanocomposites and change the results up to an order of magnitude. The procedure to produce the nanocomposites (chapter 3) was decided after a trial error type of analysis, considering the properties of the material from the same tests that are here presented.

4.2 Properties of epoxy-clay nanocomposites

As largely discussed in the literature review of chapter 2, nanoclay nanocomposites show overall better properties that the pure resin, but the changes are often modest. Nanoclays increase stiffness and mechanical resistance, but often diminish toughness, since the final nanocomposite is more brittle that the constituent pure resin. Nanoclays have beneficial effect on the flame resistance, but sometimes the effects can be very small, and it is not uncommon to have worse flame retardation. It is still unclear if the beneficial effects justify the use of nanoclays, even if their cost is low and it is going down further with time. Better dispersion creates bigger improvements, thus investigations to produce a more even dispersion and exfoliation can be the key to understand the usefulness of nanoclay nanocomposites.

4.2.1 Fracture tests on epoxy-clay nanocomposites

Fracture tests on nanoclay-epoxy nanocomposites show that the addition of nanoclays lowers the Izod impact strength and in general lowers the fracture toughness.

4.2.1.1 Impact tests on epoxy-clay nanocomposites

Impact tests on epoxy-clay nanocomposites show significant reduction of impact strength with the addition of nanoclays. Also the quantity of clays determines the magnitude of the reduction, i.e. the higher is the weight content of nanoclays the lower is the impact strength (figure 4.1). The impact strength calculated is the net value, which means that the energy to toss the broken part of the sample was subtracted from the value recorded during testing. This procedure is advisable for brittle materials. The fracture surface of the sample, which is flat and smooth, and the low value, around 0.45 kJ/m^2 for pure epoxy, suggests that the behavior of the materials is brittle. For 6% weight content of nanoclay, the net Izod impact strength is half of the

value for pure epoxy, which means that the addition of nanoclay produces drastic reduction of impact strength. This can be explained through the observation that the introduction of nanoparticles is usually coupled with the introduction of bubble and voids, which creates a path for crack propagation. Also the epoxy polymer chains tend to be entangled around the nanoclays, producing a more brittle material.

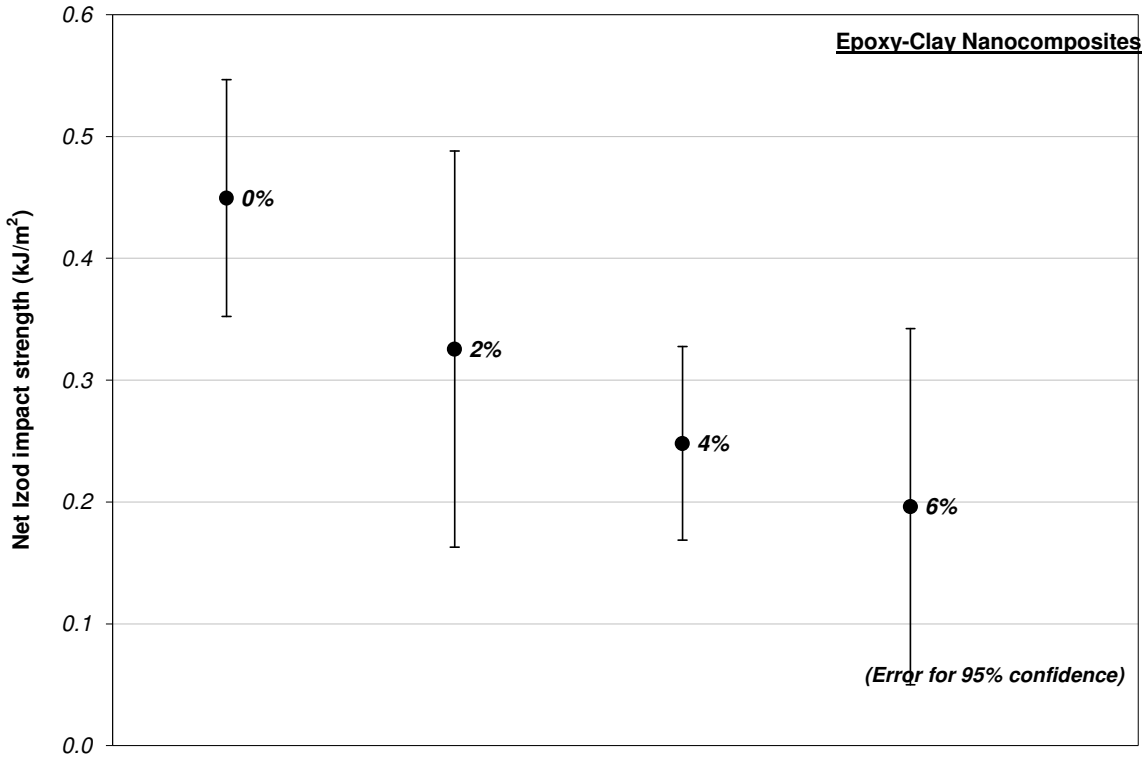

Figure 4.1: net Izod impact strength for epoxy-clay nanocomposites

4.2.1.2 Fracture toughness tests on epoxy-clay nanocomposites

Fracture toughness tests are static, while Izod impact tests are dynamic. With these tests it is possible to understand the stress and energy required to propagate a pre-made crack into the material. Results show that the addition of nanoclays has a negative effect on the fracture properties of epoxy. The stress intensity factor K_{IC} diminishes with addition of nanoclay and it is proportional to the quantity of nanoparticles added (Fig. 4.2). The critical energy release rate G_{IC}

also diminishes proportionally with addition of nanoclays (Fig. 4.3). The values of both K_{IC} and G_{IC} are low and typical for a brittle material. The correlation between K_{IC} and G_{IC} is expressed in equation (4.1) for linear behavior of crack propagation:

$$G_{IC} = \frac{K_{IC}^2}{E} \tag{4.1}$$

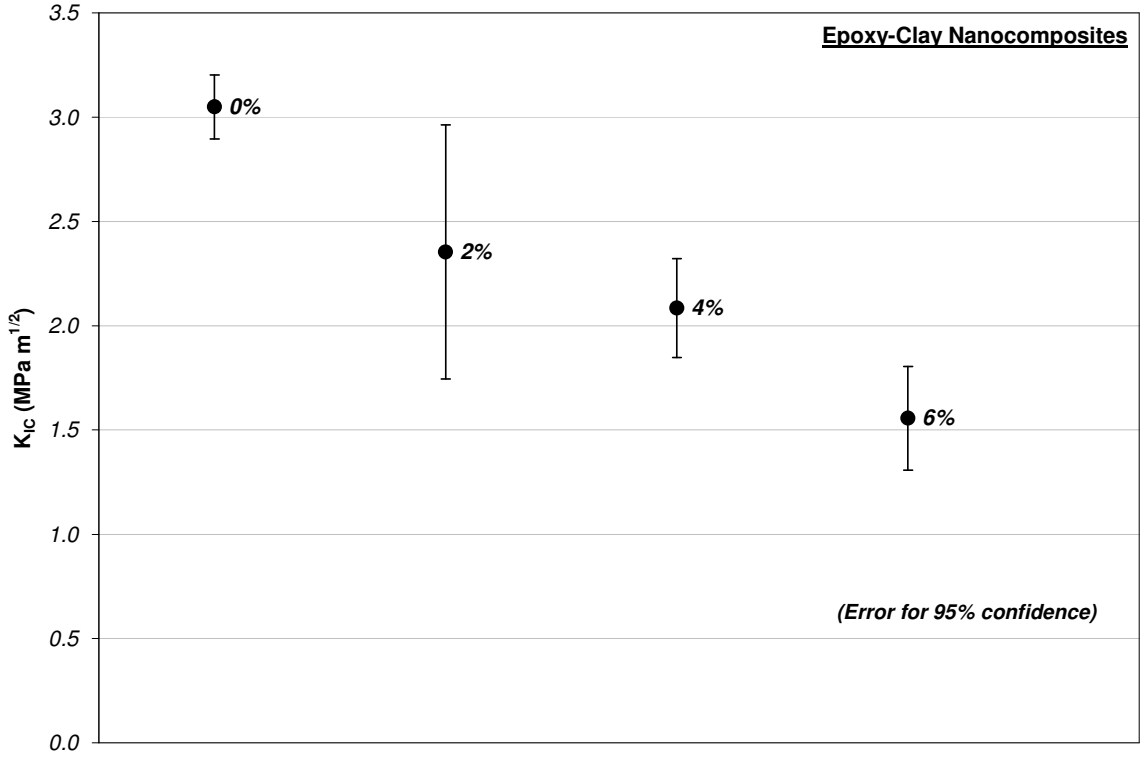

Figure 4.2: stress intensity factor for epoxy-clay nanocomposites

G_{IC} represents the energy required to have unstable crack propagation and it can be calculated either with equation (4.1) or calculating the area under the stress-strain curve for fracture toughness tests on SENB specimens. The more drastic drop of G_{IC} with respect to the drop of stress intensity factor suggests that the material is stiffer with addition of nanoclays and thus less energy is employed to deform the material. The deflection is in fact smaller with addition of nanoclays and thus the area under the stress-strain curve is smaller. This can be also

explained considering the effect of the Young's modulus E in equation (4.1). The Young's modulus is bigger with addition of clays (as it will be shown in section 4.2.2) and thus less energy is employed to bend the nanocomposites specimen with respect to the pure resin specimen. The shape of the stress strain curve generated by these tests show a linear fracture behavior, with brittle type of failure.

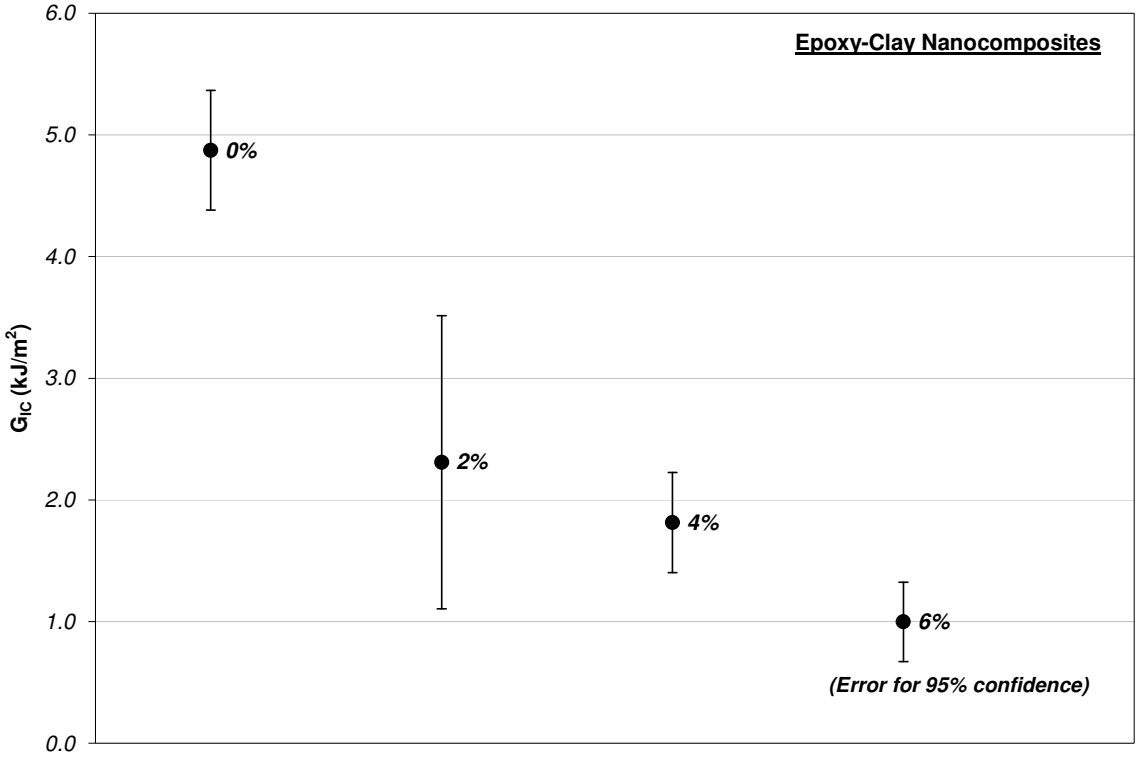

Figure 4.3; critical energy release rate for epoxy-clay nanocomposites

It is interesting to observe the similarities between the impact strength and the energy release rate plots. The plots are however slightly different because in the impact tests part of the energy is converted in vibrations and it is transmitted and absorbed by elements constituting the surrounding mounting and equipment elements. Also the values of impact strength and energy release rate are one order of magnitude different, with the impact strength smaller than the energy release rate. For this reason it is important to have both information when we test a

material at fracture. The Izod test is in fact a dynamic test and can give different information than fracture toughness tests. If instead of nanoclays the reinforcements were for instance rubber micro-spheres, their capacity of energy absorption will generate impact values and energy release rates values with completely different trend. For our case anyway the trends are similar, because the samples are brittle and no significant portion of energy in the impact tests is absorbed by the material itself.

4.2.2 Static mechanical tests on epoxy-clay nanocomposites

Static mechanical tests on epoxy nanoclay nanocomposites show that nanoclays are beneficial in terms of adding stiffness and ultimate strength, although the effect is often modest.

4.2.2.1 Tensile tests on epoxy-clay nanocomposites

Tensile tests performed on clay-epoxy nanocomposites reveal that the mechanical behavior of the nanocomposite with respect to the pure epoxy is considerably different. Yield is observed only for pure resin, while a less ductile behavior is observed for the nanocomposites (Fig. 4.4). The strain at break is reduced proportionally with the amount of nanoclays as observed in figure 4.4, where a representative sample for each mixture ratio is plotted, and in figure 4.5. The error in figure 4.5 is big, but a pattern is easily recognizable, showing lower strain for higher quantity of clay. For epoxy-nanoclay nanocomposites, the strain at break is approximately 35% lower for 6% weight content of nanoclays, and about 20% lower for 2% and 4% weight content of nanoclays. This diminishment can be acceptable if it is compensated by a higher tensile strength and Young's modulus.

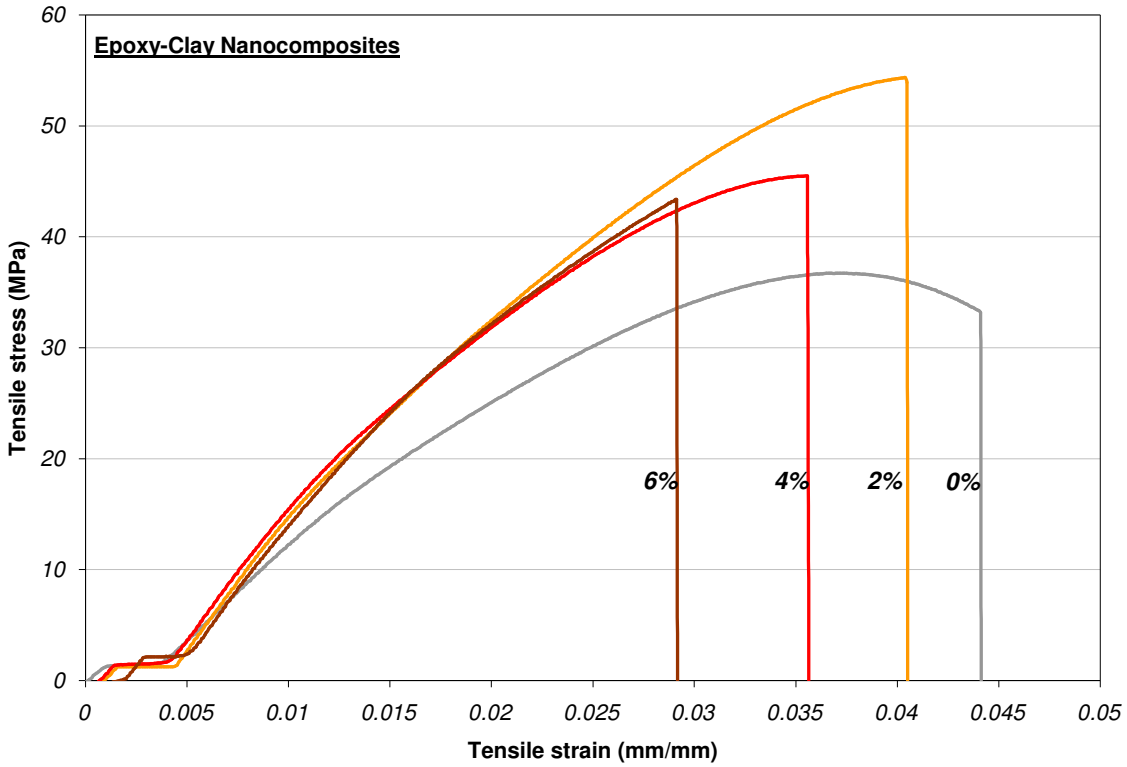

Figure 4.4: tensile tests plot for epoxy-clay nanocomposites

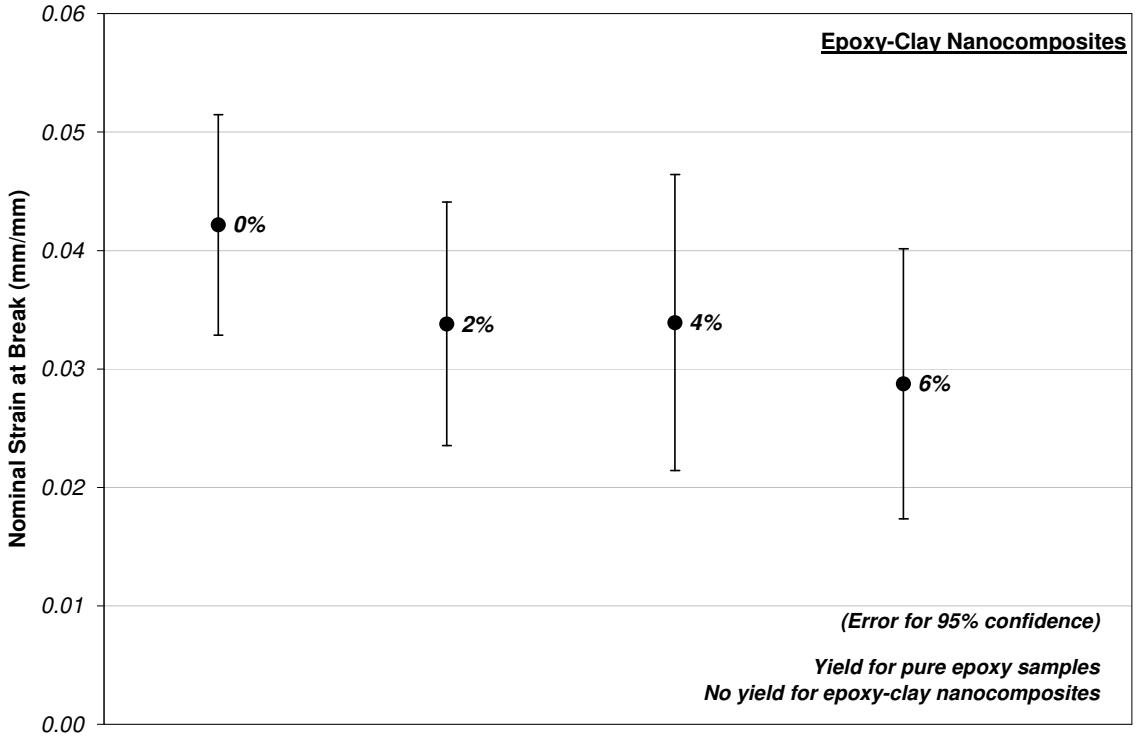

Figure 4.5: strain at break for epoxy-clay nanocomposites

Figure 4.6 shows the tensile strength. The addition of nanoclays improves the tensile strength only for percentage near 2% in weight with 23% increase. For higher percentages the properties degrade and reach the same level of the pure epoxy. This suggests that the dispersion for 2% is more even and produces major change in the properties of the resin. Perhaps a certain level of exfoliation was reached. Higher quantities of nanoclays are more difficult to disperse and the benefit in terms of tensile strength is annihilated by premature failure due to crack formation around clusters of nanoparticles. This brings the resistance of the material back to the level of pure epoxy. A different effect is observed for the Young's modulus (Fig. 4.7). All percentages of nanoparticles bring an increase in the Young's modulus of about 25%. The increase is not proportional to the amount of clay added.

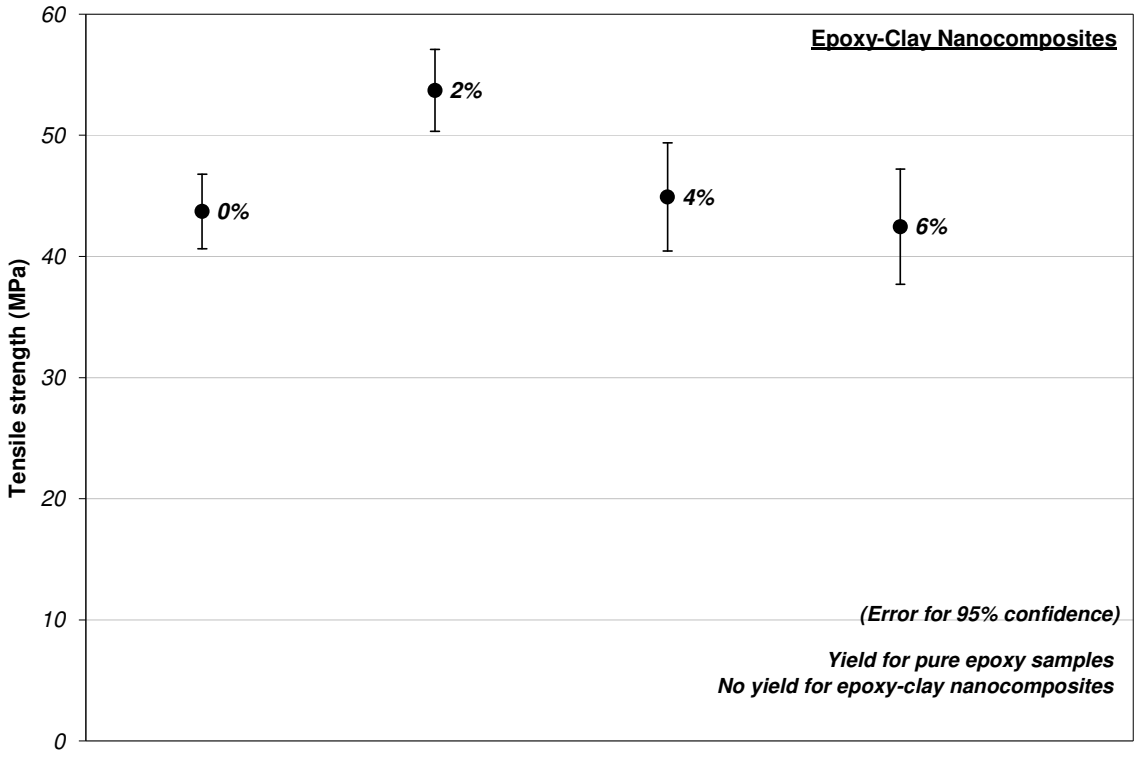

Figure 4.6: tensile strength for epoxy-clay nanocomposites

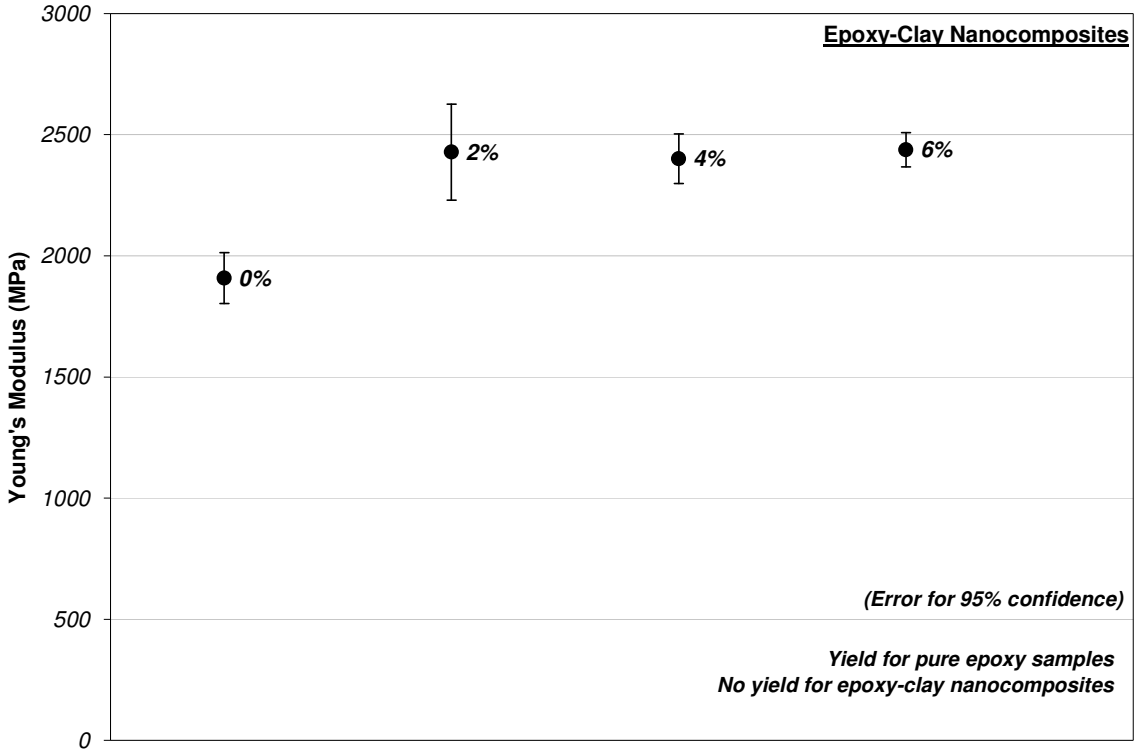

Figure 4.7: Young's modulus of epoxy-clay nanocomposites

Therefore, the tensile tests show that 2% of nanoclay seem to be an optimal weight percentage to disperse in epoxy because of increase in Young's modulus and tensile strength and only a 20% decrease in extension at break. If we estimate the area under the tensile plots in figure 4.4, which represents the "toughness" of a material, it is evident that 2% of nanoclay produces a bigger area thus a higher toughness. Also, the smaller extension at break translates in dimensional stability, since, if we compare 2% clay nanocomposite and pure epoxy, with the same load, epoxy tents to deform more than the 2% nanocomposites.

4.2.2.2 Flexural tests on epoxy-clay nanocomposites

The addition of nanoclay particles into epoxy resin produces higher flexural modulus and higher flexural strength. However the maximum deflection for nanocomposites is lower than pure resin, with little difference between the different percentages. Figure 4.8 shows 4 representative plots for different percentages in weight of clay reinforcement.

The highest flexural strength is again for 2% clay nanocomposite, with no change for 4% and 6% with respect the pure resin, like it was for the tensile tests (Fig. 4.9). The increase in flexural strength is modest (only 15%), but the maximum deflection of the nanocomposites is 50% of the one of pure epoxy and it is not proportional to the percentage in weight of the nanoparticles (Fig. 4.10).

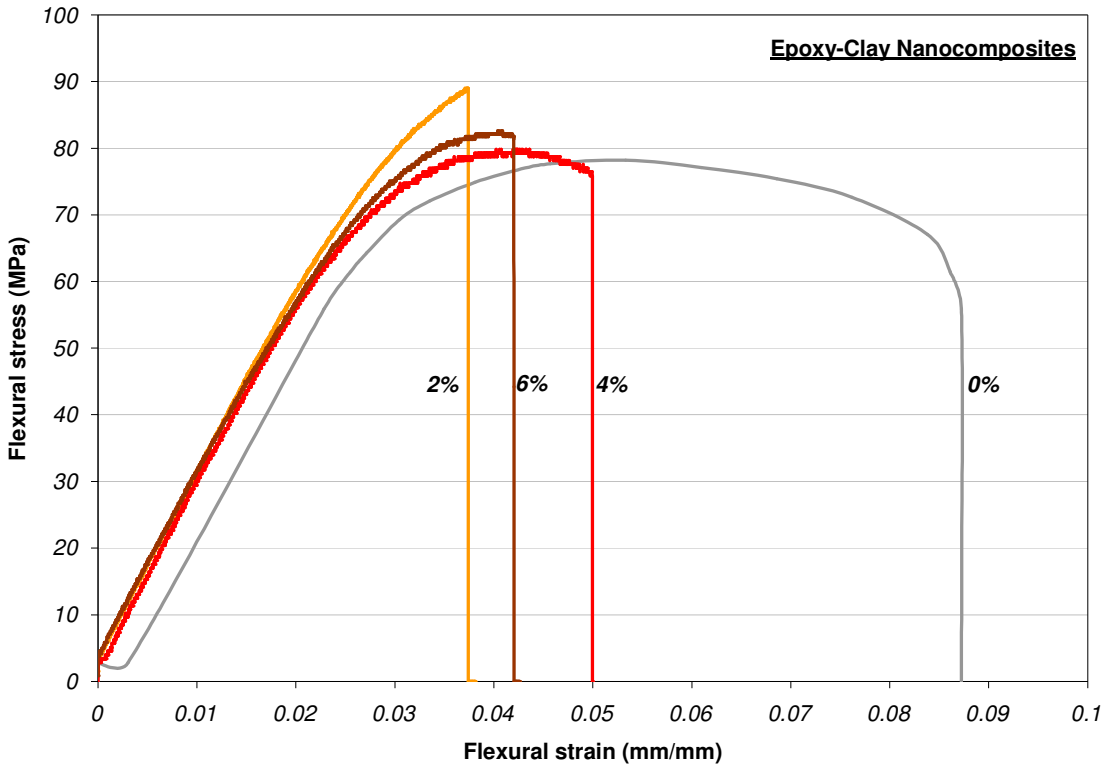

Figure 4.8: flexural tests plot for epoxy clay nanocomposites

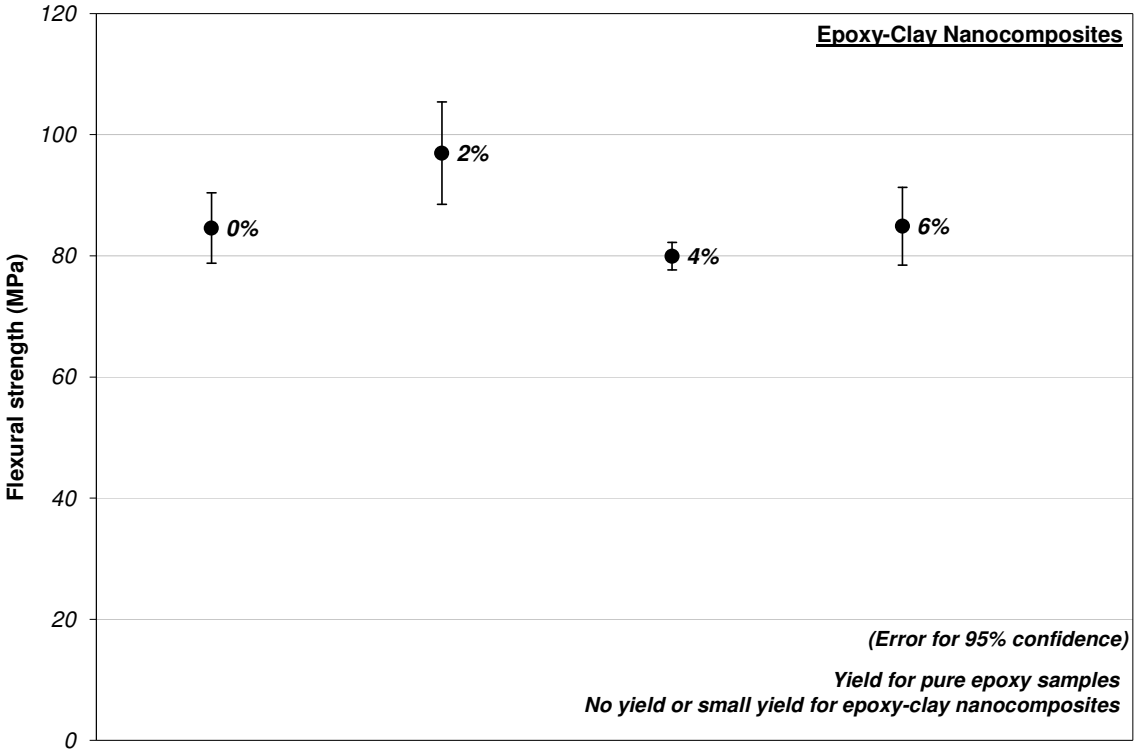

Figure 4.9: flexural strength of epoxy nanoclay nanocomposites

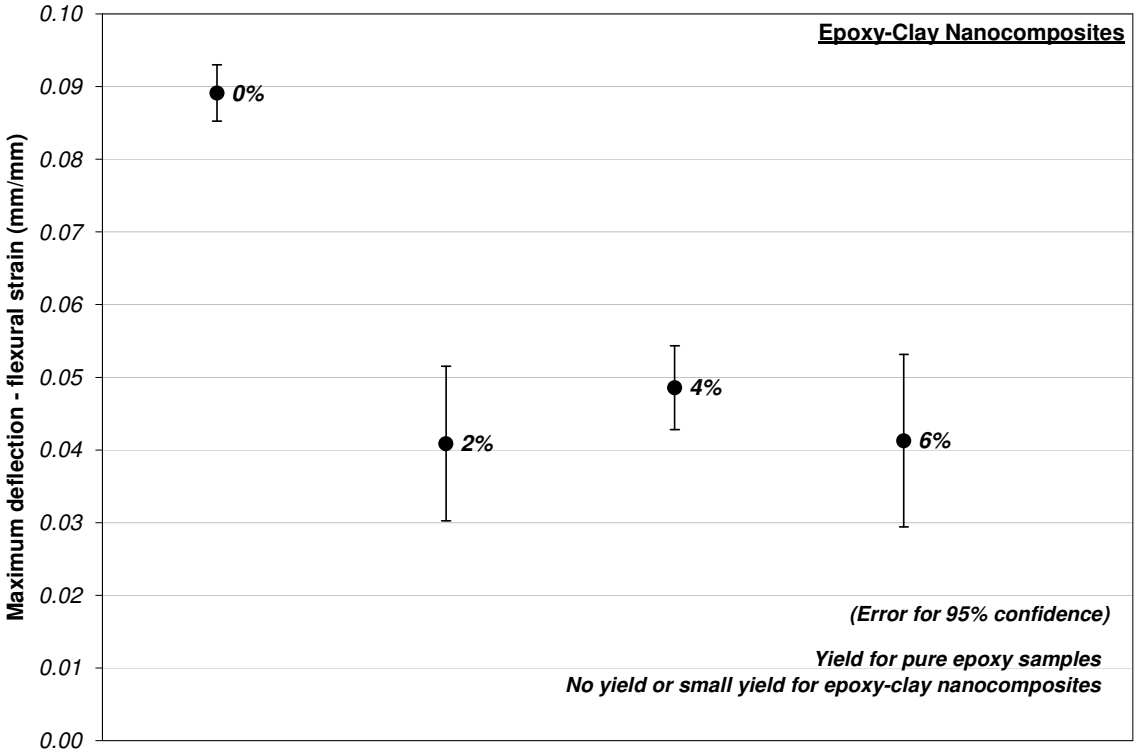

Figure 4.10: deflection (strain) at flexural peak load for epoxy-clay nanocomposites

The modulus of elasticity in bending, or flexural modulus, is slightly higher for 2% clay nanocomposite, but the difference is very small in the order of 15% increase (Fig. 4.11).

After testing, it was possible to observe that nanoclays don't improve considerably the flexural properties of epoxy, and even if the flexural modulus and the flexural strength are slightly higher for 2% clay nanocomposites, this gain does not justify the loss in toughness due to the diminishment of maximum deflection before failure. The static mechanical properties of epoxy-clay nanocomposites improve slightly for tensile characteristics and for 2% of nanoclay, but they get worse in bending for every percentage of clay. 2% seem to behave differently from other percentages, suggesting that the dispersion reached is more effective. 4% and 6% amount of clay do not bring any improvement in static mechanical properties and thus their employment is not worthwhile.

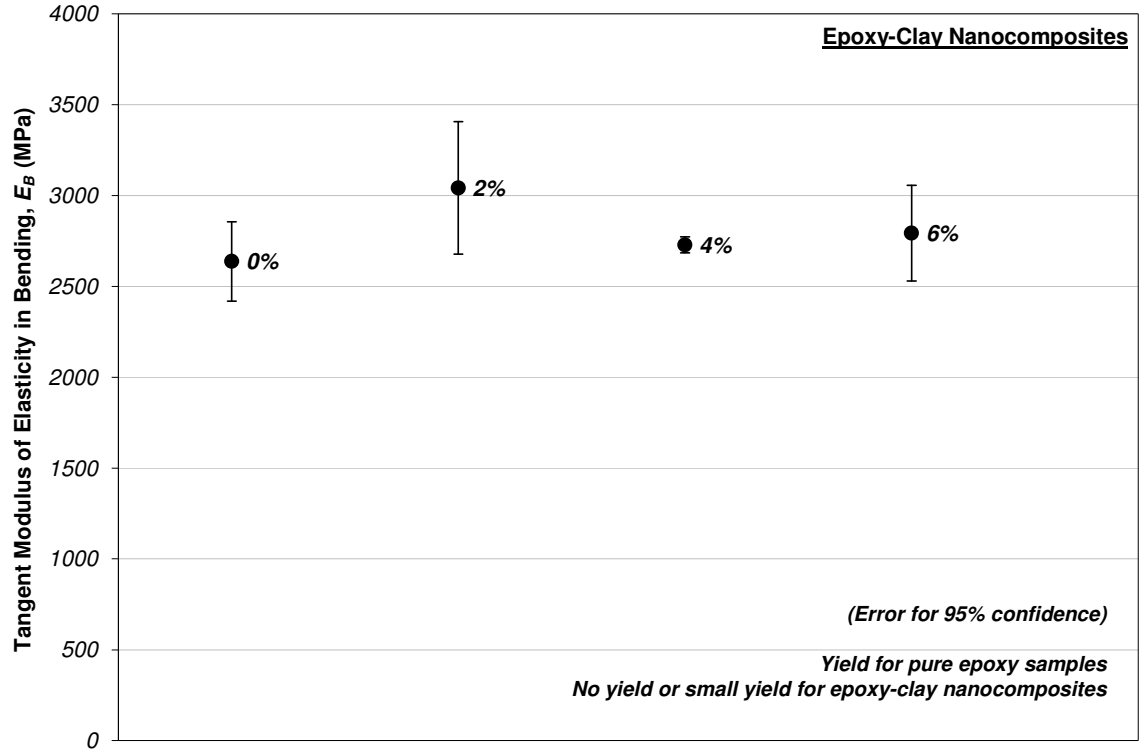

Figure 4.11: flexural modulus for epoxy clay nanocomposites

4.2.3 Flammability tests on epoxy-clay nanocomposites

It is proved that nanoclays have flame retardation characteristics. Nanoclay nanocomposites in general show improvements in terms of many flammability properties when compared to the pure matrix system, as mentioned in the literature review. The tests made for this dissertation confirm the positive effects of nanoclays when mixed with epoxy for flame retardation, even if the effect is limited for the weight percentages of clay used here. The tests were run with 50 kW/m^2 of heat flux. For 6% weight content of nanoclays the flame behavior shows the biggest improvement and we believe that for higher loading of nanoclays the effect will be more visible. All tests conditions are for samples 5 mm thick (refer to chapter 3).

The trend for HRR of epoxy with 6%wt of clay is shown in figure 4.12. The HRR increases drastically within 100 seconds from ignition and then stabilizes for other 100 seconds, after which it increases again to reach its maximum (Peak of HRR). After reaching the peak the HRR decreases and it maintains a low value until extinction, which is after about 800 seconds from the ignition. The HRR for pristine epoxy and for other weight content of nanoclays in epoxy have a similar trend, with different values. A more accurate analysis of all the values for all different clays weight percentages will follow. The values of HRR change along with thickness of the sample (higher thickness – lower PHRR), so the values of figure 4.12 should be considered only qualitatively, since all values will be standardized for a 5 mm thick sample.

In figure 4.13 the Peak of Heat Release Rate (PHRR) and the Mean of Heat Release Rate (MHRR) is plotted for different weight percentages of nanoclays. The PHRR decreases proportionally with addition of nanoclays. With 6% weight content of nanoclays the reduction is 30% with respect to the pristine epoxy. A lower PHRR is important because a high HRR can create ignition of neighboring elements and thus catastrophic effects. Moreover a more uniform

burning is easier to control and a fire is easier to extinguish when in real life it needs to be tamed by personnel. The higher is the HRR, the greater is the distance that human beings can withstand and therefore the fire suppression intervention becomes less effective. The MHRR is similar for all percentages of nanoclays. However, for higher loading of nanoclays (6%), it starts to decrease. It is arguable that higher loading will decrease further the MHRR and this is confirmed by literature. The MHRR is directly connected to the total time of burning: a higher MHRR produces a faster burning. Therefore, nanoclays decrease the total time of burning, which is a negative effect, but the difference is negligible, since the difference of MHRR is small. Also for 6% the value of MHRR is close to the one of pure epoxy.

In figure 4.14 the Mass Loss Rate (MLR) is plotted for 6% weight content of nanoclays in epoxy. Other percentages of nanoclays behave similarly.

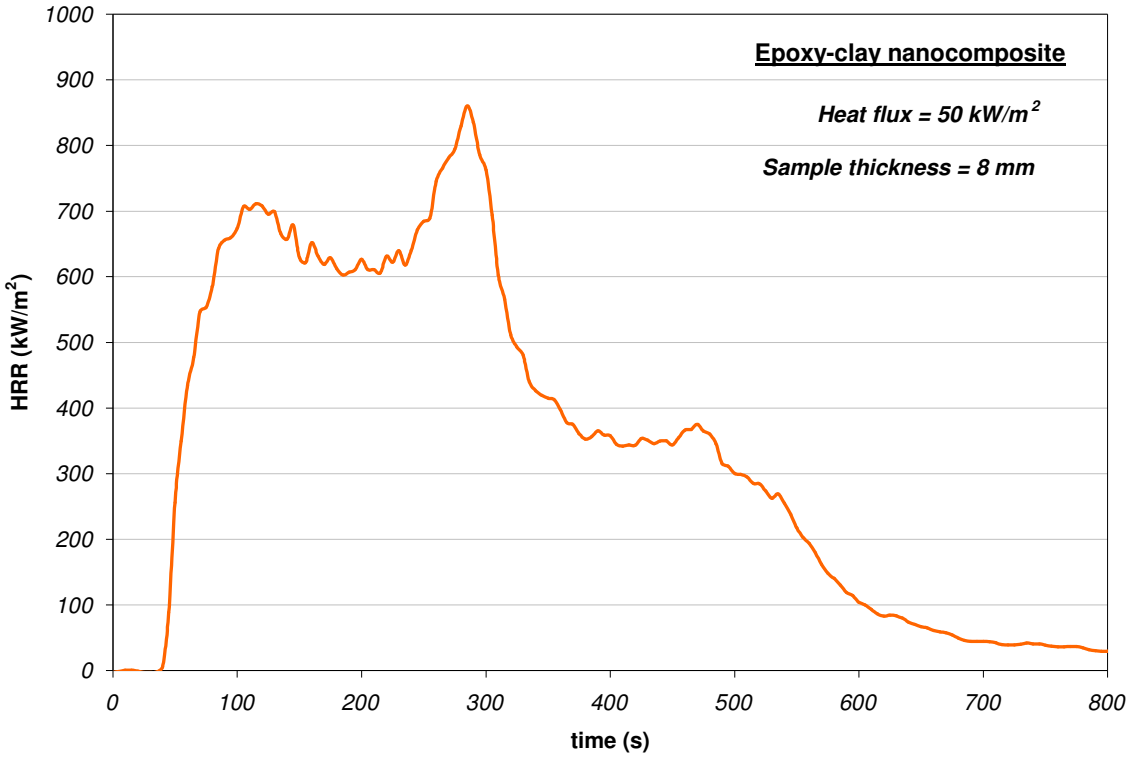

Figure 4.12: Heat Release Rate for 6% nanoclay-epoxy nanocomposite

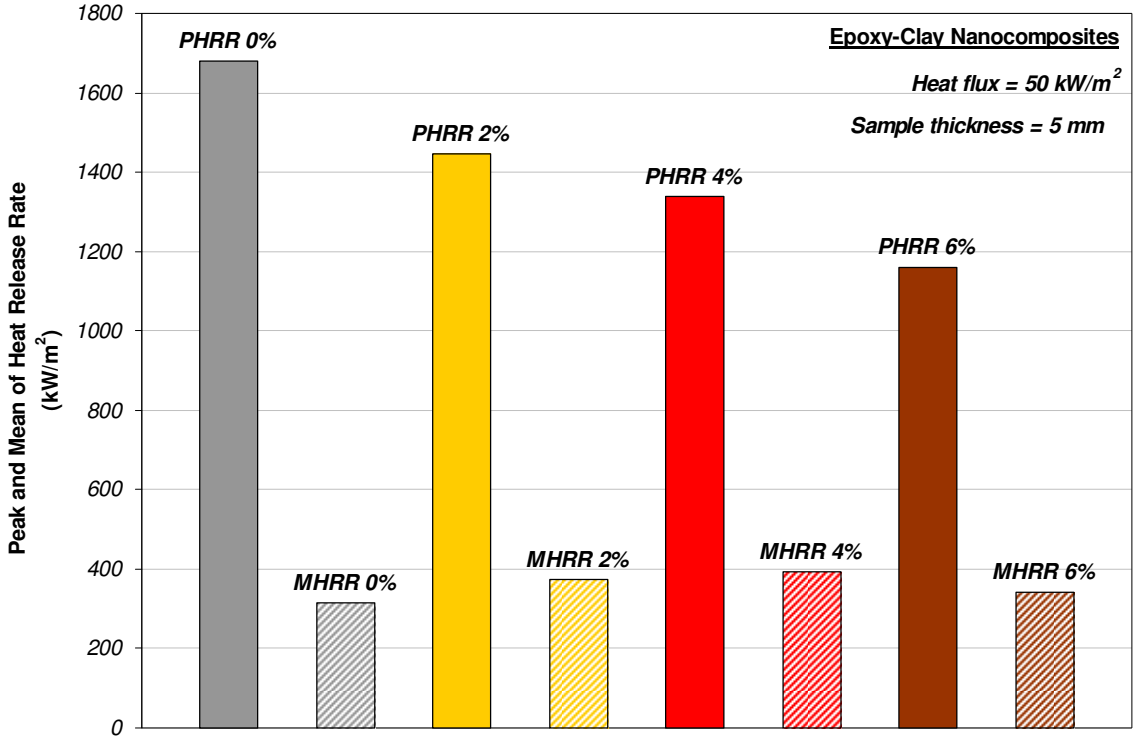

Figure 4.13: Peak and Mean of Heat Release Rate for epoxy-clay nanocomposites

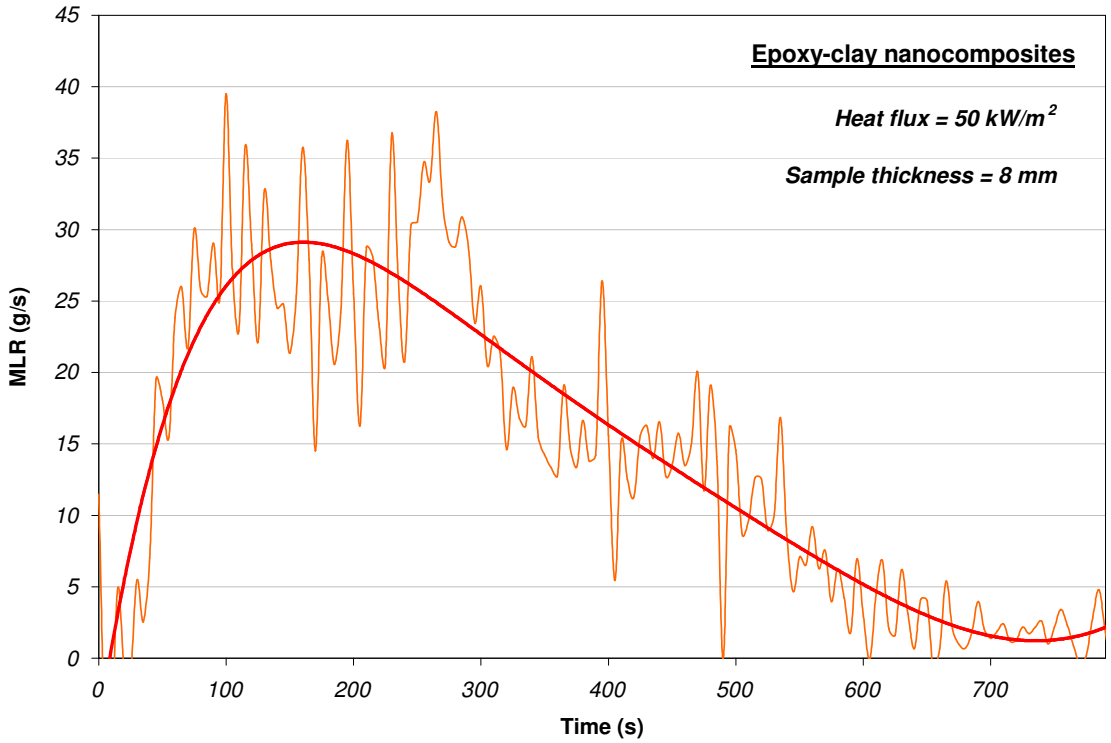

Figure 4.14: Mass Loss Rate for 6% nanoclay-epoxy nanocomposite

The MLR is a less precise measurement than the HRR, as it is evident from figure 4.14. For this reason the HRR is usually utilized, since the trend of HRR and MLR are similar. In figure 4.15 the Peak of Mass Loss Rate (PMLR) and the Mean of Mass Loss Rate (MMLR) are plotted. As expected the behavior is similar to the HRR, with the PMLR decreasing along with the clay content. The biggest reduction with respect to the pristine epoxy is observed for 6% weight content of clay. The MMLR is about the same for pure epoxy and with addition of 2% and 4% of nanoclays, and then it decreases again for higher clay loading (6%). The average MLR is about 0.12 g/s, which suggest that epoxy in general is highly flammable.

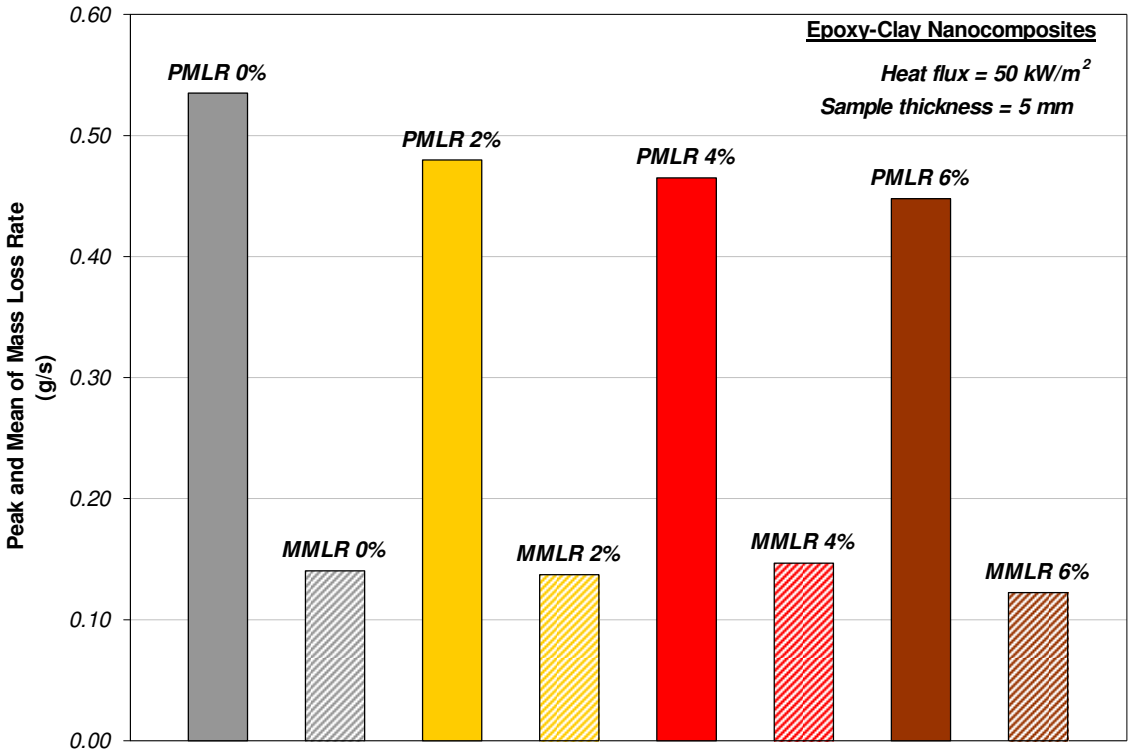

Figure 4.15: Peak and Mean of Mass Loss Rate for epoxy-clay nanocomposites

The time of burning is another important parameter for flammability tests. The three more representative times that can be recorded are the time to ignition, the time to PHRR, and the time to flameout. The time to ignition increases with addition of clays (figure 4.16). For 6% weight content of nanoclays the time to ignition is double that the one for pristine epoxy. This is a positive effect, since having a bigger ignition time means having less probability of elements catching of fire. If the detonation is in fact shorter than the time of ignition or if the element is exposed to ignition conditions for a time shorter than the ignition time, fire does not occur. The time to PHRR is bigger for clay nanocomposites than for pure resin. This is a positive factor too, since the PHRR is critical negative event and for epoxy-clay nanocomposites occurs later. The time to flameout is about the same for pure epoxy and for nanocomposites with 2% and 4% weight content of nanoclays. However, for 6% weight content of nanoclays the time to flameout is larger (as expected observing the plot for the HRR), meaning that epoxy takes more time to burn out if 6% clays are present. The time to ignition is in the order of 15-30 seconds, PHRR occurs 100-160 seconds after ignition and 5 mm thick samples burn out usually in 400-500 seconds.

Figure 4.17 shows the total smoke and heat produced during burning. The total smoke produced is important because it gives information about the toxicity of the burning process. The value is about the same for all percentages of nanoclays and for the pure epoxy, meaning that not significant reduction or increase of smoke was observed. However the nanocomposites tent to liberate a small percentage of nanoclays during burning. This might be hazardous since the diameter of these particles is extremely small. Anyway most of the nanoclays are left in form of a solid char and only a tiny percentage was transported by the fumes. The total heat release is the same for all samples, suggesting that all resin was burned out

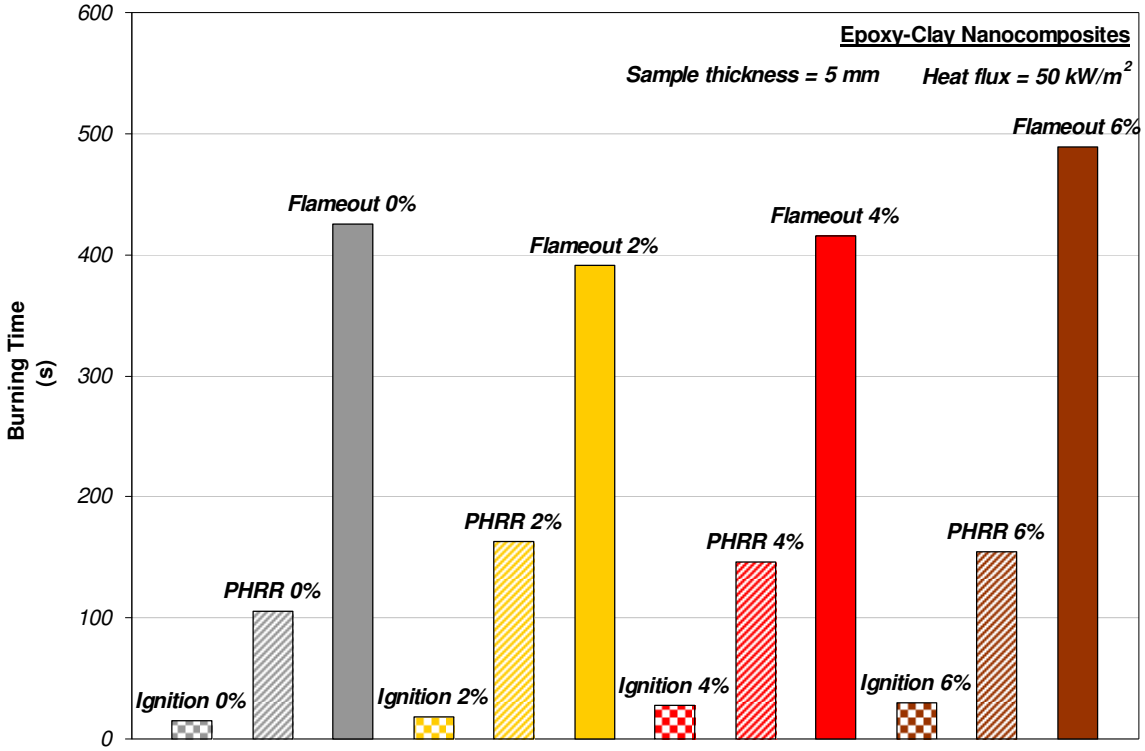

Figure 4.16: time to ignition, time to PHRR, and time to flameout for epoxy-clay nanocomposites

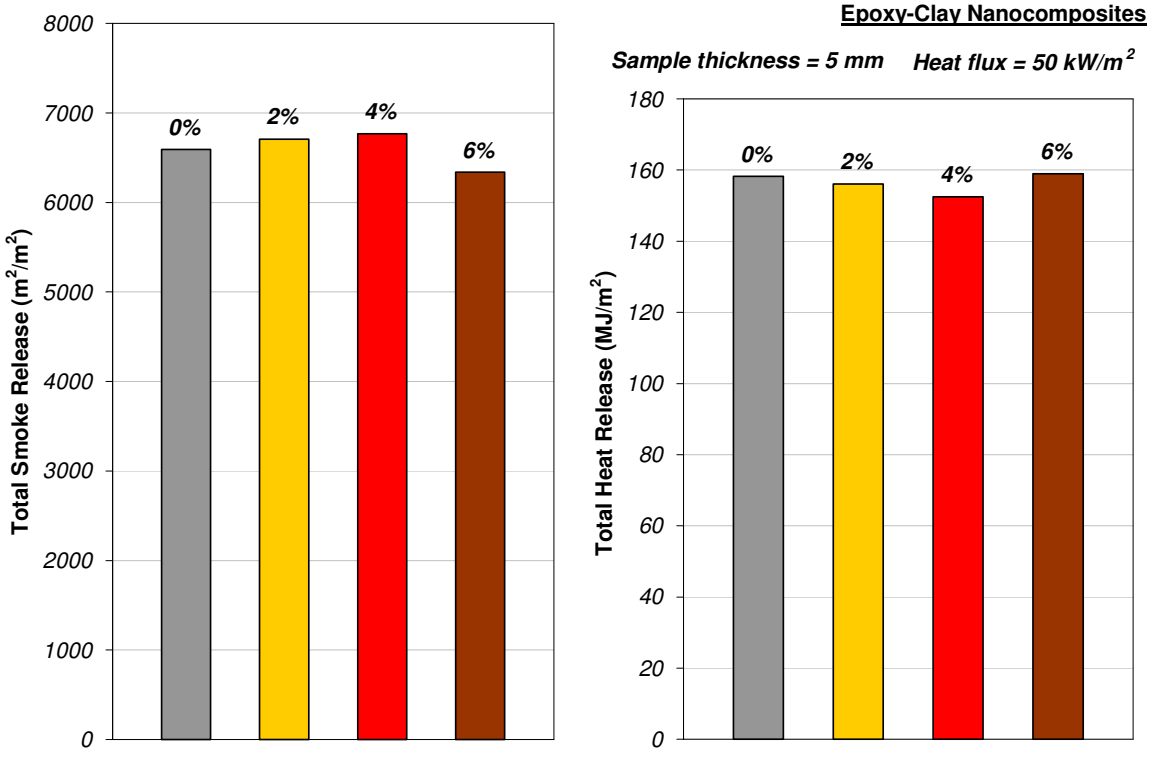

Figure 4.17: Total Smoke Release and Total Heat Release for epoxy-clay nanocomposites

4.3 Properties of epoxy-carbon nanofiber nanocomposites

In the literature review of chapter 2, it is shown that carbon nanofibers can visibly increase the overall mechanical properties of a polymer matrix. However, the strain at break diminishes when compared to clay nanocomposites and fracture properties gives more modest changes. The Young's modulus and tensile strength are higher for all percentages of carbon nanofibers tested. Also the flexural properties increase with addition of CNFs. Flammability properties improve after addition of carbon nanofibers, even if smoke and toxicity can become an issue. In general a polymer matrix with CNFs becomes more resistant and stiff with additional flame retardation properties. The use of such nanofibers seems completely justified, but the cost of carbon nanofibers is still too high to foresee an immediate commercial employment.

4.3.1 Fracture tests on epoxy-carbon nanofiber nanocomposites

Fracture tests on epoxy-carbon nanofibers nanocomposites show that the addition of CNFs in general produces lower fracture properties, even if the negative effect is less severe than for nanoclay reinforcements.

4.3.1.1 Impact tests on epoxy-carbon nanofiber nanocomposites

The net Izod impact strength is lower with addition of carbon nanofibers as depicted in figure 4.18. For these tests, as for epoxy-clay nanocomposites, the energy used for tossing the broken part of the sample was subtracted from the value recorded during testing. The behavior of the nanocomposite produced with CNFs is brittle as for pristine epoxy. The biggest reduction is observed for 1% weight content of CNFs, with Izod strength less than half of the one for pure epoxy. Less severe reduction is observed for 2% and 3% CNFs weight content, with impact strength of about 0.3 kJ/m^2.

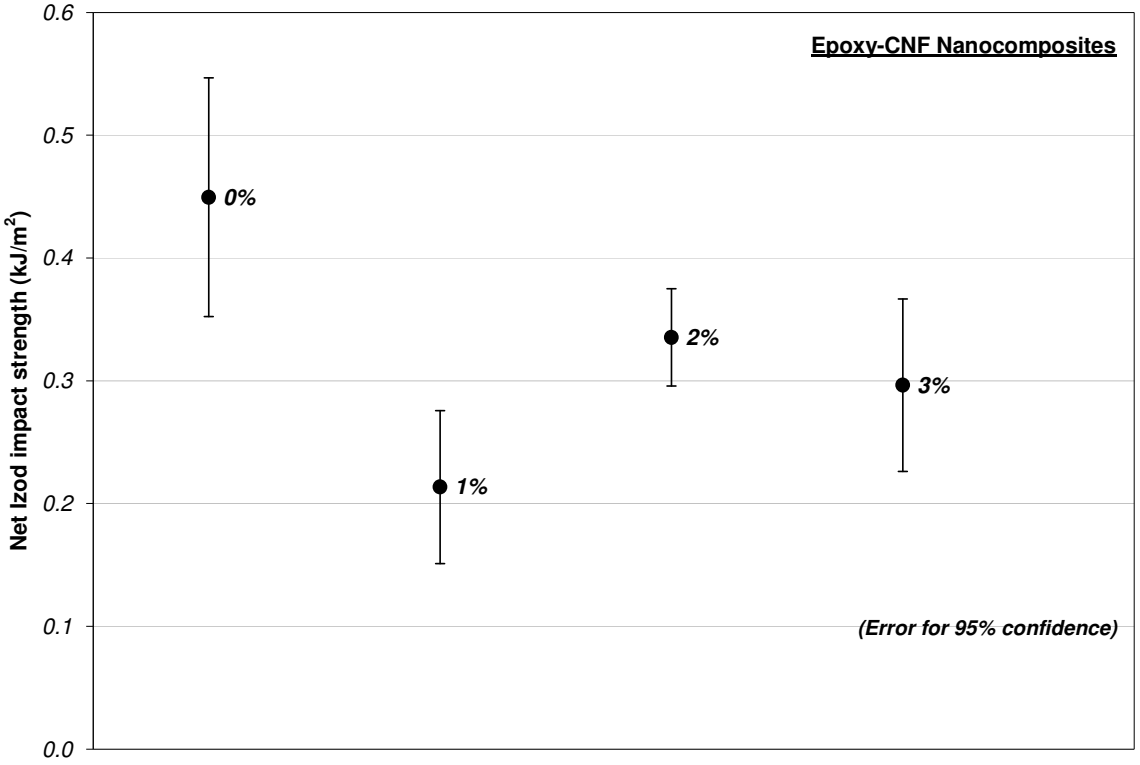

Figure 4.18: Izod impact strength on epoxy-carbon nanofiber nanocomposites

4.3.1.2 Fracture toughness tests on epoxy-carbon nanofiber nanocomposites

Fracture tests show that the addition of carbon nanofibers is beneficial in terms of stress intensity factor K_{IC} with addition of 2%wt of CNFs, but the energy release rate G_{IC} is lower for epoxy-CNF nanocomposites. The stress intensity factor is 10% higher for 2% weight content of CNFs as shown in figure 4.19, but it is lower for the other CNFs loading percentages. The trend for G_{IC} is different, due to the effect of the Young's modulus (see equation 4.1), which will be shown in the following section. As explained in section 4.2.1.2 the energy release rate represents the energy required to make a pre-made crack to propagate unstably. Part of this energy is used to deform the material (influence of the Young's modulus in equation 4.1 and displacement in the stress-strain curve for fracture toughness, which influences the area underneath the curve and thus the total energy used). The energy release rate is lower for all CNFs weight percentages than

for pure epoxy (figure 4.20). The trend is similar to the one for the Izod impact strength, like it was for epoxy-clay nanocomposites, but the values G_{IC} is one order of magnitude bigger.

Literature shows that CNFs usually improve the fracture properties. This was not observed here for epoxy-CNF nanocomposites. Higher weight percentages, like 3%, create clusters with voids during the mixing process that produce a preferred path for the crack. Lower weight percentages, like 1%, make only the material stiffer and more brittle, without a sufficient fiber loading to have the "crack stopping" effect observed in traditional advance composites. 2% seem to have more equilibrated behavior, with not too many voids produced in the mixing process and more fibers than for 1%. If the mixing procedure for high weight contents of CNFs is improved and the dispersion reaches the quality of 2% weight content, it is arguable that the fracture properties will improve further.

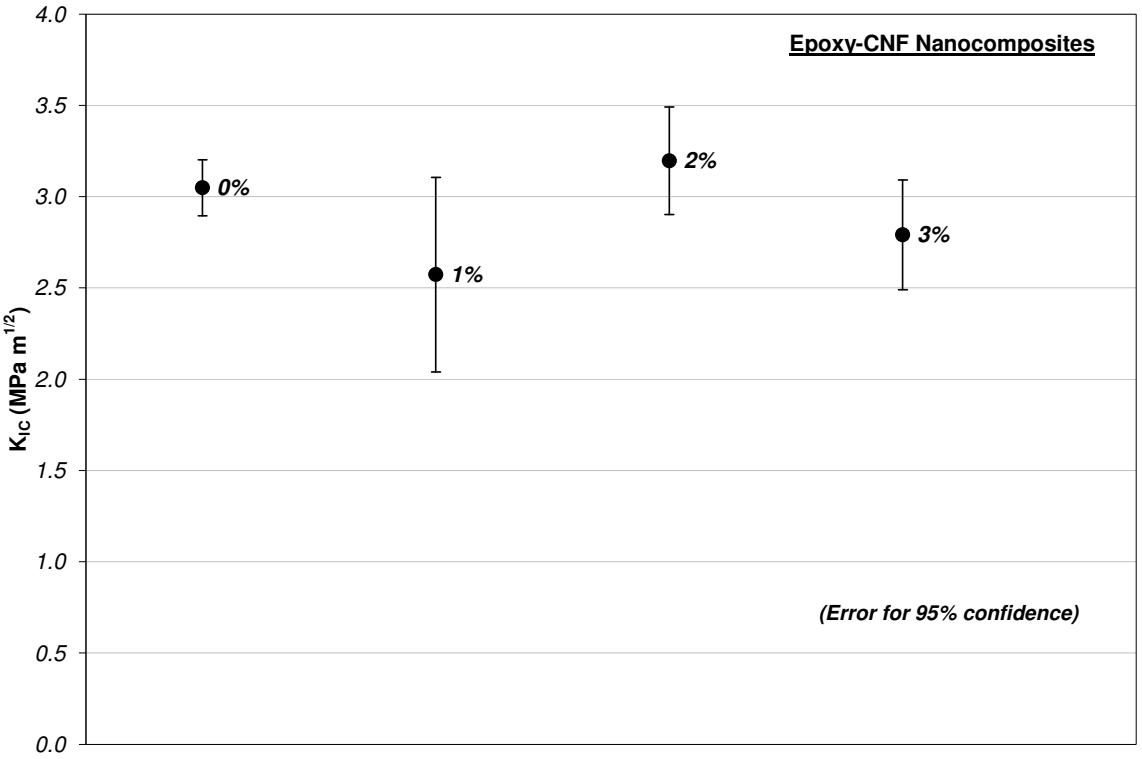

Figure 4.19: stress intensity factor for epoxy-carbon nanofiber nanocomposites

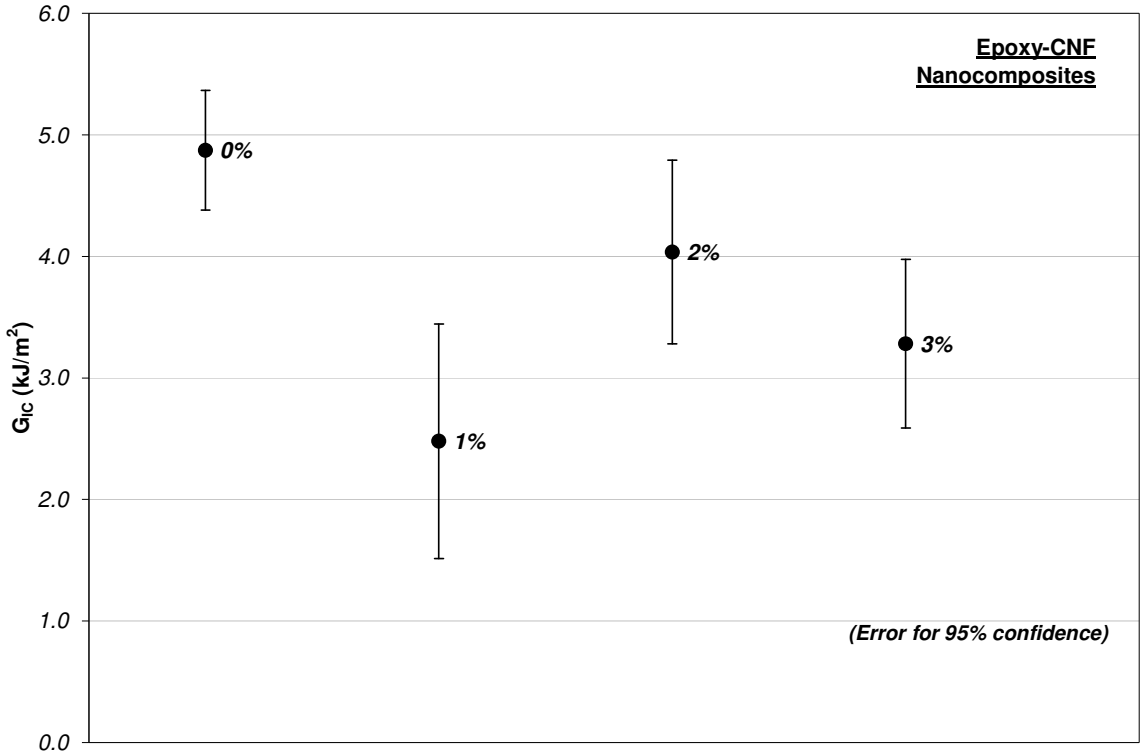

Figure 4.20: energy release rate for epoxy-carbon nanofiber nanocomposites

4.3.2 Static mechanical tests on epoxy-carbon nanofiber nanocomposites

Static mechanical tests on epoxy-carbon nanofiber nanocomposites show that CNFs bring positive effects in terms of mechanical strength and stiffness.

4.3.2.1 Tensile tests on epoxy-carbon nanofiber nanocomposites

Tensile tests on epoxy-carbon nanofibers nanocomposites demonstrate that carbon nanofibers add tensile strength and stiffness to epoxy. The stress-strain plot in figure 4.19 shows that moderate yield occurs for pure epoxy and then gradually diminishes with increasing amount of CNFs. The strain at break (figure 4.22) decreases with increasing weight percentage of nanofibers and becomes more severe with higher nanofibers content. The small strain at break (between 0.045 and 0.035) suggests a non-ductile behavior of the material.

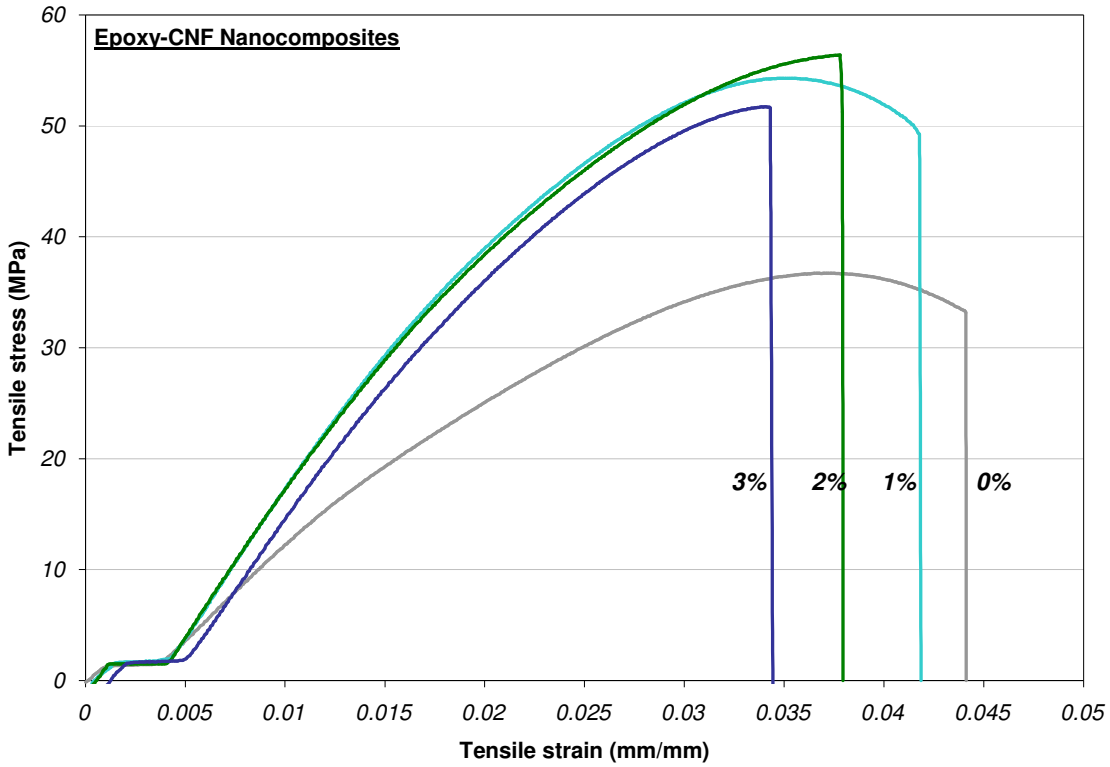

Figure 4.21: tensile tests plot for epoxy-carbon nanofiber nanocomposites

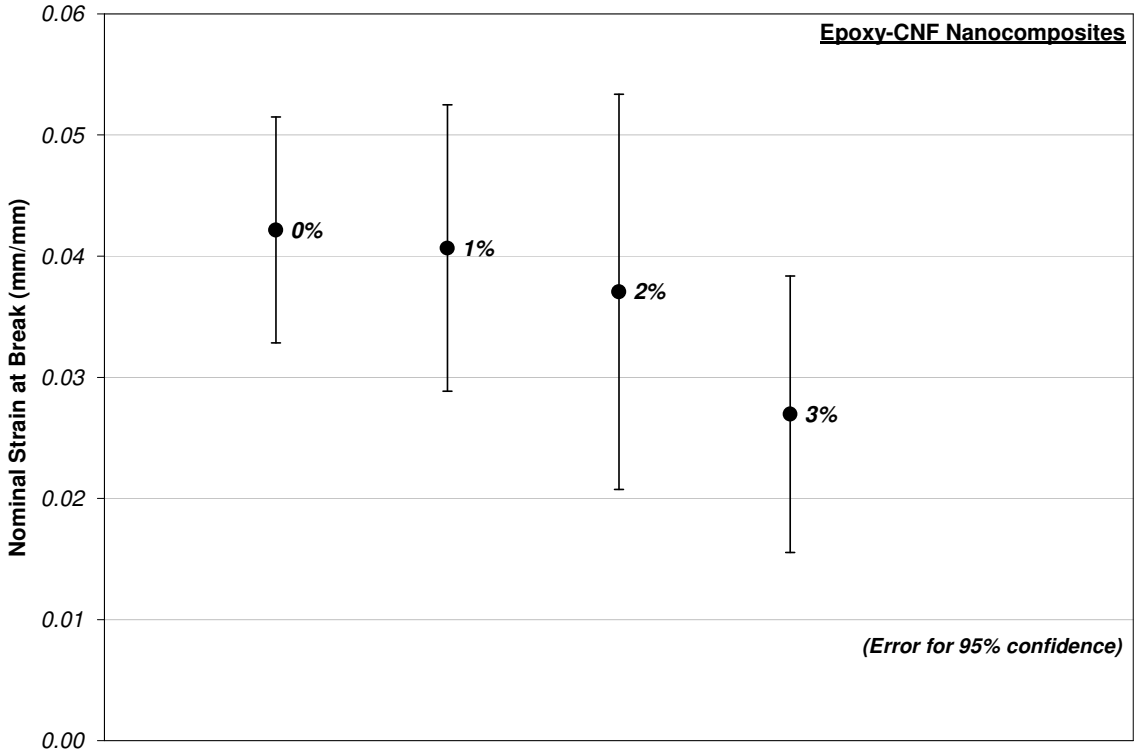

Figure 4.22: nominal strain at break for epoxy-carbon nanofiber nanocomposites

The tensile strength is higher for the nanocomposites than for pure resin. The increase produced is between 15% and 25% with higher increase for 2% weight content of nanofibers. 1% of nanofibers generates improvements similar to 2%, while 3% weight content has lower tensile strength, but still higher that the pure polymer (figure 4.23).

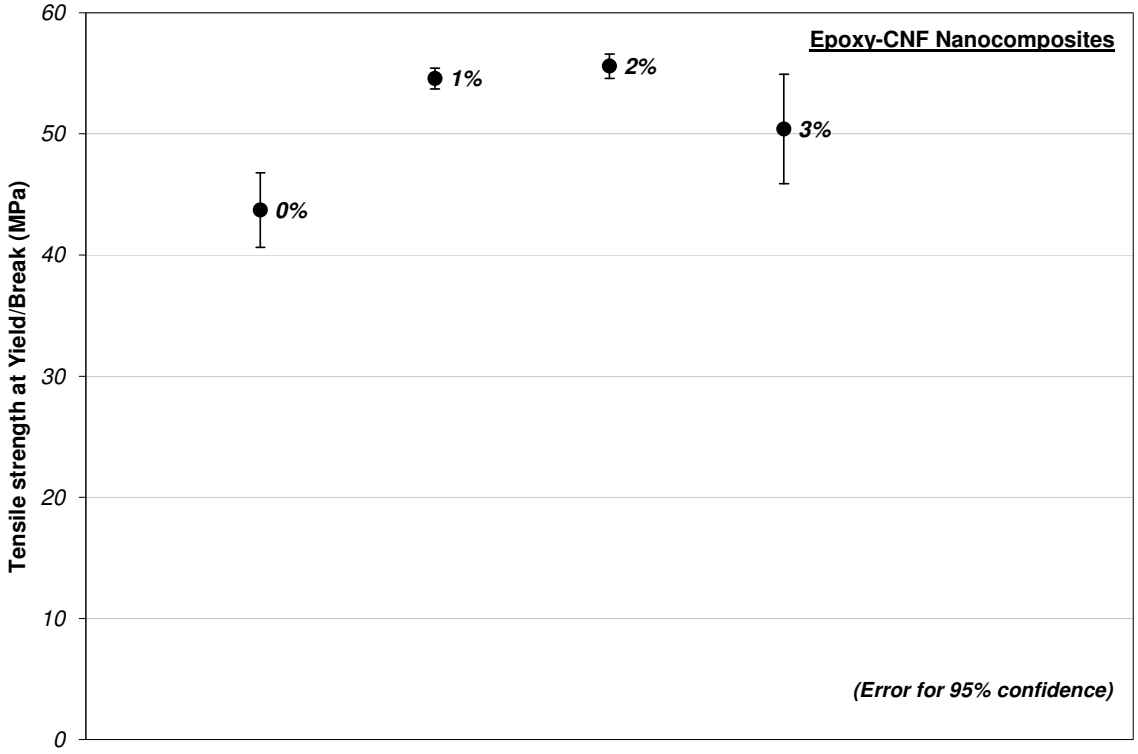

Figure 4.23: tensile strength for epoxy-carbon nanofiber nanocomposites

The Young's modulus (figure 4.24) is higher for the carbon nanofibers, with increase up to 30% for 2% weight content of CNFs. The Young's modulus has a peak for 2%, similarly than for the tensile strength and for all fracture tests, demonstrating that the best equilibrium between fibers loading and dispersion was reached for this content of CNFs. The increase in elastic modulus for 3% content of CNFs is still 25% higher than pure epoxy. These results prove that even small percentages of carbon nanofibers produce non-negligible increase in tensile strength

and elastic modulus with 2% having improvements in the order of 25-30%. Moreover for 2% weight content of carbon nanofibers the reduction of strain at break is relatively small.

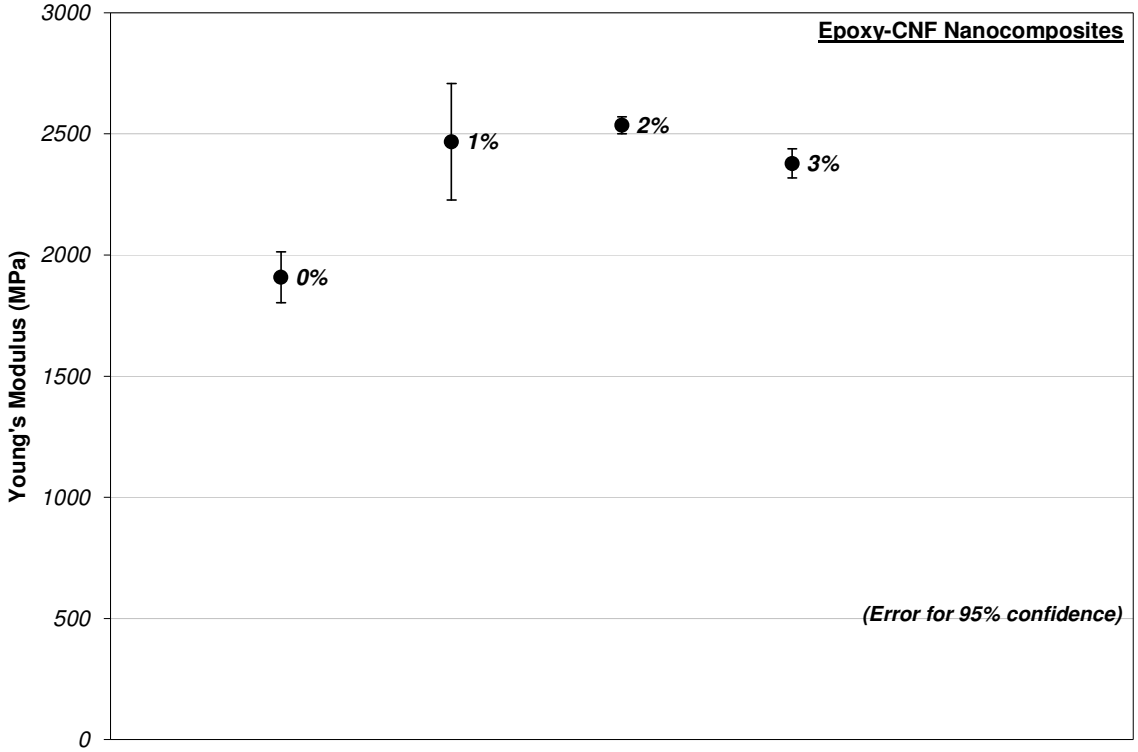

Figure 4.24: Young's modulus for epoxy-carbon nanofiber nanocomposites

4.3.2.2 Flexural tests on epoxy-carbon nanofiber nanocomposites

The flexural tests confirm the superior mechanical properties of carbon nanofiber nanocomposites with respect the pure matrix. Figure 4.25 shows a representative stress-strain plot where the higher strength of the nanocomposites is evident. Another peculiar element is that using the ASTM D 790-03 standards for flexural tests on plastics, it was not possible to reach rupture for CNFs nanocomposites (all epoxy-clay nanocomposites broke instead).

The highest flexural strength is reported for 2% weight content of CNFs, like for tensile tests (figure 4.26). The increase is very evident: 20% for 1% CNFs content, 45% for 2% CNFs content, and 22% for 3% CNFs content.

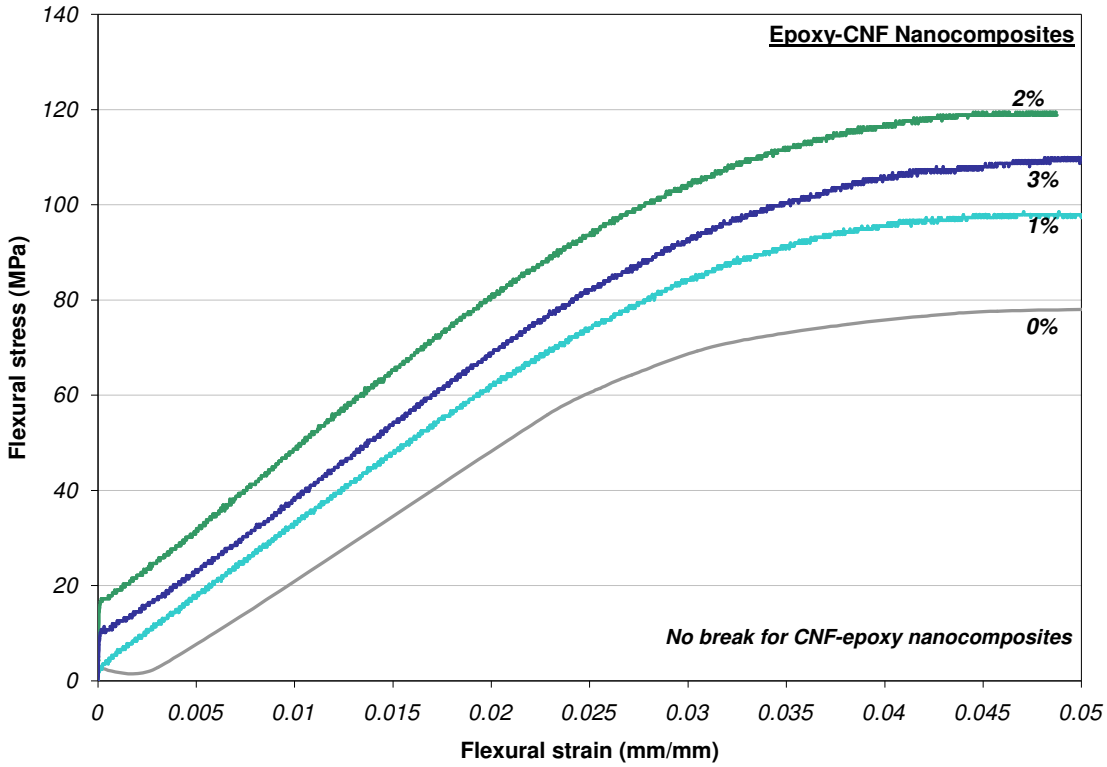

Figure 4.25: flexural tests plot for epoxy-carbon nanofiber nanocomposites

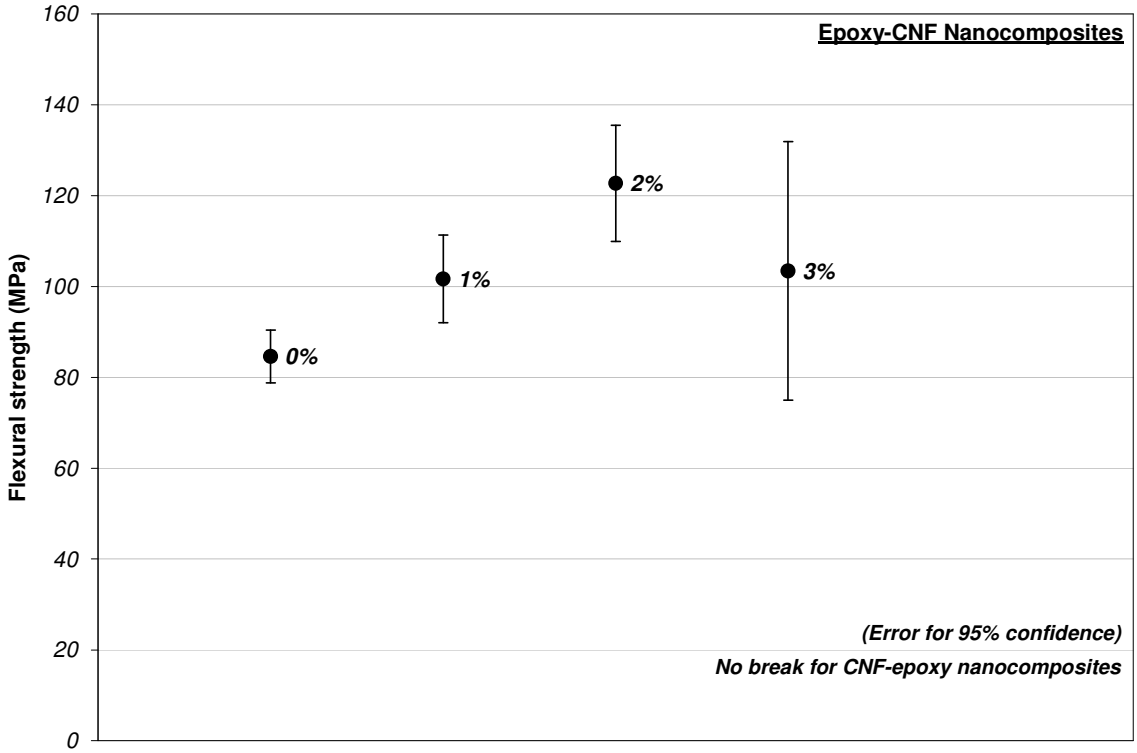

Figure 4.26: flexural strength for epoxy-carbon nanofiber nanocomposites

The deflection (strain) at flexural peak load is sensibly lower for CNFs nanocomposites than for pure resin, like it was for clay nanocomposites (figure 4.27). The flexural strain is almost half than the one of pure epoxy, with virtually no change for the different nanofibers percentages.

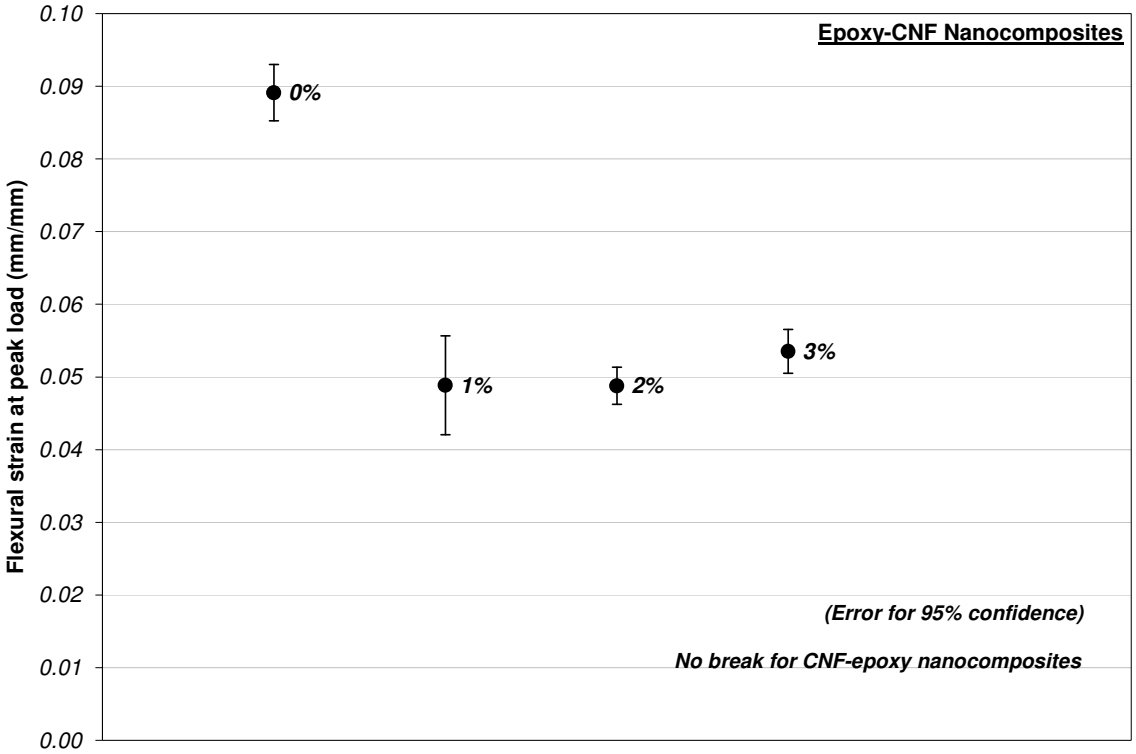

Figure 4.27: deflection (strain) at flexural peak load for epoxy-carbon nanofiber nanocomposites

The tangent modulus of elasticity in bending is higher for all percentages of CNFs, with a peak for 2% weight content of carbon nanofibers (figure 4.28). The increase is evident and ranges from 10 to 27%.

The flexural tests show again that carbon nanofibers produce better static mechanical properties, increasing ultimate flexural strength and stiffness, and decreasing the strain deflection

at the peak load. It is encouraging that it did not reach rupture using the ASTM D 790 standards. CNF-epoxy seems to be a suitable solution to reach superior flexural properties.

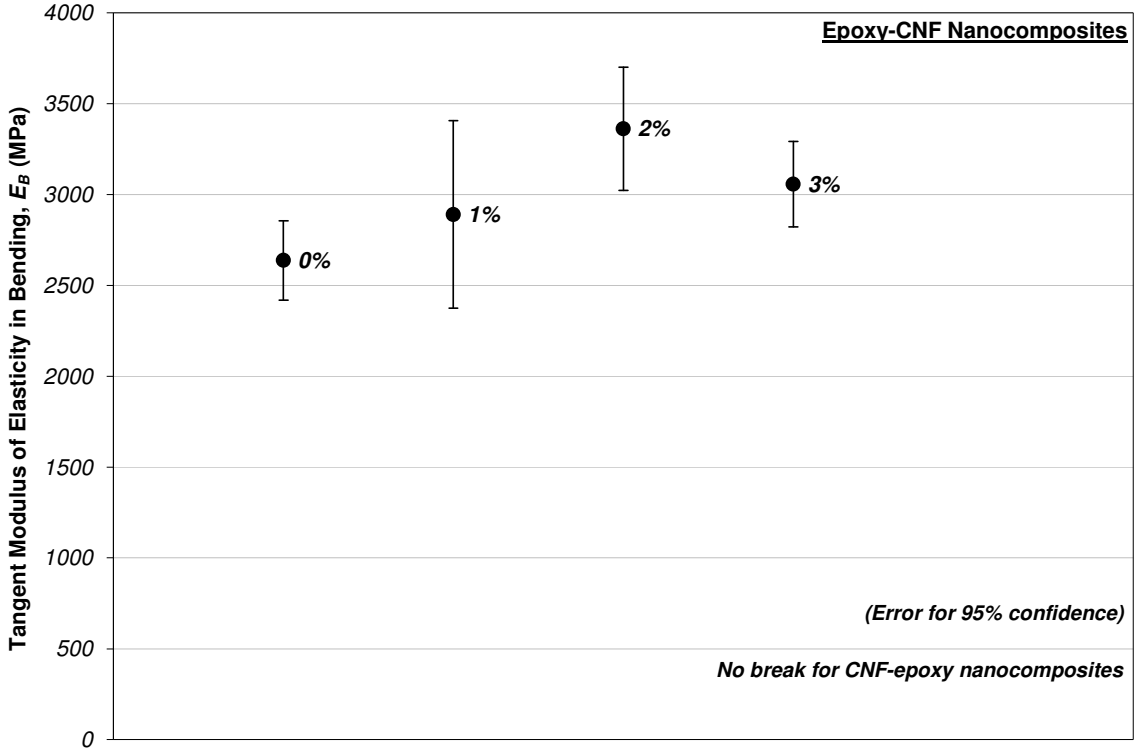

Figure 4.28: tangent modulus of elasticity in bending for epoxy-carbon nanofiber nanocomposites

4.3.3 Flammability tests on epoxy-carbon nanofiber nanocomposites

Flammability tests on carbon nanofiber nanocomposites are not as common as for nanoclays nanocomposites. Connected with the burning of CNFs nanocomposites there is the hazard of liberating carbon nanofibers through the fumes produced during burning. It is still not clear if the carbon particles released are in the form of carbon nanofibers, or they are bigger agglomerate. In both cases anyway the danger of breathing these particles in is at least in the level of carbon black and it is not advisable to use CNFs as a mere flame retardant. Nevertheless, the flame retardation properties of CNFs additive are greater than the ones produced by nanoclays.

In figure 4.29 the trend of the HRR versus time is plotted. This graph, like for the case of nanoclays, is to be considered from a qualitative point of view, since the quantitative evaluation will be for samples with a 5 mm thickness. The HRR has a sharp peak, and in general the trend is similar to the one of epoxy and epoxy-clay nanocomposites.

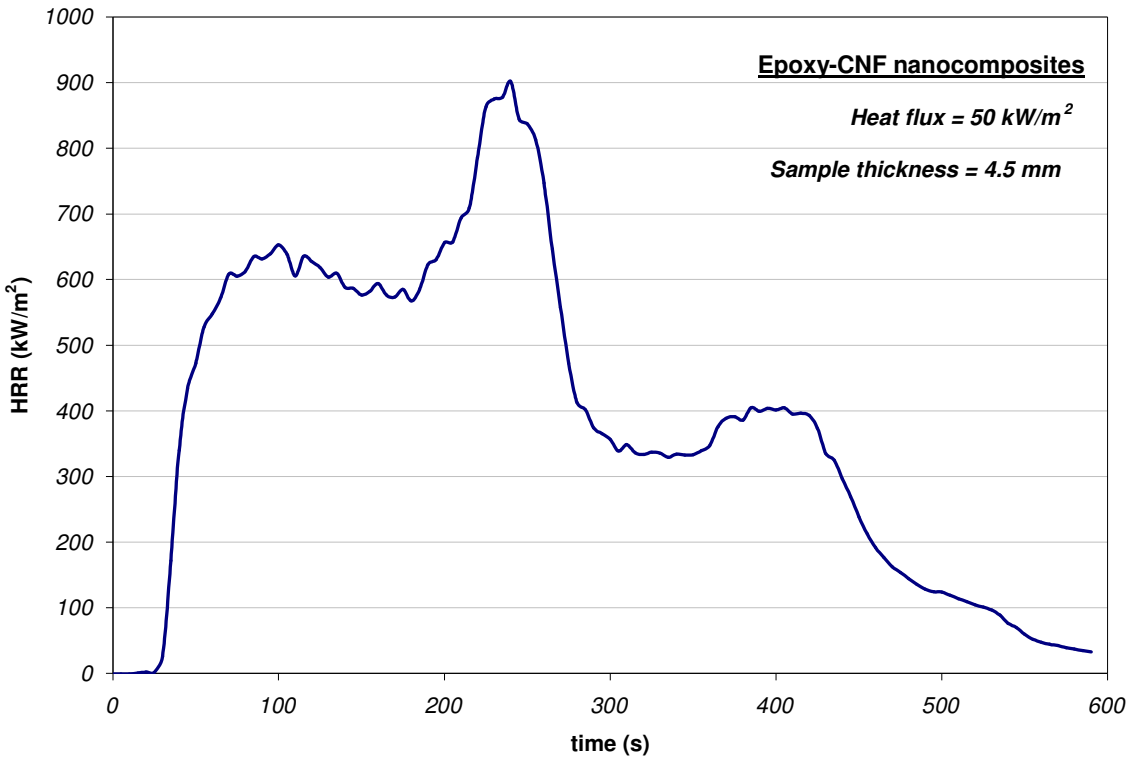

Figure 4.29: Heat Release Rate for 1% CNF-epoxy nanocomposite

The PHRR and the MHRR are plotted in figure 4.30. The PHRR is higher for pure epoxy than for epoxy with addition of CNFs. The difference is evident and with 3% weight content of CNFs the value is half of the value for pristine epoxy. The reduction for 1% and 2% are respectively 36% and 45% of the value for pure epoxy, which makes the CNFs a very effective additive to reduce the PHRR. The MHRR is approximately the same for all cases studied, with slighter lower values for 2% and 3% CNFs weight content.

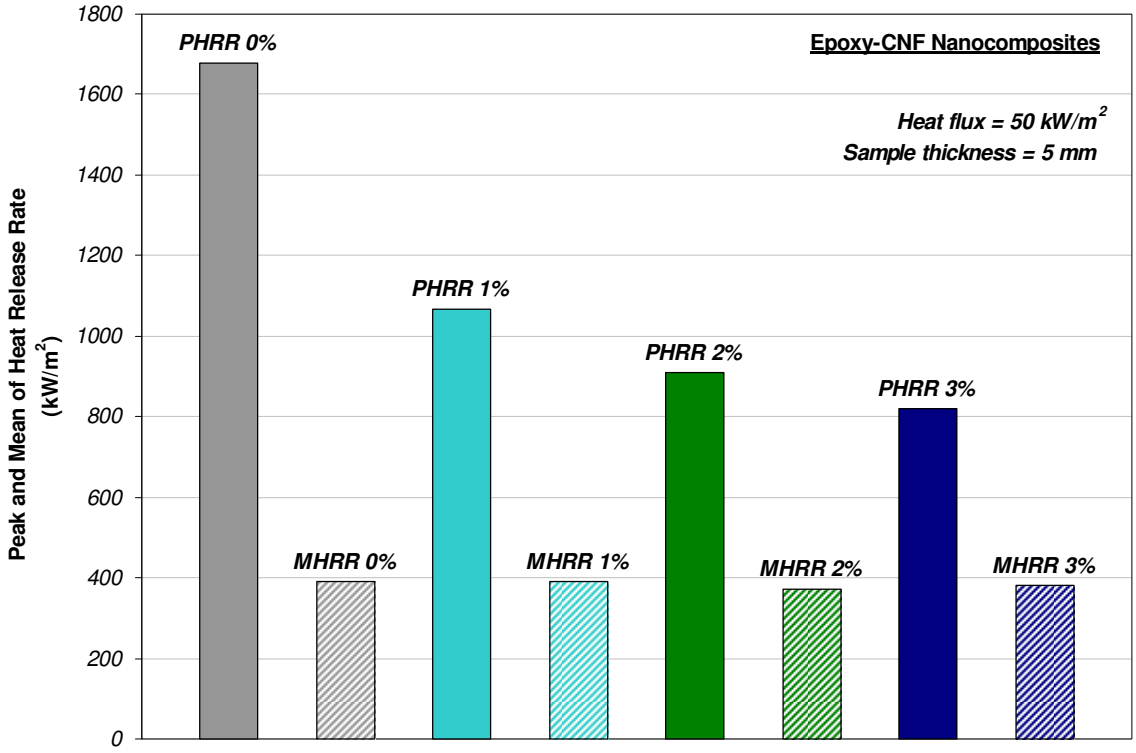

Figure 4.30: Peak and Mean of Heat Release Rate for epoxy-CNF nanocomposites

Figure 4.31 shows the trend for the MLR, which is similar to the one of epoxy-clay nanocomposites. The PMLR and MML are plotted in figure 4.32, and it shows significant reduction in PMLR with addition of CNFs. The reduction is proportional to the weight content of CNFs, and with 3%wt of CNFs we have 33% reduction of PMLR. The MMLR is about the same for all cases studies. The HRR and MLR are connected and usually the behavior for these two properties is very similar. The high values for the MLR suggests that both pure epoxy and epoxy-CNFs nanocomposites are highly flammable. This was also noticed through observation of the very tall flames during testing.

The HRR is a more precise measurement than MLR, as it is evident comparing the plots in figure in figure 4.29 and 4.31. It is for this reason advisable to select the HRR as a reference for the fire behavior of a material, rather than the MLR.

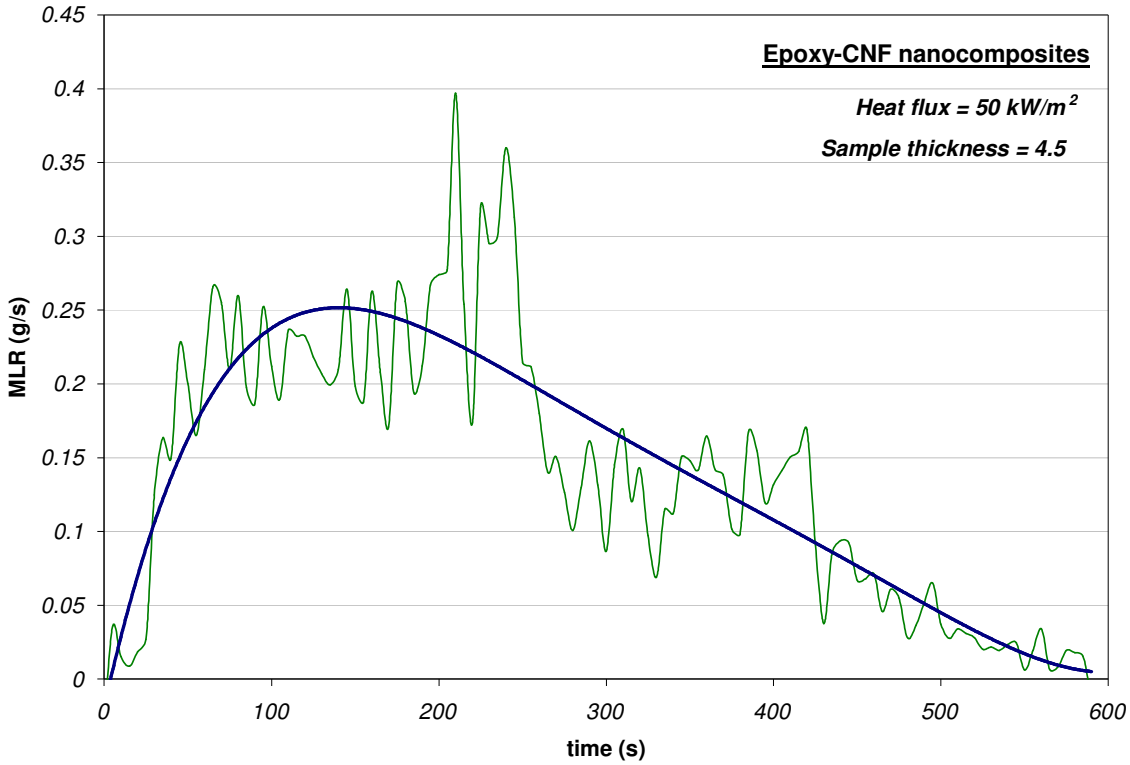

Figure 4.31: Mass Loss Rate for 1% CNF-epoxy nanocomposite

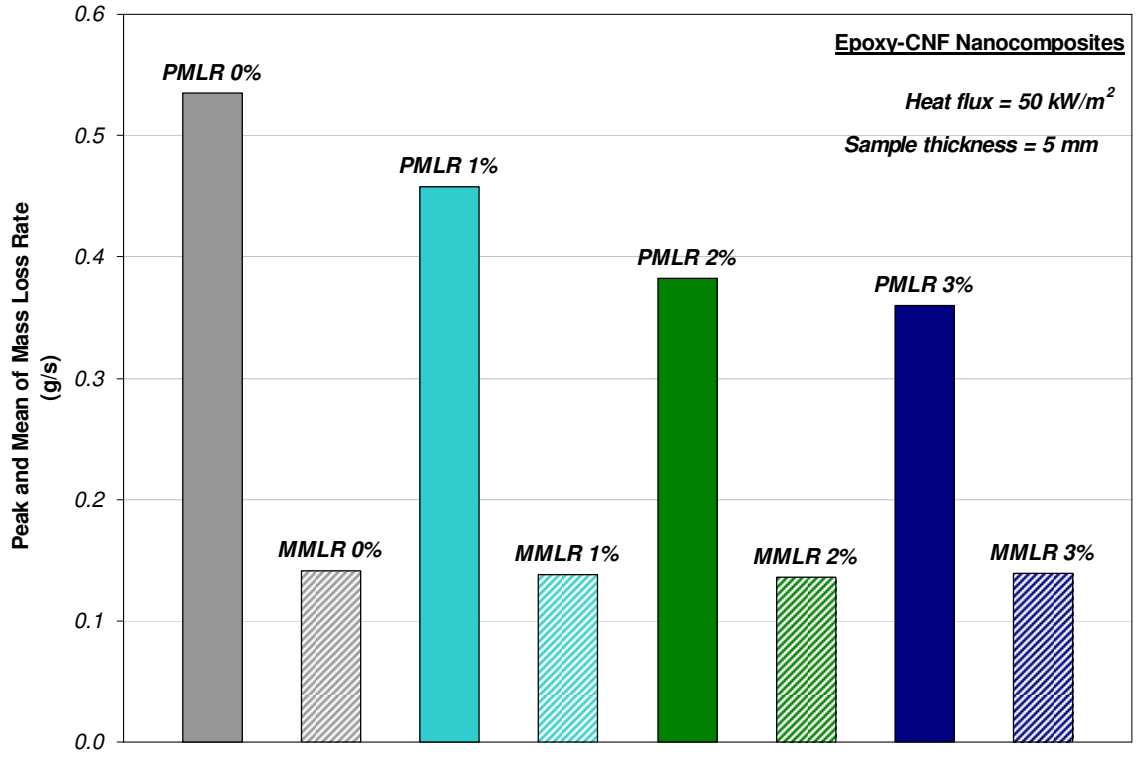

Figure 4.32: Peak and Mean of Mass Loss Rate for epoxy-CNF nanocomposites

The time of ignition is plotted in figure 4.33 and the results do not show evident differences for all cases studied. The time to ignition seems to be higher for 3% of CNFs, but the difference is within the error of measurement. The time to PHRR is higher for CNFs nanocomposites, which means that the PHRR occurs later, like observed for clay nanocomposites. The time to flameout grows with addition of CNFs, with 12% increase for 2% weight content of CNFs. The gain in time to flameout is not very high and the error for this measurement is extremely high, since at the end of the burning process only small isolated flames survive and it is difficult to decide when the burning should be considered concluded. To reduce this uncertainty, it was considered time to flameout the time when the HRR goes below 30 kW/m^2.

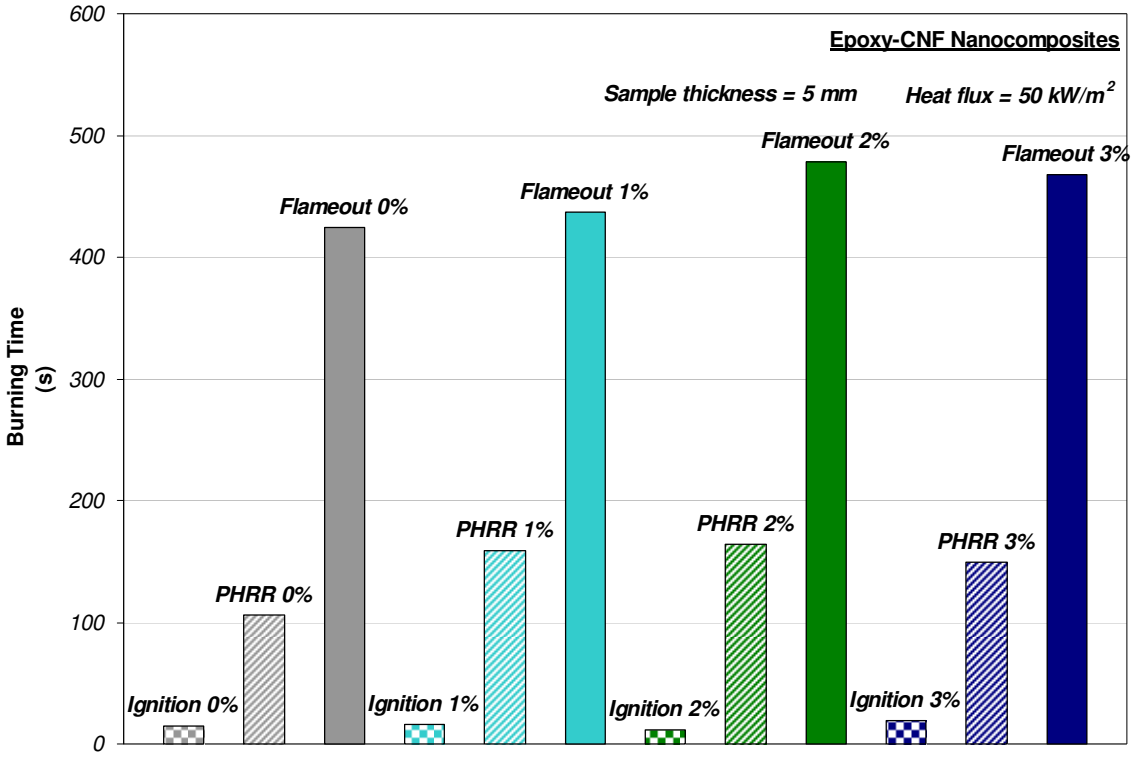

Figure 4.33: time to ignition, time to PHRR, and time to flameout for epoxy-CNF nanocomposites

Figure 4.34 shows the total smoke release and the total heat released. The total heat release is the same for all cases studied, meaning that all resin is burned out. The total smoke release is also about the same for all cases studied. The carbon nanofibers do not contribute in a visible way to production of smoke and observing the char left after testing, it is evident that most of the nano-reinforcements are not transported by the fumes. However the filters of the cone calorimeters collect a lot of black particles, certainly carbon. There is thus the hazard produced by carbon particles, as suspected. Most of the particles are visible, but it is believed that many others were micro or nano sized. These small dimensions are believed to constitute a great danger for living beings.

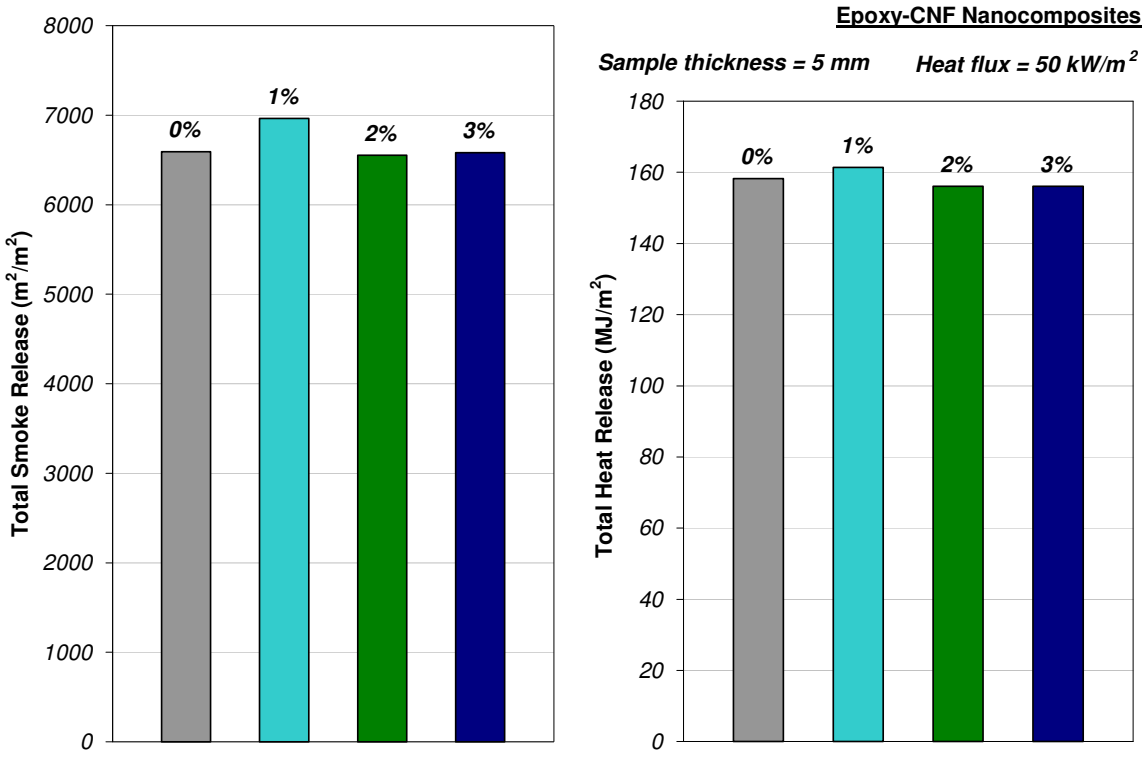

Figure 4.34: Total Smoke Release and Total Heat Release for epoxy-CNF nanocomposites

4.4 Properties of epoxy-clay-CNF nanocomposites

A new class of nanocomposites was developed here mixing two different nanoparticles (nanoclay and CNFs) into epoxy resin. The results are compared with nanocomposites with 2% weight content of nanoclays and CNFs and with pure epoxy. The study was carried out to understand if the superimposition principle is applicable and if the two nanoparticles together produce a combined effect to enhance the overall properties of the nanocomposite. The percentages mixed were 1%-1% and 2%-2% weight content of nanoclays and CNFs. The results show improvements with respect to the pristine resin for both mechanical and flammability properties. The best results are for 2% weight content of CNFs, where both static mechanical and flammability results are superior to pure epoxy. For 1%-1% clays-CNFs good mechanical properties are recorded and superior flame resistance is observed when compared to clay-epoxy nanocomposites. 2%clay-2%CNF nanocomposites demonstrates to be too loaded of nanoparticles and good dispersion cannot be reached with the methodology developed for this dissertation. The properties are lower than for 2% CNF nanocomposites and 1%clay-1%CNF, indicating that it is not a suitable solution.

4.4.1 Fracture tests on epoxy-clay-CNF nanocomposites

Izod impact tests and fracture toughness tests show that the addition of nanoclays and carbon nanofibers make the material more brittle and less fracture resistance. 2% weight content of CNFs seems to be still more fracture resistance than other nanocomposites, but the values are inferior to the ones of pristine epoxy.

4.4.1.1 Impact tests on epoxy-clay-CNF nanocomposites

The net Izod impact strength of nanocomposites produced with both nano-reinforcements together is plotted in figure 4.35. The value is compared with pure epoxy (in figure represented

by red lines) and with nanocomposites with 2% weight content of nanoclays and 2% weight content of CNFs. The pure epoxy is still the most resistant to impact, while the nanocomposites produced with the two nanoparticles together are the one with the lower values. The superimposition principle seem not to work here, since the value for 1%clay-1%CNF is lower that the 2%clay and the 2%CNF, and since the nano-reinforcement loading is 2% for all of them. As expected 2%clay-2%CNF nanocomposites have lower impact strength, as observed for clays nanocomposites and CNFs nanocomposites where high reinforcements content where producing low impact resistance. After testing nanocomposites made with nanoclays, carbon nanofibers and both nano-reinforcements together it is evident that the nanocomposites produced have lower impact resistance and that the best results are reached with 2% weight content of nanoclays or 2% weight content of CNFs.

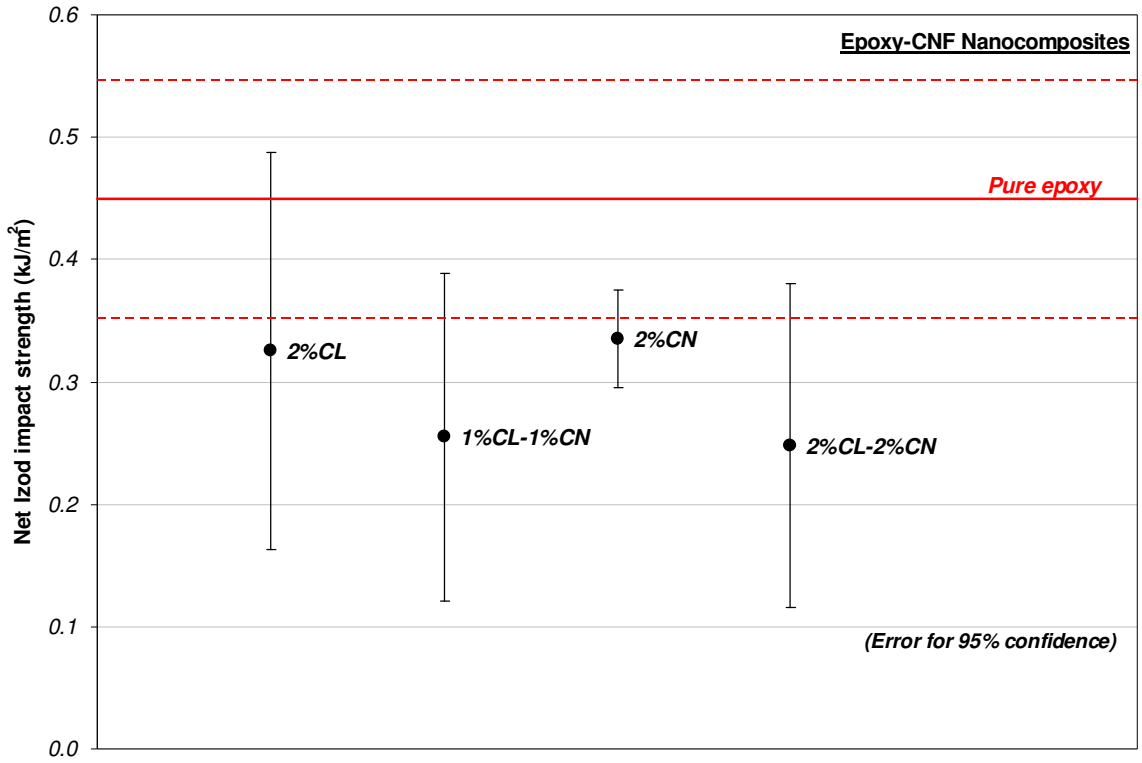

Figure 4.35: Izod impact strength on epoxy-clay-CNF nanocomposites

4.4.1.2 Fracture toughness tests on epoxy-clay-CNF nanocomposites

The stress intensity factor is lower for all percentages of nano-reinforcements, except that with 2% content of CNFs (figure 4.36). The increase in K_{IC} is however modest and within the boundary of the measurement error, which suggest that no significant improvement was brought. 2%clay-2%CNF has the lowest value, which confirms that the mixing process was ineffective for such high nano-reinforcement loading. Bubbles and voids created during the ultrasonication make the material less fracture resistant and more brittle. This is confirmed by the results for the energy release rate (figure 4.37) where all values of nanocomposites are lower than the one for pure epoxy. The best results are again observed for 2% carbon nanofibers weight content, where the reduction in energy release rate is within 20%.

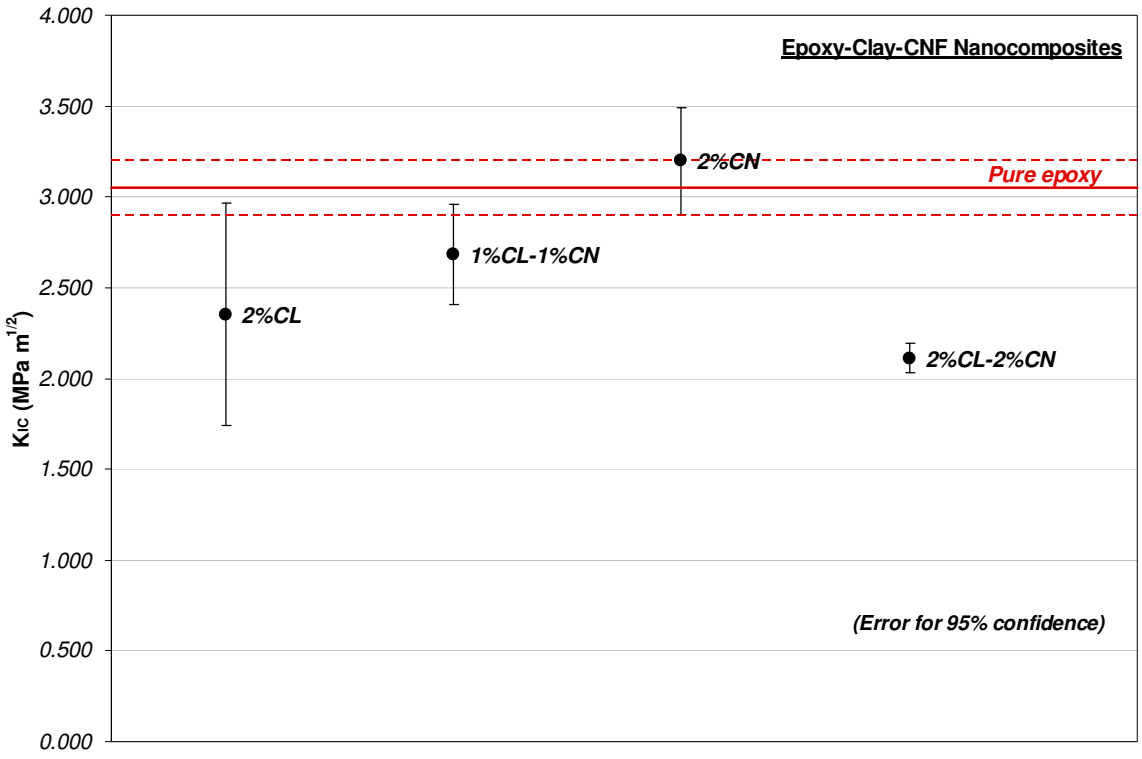

Figure 4.36: stress intensity factor for epoxy-clay-CNF nanocomposites

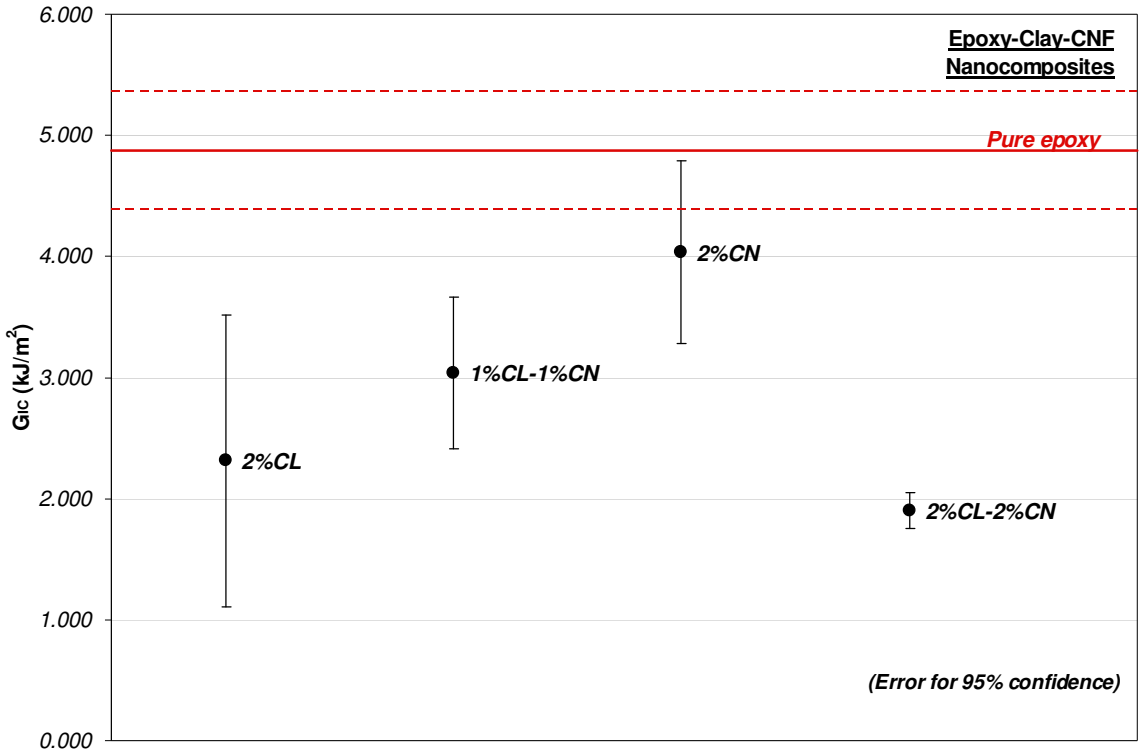

Figure 4.37: energy release rate for epoxy-clay-CNF nanocomposites

4.4.2 Static mechanical tests on epoxy-clay-CNF nanocomposites

Static mechanical tests demonstrates that nanocomposites with 2%wt of nanoclays, 1%-1%wt of nanoclay-CNF, 2%wt of CNFs, and 2%-2%wt of nanoclay-CNF have better mechanical properties than pure epoxy.

4.4.2.1 Tensile tests on epoxy-clay-CNF nanocomposites

The tensile properties of the nanocomposites produced with both nanoclays and CNFs are overall better than the ones of pure epoxy. However, the strain at break is smaller as shown in figure 4.38. The biggest reduction of strain at break is reached with 2%-2%wt clay-CNF, as expected, considering the high amount of nano-reinforcements added. The smallest reduction can be observed for 2%wt of CNFs, which have also the highest tensile strength (figure 4.39).

The tensile strength is higher for all cases studied compared to the pristine epoxy, but again the smallest increase was obtained for 2%-2%wt clay-CNF nanocomposites. The other percentages roughly behave similarly, with the biggest improvements for 2% weight content of CNFs.

The Young's modulus is 25%-30% higher for all cases studied (figure 4.40), with biggest increase for 2%wt of CNFs and smallest increase for 2%-2%wt clay-CNF.

The tensile tests show that 2% weight content of CNFs has higher tensile strength, higher Young's modulus, and higher strain at break than any other nanocomposites produced. 1%-1%wt clay-CNF nanocomposites seem to have also properties comparable to 2%wt CNF nanocomposites, and considering the specific costs (lower for nanoclays than for CNFs) it seems to be a reasonable choice. 2%-2%wt clay-CNF nanocomposites have instead inferior tensile properties and they come with the highest price, and thus this solution is not advisable.

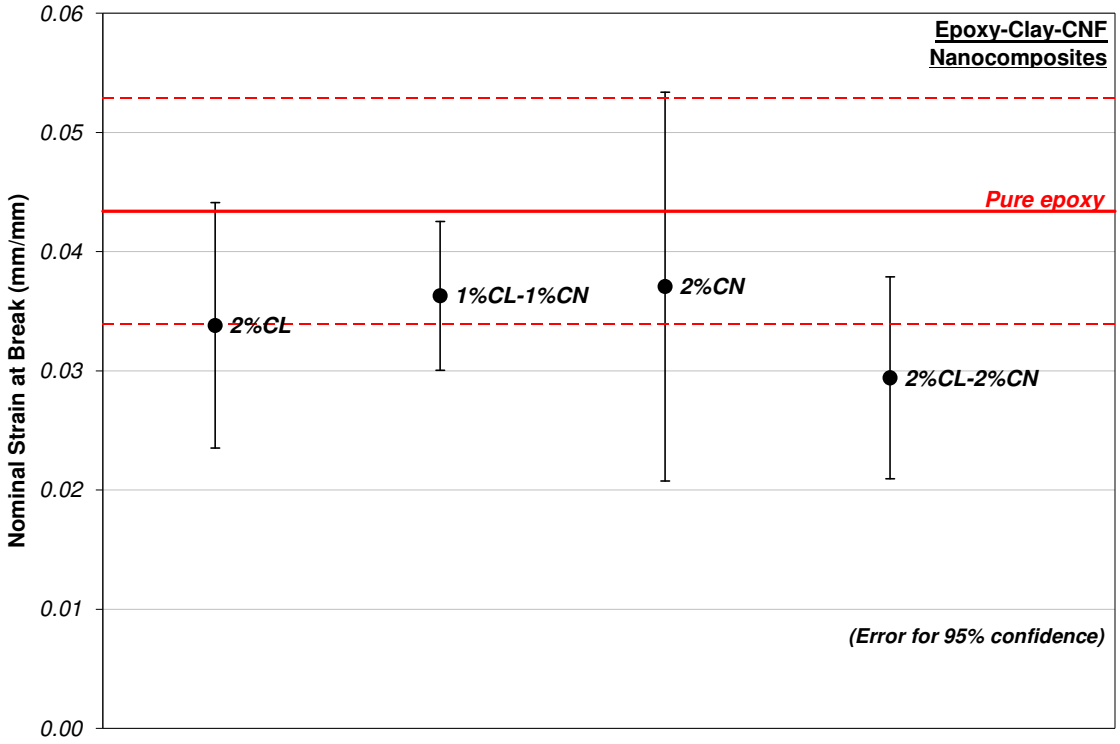

Figure 4.38: nominal strain at break for epoxy-clay-CNF nanocomposites

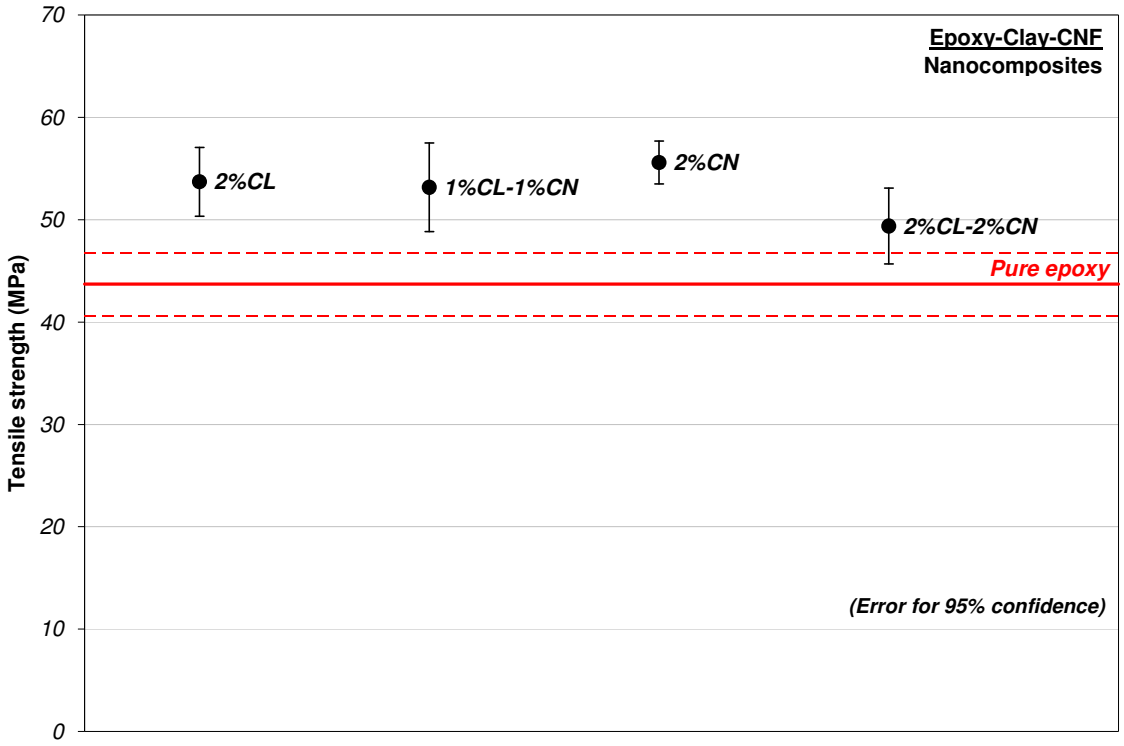

Figure 4.39: tensile strength for epoxy-clay-CNF nanocomposites

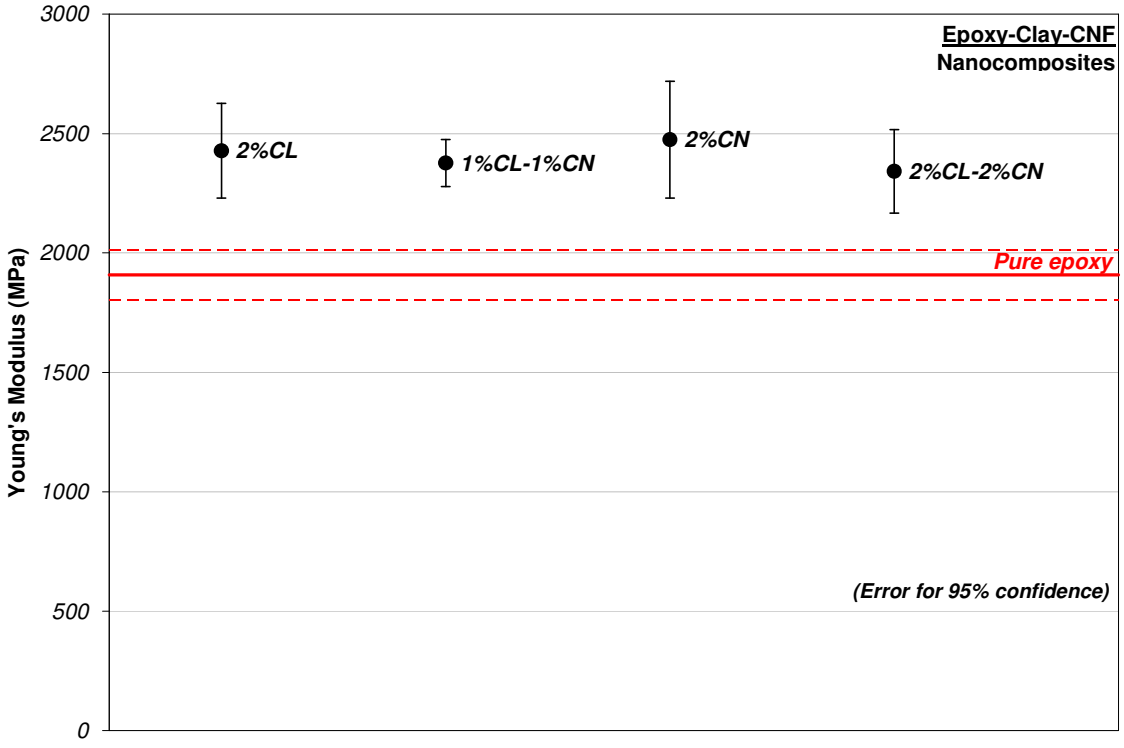

Figure 4.40: Young's modulus for epoxy-clay-CNF nanocomposites

4.4.2.2 Flexural tests on epoxy-clay-CNF nanocomposites

The flexural strength for the nanocomposites produced with both nanoparticles in epoxy is shown in figure 4.41. For this property, the addition of 2% of CNFs creates the best result, with increase of 45% in flexural strength. All other cases studied have better flexural strength than pristine epoxy, but with a similar gain within 20%.

The strain at peak load is lower for all cases studied, when compared to pure epoxy. The reduction is dramatic and it is in the order of approximately half of the value of epoxy. The smallest reduction is achieved with 2% of CNFs (both 2% CNFs alone, and 2%-2% clay-CNF nanocomposites), meaning that carbon nanofibers make the nanocomposites a little bit tougher at bending. 1%-1% clay-CNF has an intermediated value between 2% clay and 2% CNF, meaning that the superposition principle apply for this case.

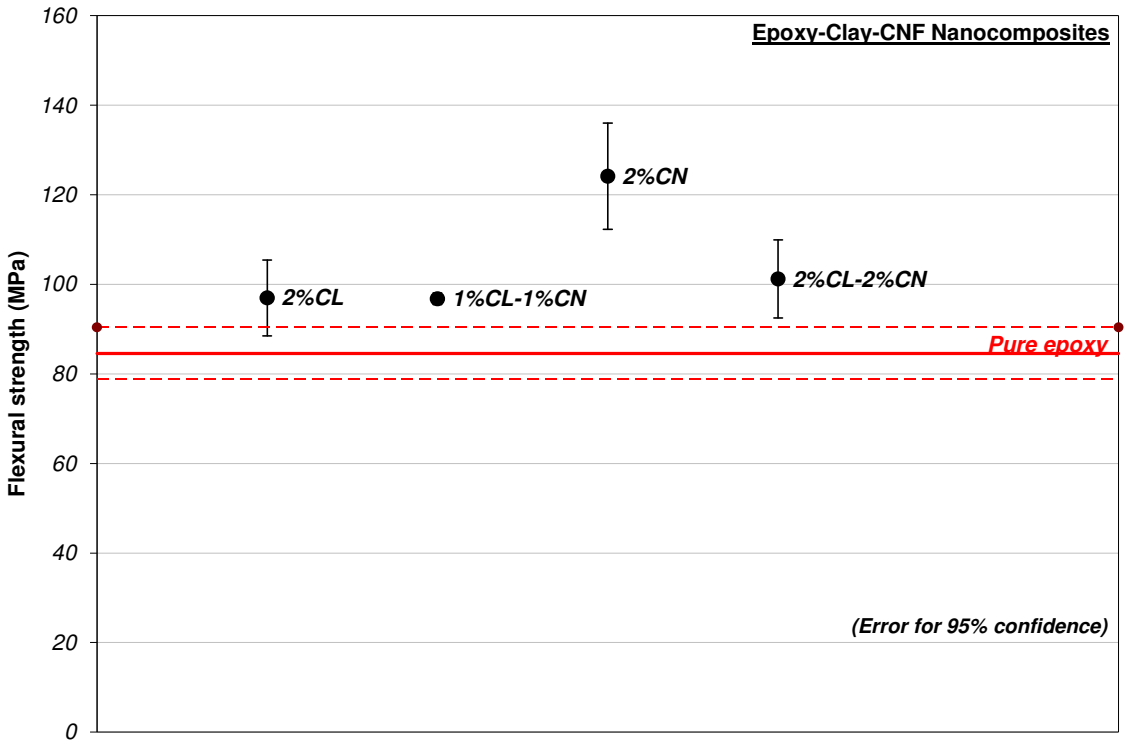

Figure 4.41: flexural strength for epoxy-clay-CNF nanocomposites

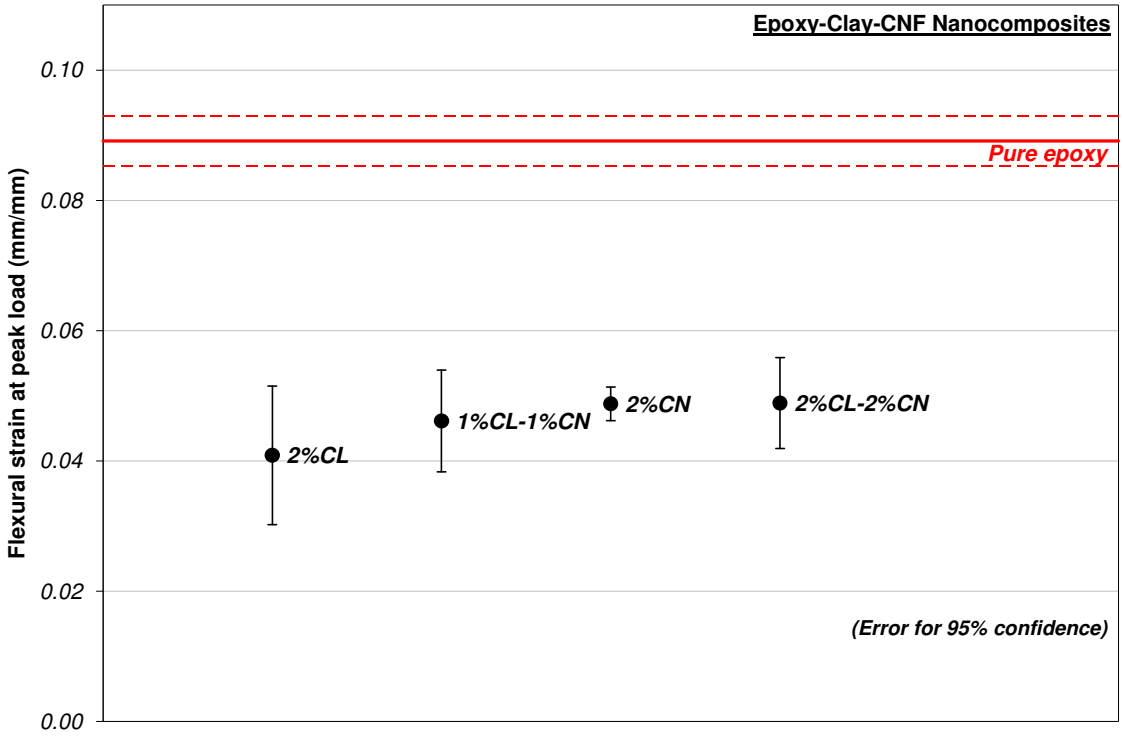

Figure 4.42: deflection (strain) at flexural peak load for epoxy-clay-CNF nanocomposites

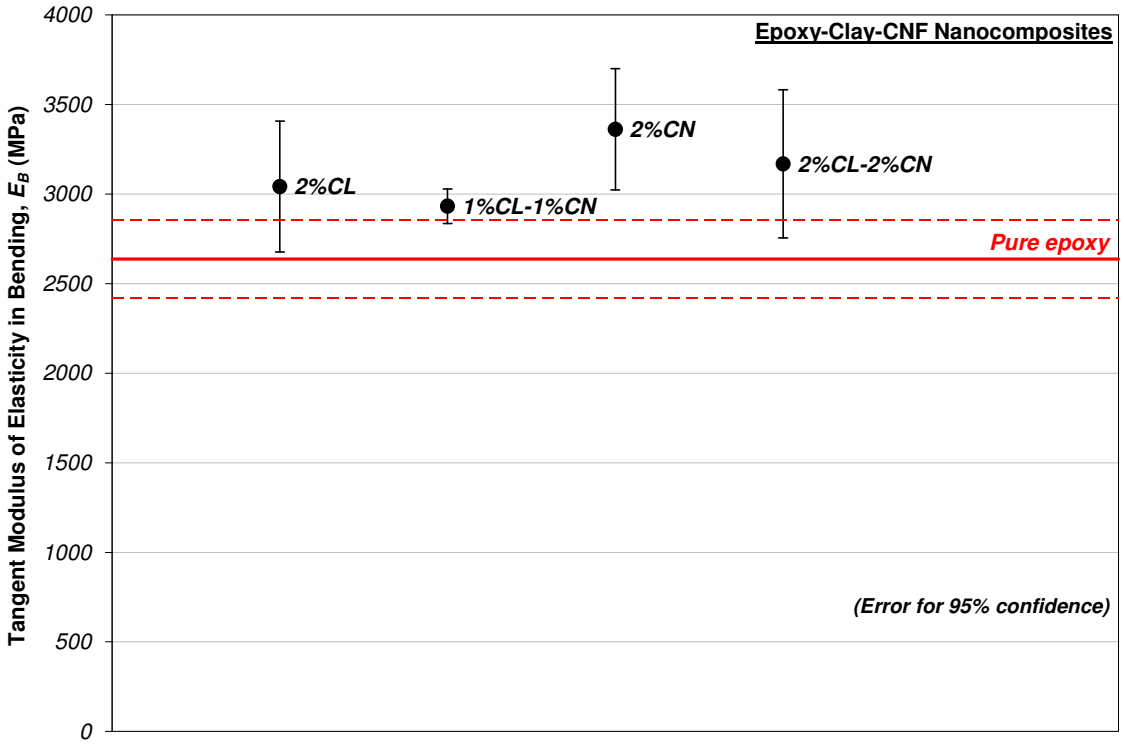

Figure 4.43: tangent modulus of elasticity in bending for epoxy-clay-CNF nanocomposites

The flexural modulus is higher for all cases studied compared to the one of pure epoxy. The biggest gain is again reached with addition of 2% weight content of CNFs, and the smallest with addition of 2% weight content of clays. 2%-2%wt clay-CNF has also a high flexural modulus.

Flexural tests show improvements with addition of 2% CNFs into epoxy. 2% nanoclays do not bring increase in flexural properties of magnitude comparable to CNFs, but the flexural resistance is still higher than pure epoxy.

4.4.3 Flammability tests on epoxy-clay-CNF nanocomposites

The flammability results of the nanocomposites produced with both nanoparticles mixed into epoxy show encouraging flame retardation properties for the cases studied. The biggest contribution was given by carbon nanofibers, as it is evident observing figure 4.44. The PHRR is half of the value for pure epoxy for all nanocomposites containing CNFs. When only 1% of carbon nanofibers is present, part of the reduction is to be attributed to the nanoclays (1%-1% clay-CNF nanocomposite). The 2%-2% clay-CNF nanocomposite was expected to be with an even lower PHRR. This does not happen here, and it is believed that the cause is the presence of voids, which allow the fire to seep through the thickness, alimenting the fire with a larger portion of epoxy. For this reason, a burning process that develops more deeply through the thickness annihilates the effect of the additional flame retardation due to a higher percentage of nanoparticles. The MHRR is slightly lower for all nanocomposites. This will have the effect to slow the burning process. The trend of PMLR and MMLR (figure 4.45) is similar to the one of PHRR and MHRR, but as explained before, even if HRR and MLR are connected, the measurements for HRR are more precise.

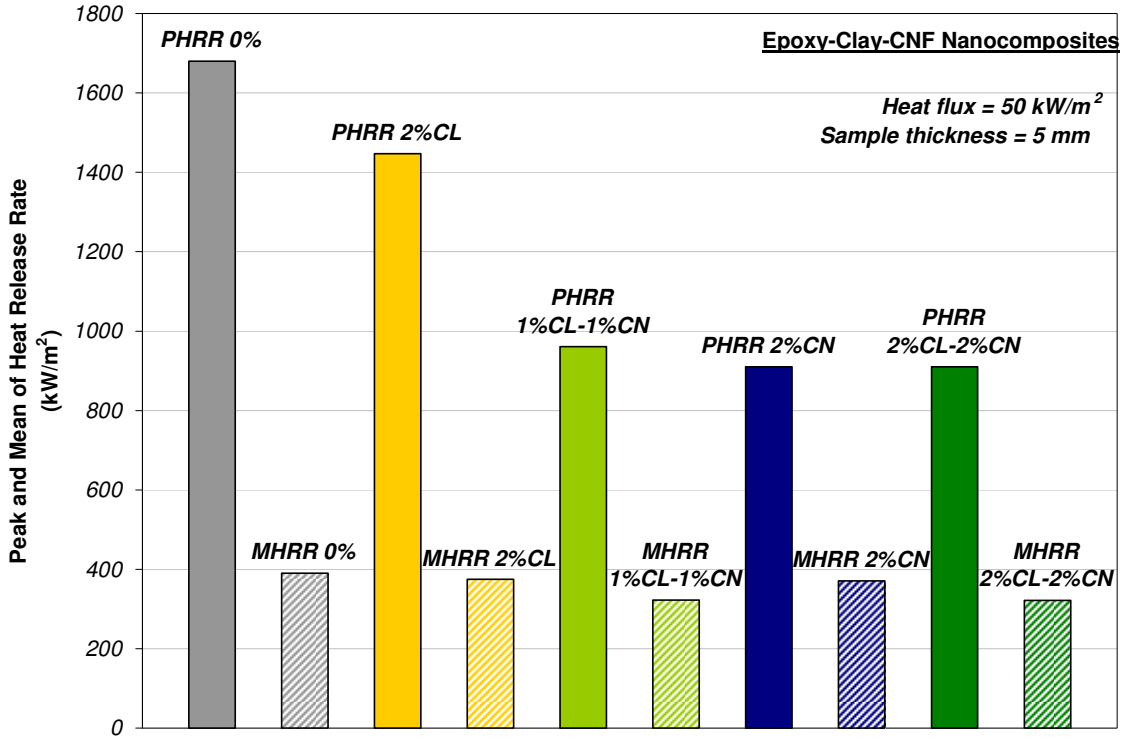

Figure 4.44: Peak and Mean of Heat Release Rate for epoxy-clay-CNF nanocomposites

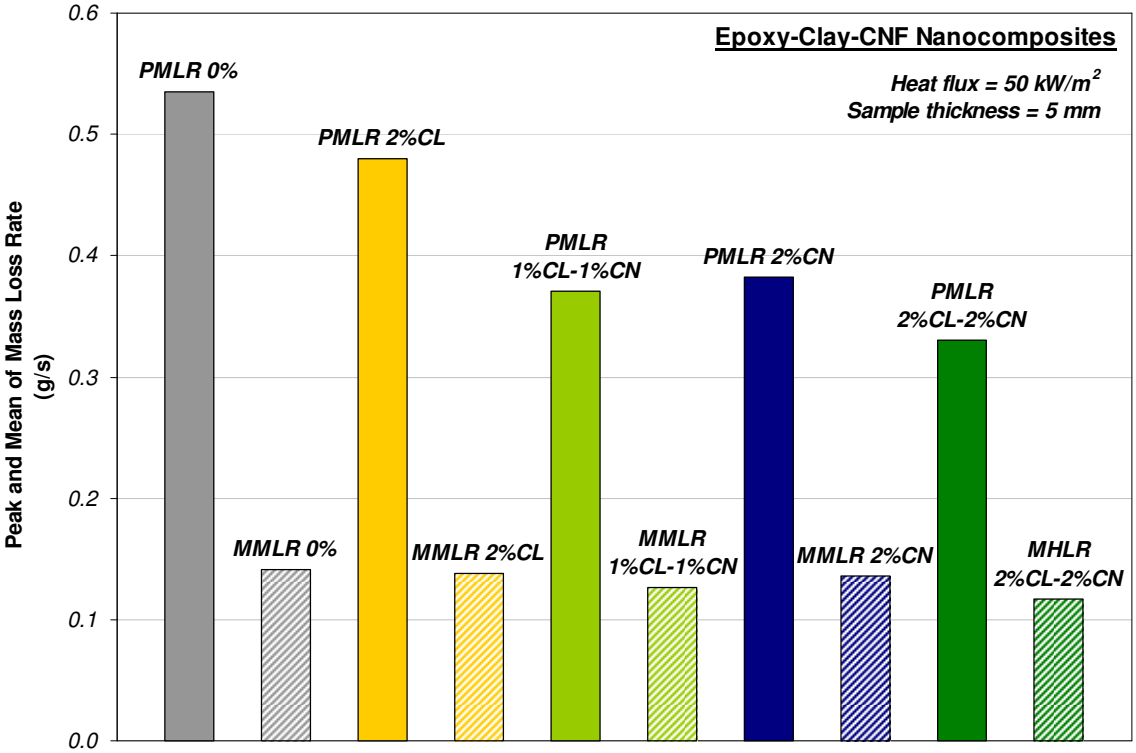

Figure 4.45: Peak and Mean of Mass Loss Rate for epoxy-clay-CNF nanocomposites

The ignition time, the time to PHRR and the time to flameout are depicted in figure 4.46. The time to ignition is higher for nanocomposites containing nanoclays, while CNFs seem not to bring any improvements, confirming what was observed before for epoxy-CNF nanocomposites. The time to PHRR occurs later for the nanocomposites, when compared to the time to PHRR of pristine epoxy. The time to flameout is longer for nanocomposites containing CNFs and this also confirms the observation made before in this chapter.

The total smoke and heat released is similar for all cases studied. This suggests that not significant increase in smoke production can be attributed to the presence of nano-reinforcements. After examining the filter in the cone calorimeter it is evident however that a percentage of nanoparticles was liberated by the fumes and this can constitute an hazard to the surrounding environment. The total heat release suggests that all epoxy resin was burned out.

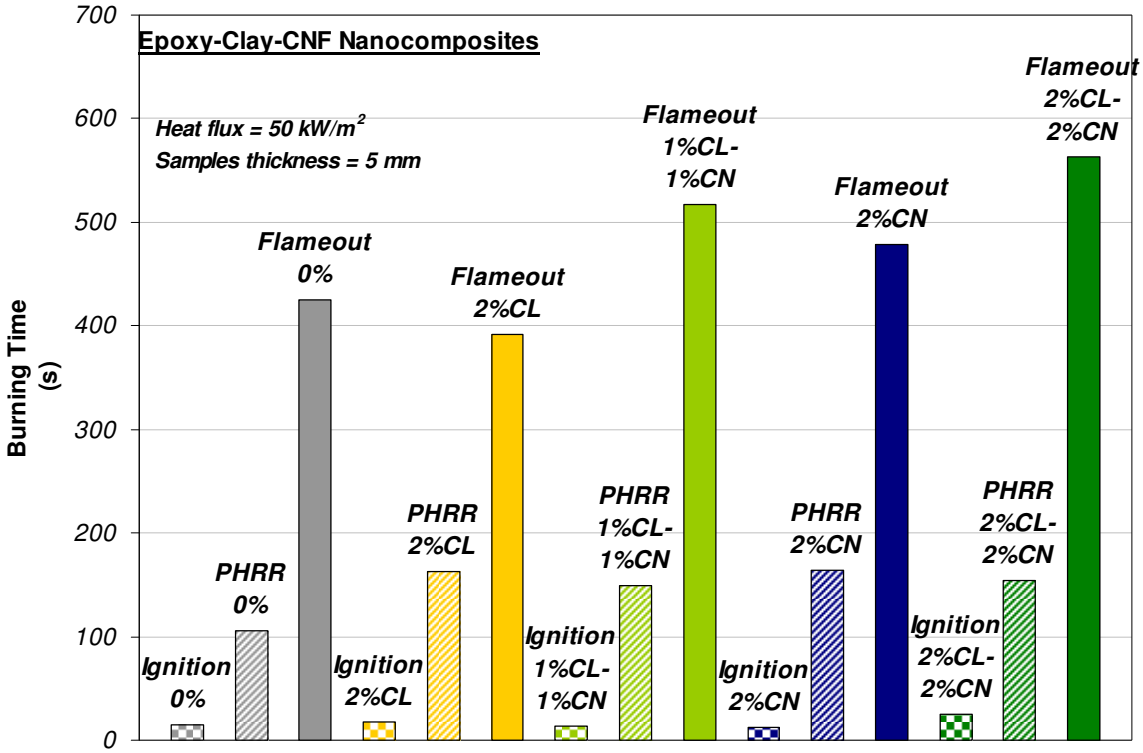

Figure 4.46: time to ignition, time to PHRR, and time to flameout for epoxy-clay-CNF nanocomposites

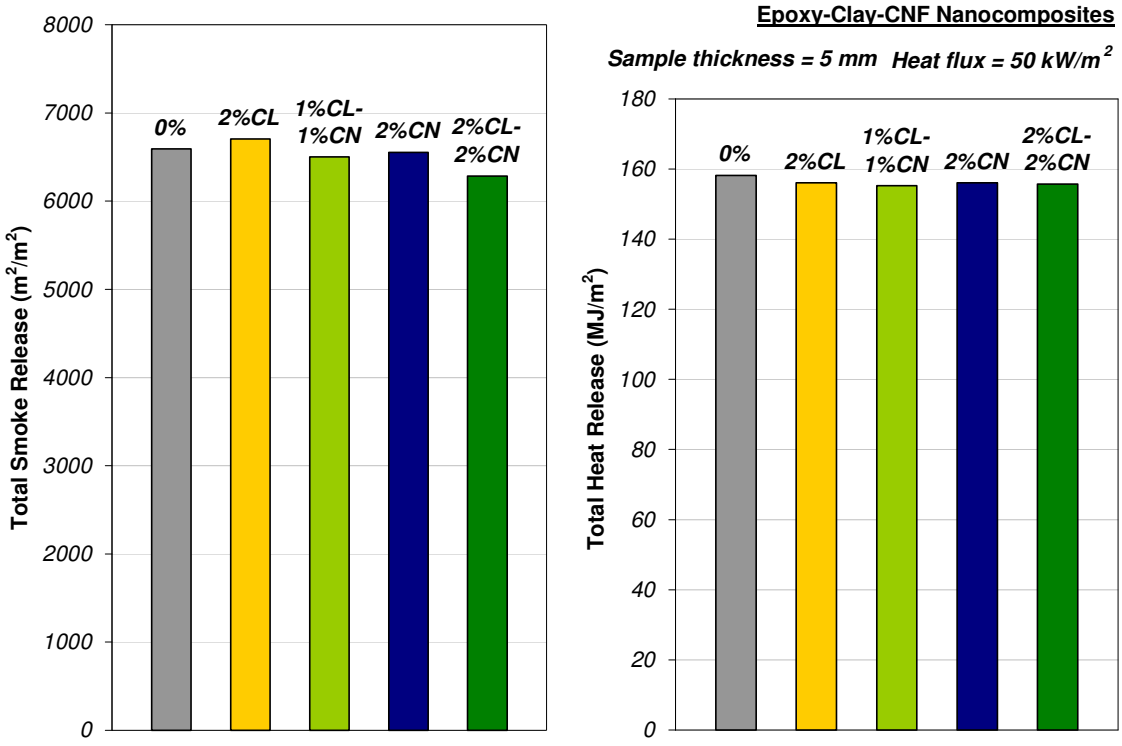

Figure 4.47: Total Smoke Release and Total Heat Release for epoxy-clay-CNF nanocomposites

Chapter 5

Modeling of stability of nanocomposites columns under fire

5.1 Introduction

Polymer matrix composites, such as epoxy fiberglass, offer many advantages when used as structural elements. Their superior mechanical properties together with their light weight make them a class of materials (or, more correctly, a class of structures) of choice for many applications. One of the benefits is that composites are "design" structures, which means that properties can be optimized and suited for specific functions. This is mainly due to the possibility of orientate the reinforcing fibers, control the fiber volume fraction, use various specific polymer matrix and various type of reinforcements. Recently the use of nanoparticles as modifier for the matrix system has opened new doors for the optimization of the composites properties. Polymer composites offer also high fatigue and corrosion resistance.

One of the principal issues connected with the use of composites is the fire performance. Polymer composites properties can be severely degraded by thermal loading by fire and usually polymers are highly flammable. Epoxy in particular is very flammable, and additives that produce fire mitigation effects usually diminish its mechanical performances.

Fire loading produces reduction of stiffness and ultimate strength, due principally to occurring chemical reactions with consequent change of material composition. Another effect is a severe thermal distribution with high temperatures under which the polymer loose most of its strength. Finally, part of the constituent material burns out (ablation), with consequent

diminishment of the resistant section. All these elements lead to premature failure compared with normally operating conditions.

In this section the stability of structural elements, specifically structural columns will be evaluated. The problem will include the element with one side burning uniformly or with a burning spot, which expand along the thickness and the length of the column. The model will be two-dimensional and time dependent, and it will use the classical theory of beams.

5.2 Buckling of composite structural elements in fire

There is a set of physical, chemical and mechanical phenomena occurring during the process of burning of flammable structural elements. The analysis of these phenomena can be performed taking into account some subset of them, which is suspected as playing the main role. Let's review some simple models reflecting few factors only.

5.2.1 Stability of a column burning uniformly along the span

Let's consider a beam axially loaded in compression (column), which is burning uniformly on one side. The thickness will diminish uniformly along the span. Due to ablation of the cross section produced by burning, the effective stiffness on tension-compression, bending and torsion is decreasing with time. If the dependencies of geometrical parameters on time are known, also the stiffness as function of time is known. Combining loads and geometrical parameters into the equations of mechanics of structures allows finding the critical time of stability of structural element from the beginning of fire. This is important for safety reason, to understand when a structure is about to fail, and thus when people or things need to be evacuated.

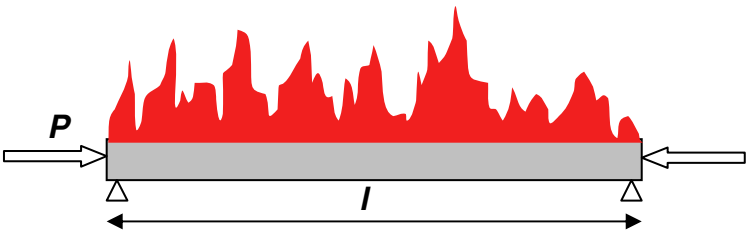

Figure 5.1: column burning uniformly along the span

Let's review the simple case of Euler instability of a column, without burning spot. Using the elementary derivation of the Euler formula with moment due to compression force, we can find the governing equation:

$$EI\frac{d^2w}{dx^2} = M \quad \text{with} \quad M = -P \cdot w \tag{5.1}$$

where w is the deflection, x the coordinate in the longitudinal direction of the column, M the momentum, P the load applied, E the elastic modulus, and I the moment of inertia. The equation of pure buckling becomes

$$EI\frac{d^2w}{dx^2} + Pw = 0$$

$$\frac{d^2w}{dx^2} + k^2 w = 0 \quad \text{with} \quad k^2 = \frac{P}{EI}$$

The general solution is

$$w = C_1 \sin kx + C_2 \cos kx$$

For the simply supported column the boundary conditions are

$$w = 0 \text{ at } x = 0 \text{ and } x = l$$

From the first condition we have

$$C_2 = 0$$

and from the second condition

$C_1 \sin kl = 0$, which leads to $kl = n\pi$

The minimal non-zero root for the first mode is

$$k = \frac{\pi}{l}$$

with Euler load becoming

$$P_E = \frac{\pi^2 EI}{l^2}$$

Let's denote the regular axial compressive load as *P*, which is less than the Euler critical load P_E. In the case of uniformly decreasing thickness of the column along its length, we can find, from Euler formula the critical time of buckling.

$$P_E = \frac{\pi^2 EI}{(\upsilon l)^2}$$

where υ is a factor depending from the type of supports. For rectangular cross-section

$$I = \frac{b[h(t)]^3}{12}$$

where *b* is the width of the column, and *h(t)* is the thickness, which depends on time due to burning. The function *h(t)* is known, and it is possible to find the inversed function of the critical thickness:

$$h_{cr}(t) = \sqrt[3]{\frac{12P(\upsilon l)^2}{\pi^2 Eb}}$$

For example, if the thickness is a linear function of time, we have

$$h = h_0\left(1 - \frac{t}{\tau}\right)$$

where τ is the time of total burning, i.e. the time when all the column burns out, and h_0 is initial thickness.

The critical time will be

$$t_{cr} = \tau\left[1 - \frac{1}{h_0}\sqrt[3]{\frac{12P(\upsilon l)^2}{\pi^2 Eb}}\right]$$

or, taking into account value of critical Euler load P_{cr} for the initial cross section

$$P_{cr} = \frac{\pi^2 E}{(\upsilon l)^2}\frac{bh_0^3}{12}$$

$$h_0 = \sqrt[3]{\frac{12P_E(\upsilon l)^2}{\pi^2 Eb}}$$

we will receive the following elementary formula

$$t_{cr} = \tau\left(1 - \sqrt[3]{\frac{P}{P_{cr}}}\right) \tag{5.2}$$

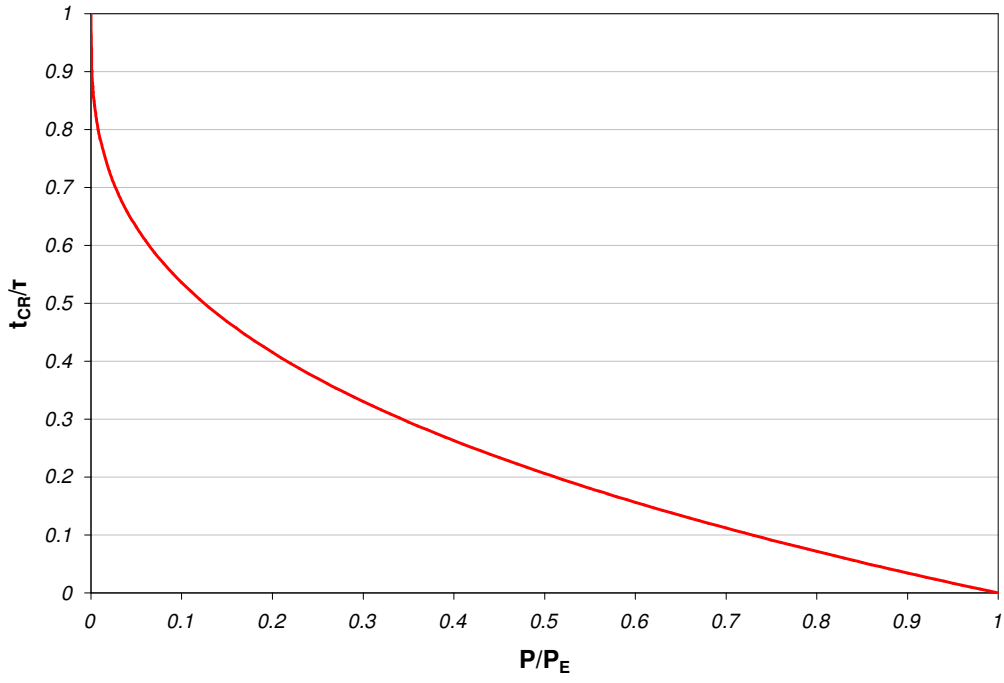

Figure 5.2: non-dimensional critical time (time of instability) vs. non-dimensional load for a column burning uniformly along the span

Figure 5.2 shows the time of instability in relation with the load applied. For loads equal to the Euler load, i.e. $P/P_{cr}=1$, instability occurs instantaneously, and for no load applied, failure occurs at the time τ, which is when the column burns completely. All other cases occur in between.

Other factors that influence the stability of a structural element under fire are dependency of elastic characteristics on temperature, effect of linear thermal expansion, acceleration of creep with temperature, and change of eccentricity of applied load with time of unilateral burning in buckling problems.

5.2.2 Stability of a column burning non-uniformly with central burning spot

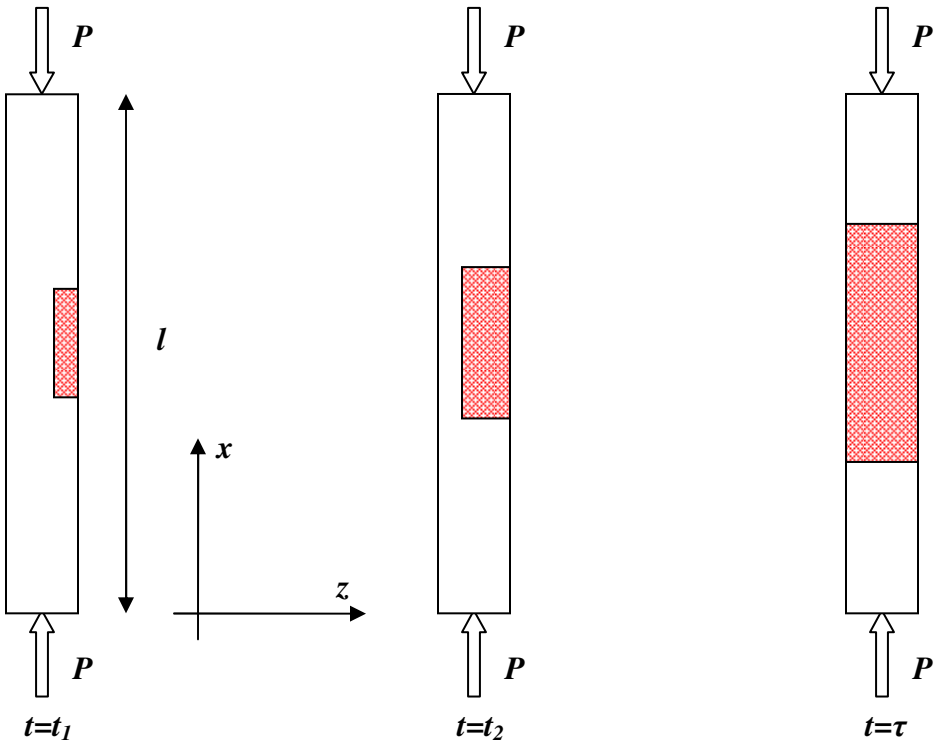

Figure 5.3: depiction of the column with a burning spot in the middle at different time frames

Let's consider a column simply supported at its extremes loaded with a longitudinal force *P*. In the middle part of the column a spot is burning continuously, ablating material and reducing the resistant section. For simplicity, the burning spot is assumed rectangular, as depicted in figure 5.3. For our problem of rectangular burning spot in the middle of the column, we can divide the structure in three areas as depicted in figure 5.4.

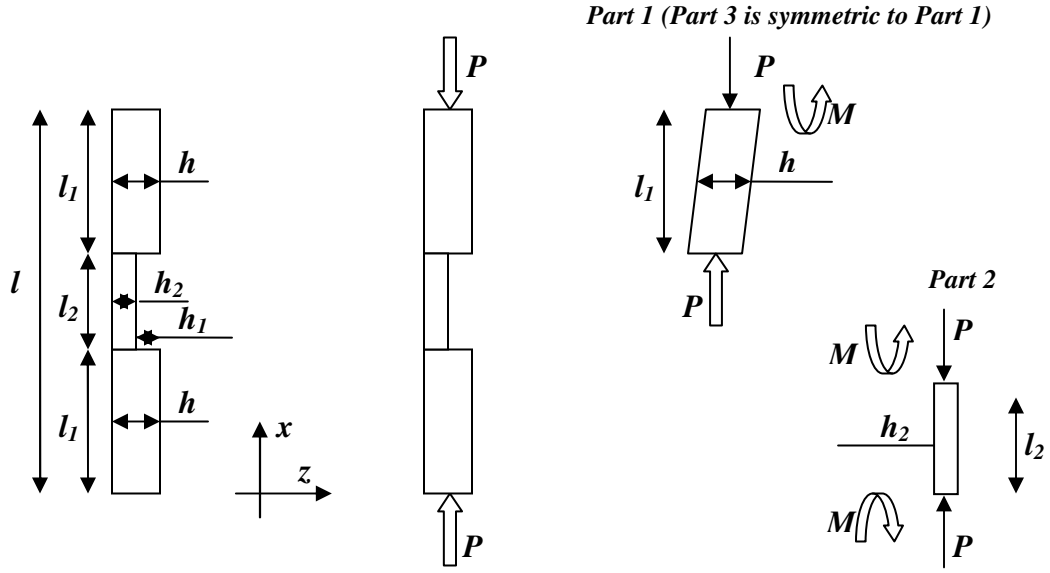

Figure 5.4: equilibrium of a column with a burning spot in the middle

From static equilibrium

$$|M| = P\frac{h-h_2}{2} = P\frac{h_1}{2}$$

The governing equations for the part 1 and 3 are

$$\frac{d^2 w^{(1)}}{dx^2} + k^2 w^{(1)} = 0 \tag{5.3}$$

with $k^2 = \frac{P}{EI}$, $I = \frac{bh^3}{12}$

The second (central) part governing equation is

$$\frac{d^2 w^{(2)}}{dx^2} + k_2^2 \left[w^{(2)} - \frac{h_1}{2} \right] = 0 \tag{5.4}$$

with $k_2^2 = \frac{P}{EI_2}$, $I_2 = \frac{bh_2^{\ 3}}{12}$

The solutions are

$$\begin{aligned} w^{(1)} &= C_1 \sin kx + C_2 \cos kx \\ w^{(2)} &= C_3 \sin k_2 x + C_4 \cos k_2 x + \frac{h_1}{2} \end{aligned} \tag{5.5}$$

We have four unknown ($C_{1,2,3,4}$) so we need four boundary/interface conditions:

$$w^{(1)} = 0 \text{, at } x = 0 \tag{5.6a}$$

$$\frac{dw^{(2)}}{dx} = 0 \text{, at } x = l_1 + \frac{l_2}{2} = \frac{l}{2} \text{ (condition of symmetry)} \tag{5.6b}$$

$$w^{(1)} = w^{(2)} \text{, at } x = l_1 \tag{5.6c}$$

$$\frac{dw^{(1)}}{dx} = \frac{dw^{(2)}}{dx} \text{, at } x = l_1 \tag{5.6d}$$

Imposing the boundary conditions, we can calculate the unknown coefficients and thus the displacements for each individual section of the column.

From (5.6a) we easily obtain

$$C_2 = 0$$

Using the condition of symmetry (5.6b) we can find

$$C_3 k_2 \cos\left(k_2 \frac{l}{2} \right) - C_4 k_2 \sin\left(k_2 \frac{l}{2} \right) = 0$$

Or $C_3 = C_4 \tan\left(k_2 \frac{l}{2} \right)$ (5.7)

From (5.6d) we obtain

$$C_1 k \cos kl_1 = C_3 k_2 \cos k_2 l_1 - C_4 k_2 \sin k_2 l_1$$

this can be written as

$$C_1 k \cos kl_1 = C_4 k_2 \left[\tan\left(k_2 \frac{l}{2} \right) \cos k_2 l_1 - \sin k_2 l_1 \right]$$

Multiplying the factor in square bracket by $\cos\left(k_2 \frac{l}{2} \right)$ and using the formulae of trigonometry for addition and subtraction of angles (knowing that $\frac{l}{2} = l_1 + \frac{l_2}{2}$), we obtain

$$C_1 = C_4 \frac{k_2 \sin\left(k_2 \frac{l_2}{2} \right)}{k \cos(kl_1) \cos\left(k_2 \frac{l}{2} \right)} \tag{5.8}$$

From (5.6c) we can write

$$C_1 \sin kl_1 = C_3 \sin k_2 l_1 + C_4 \cos k_2 l_1 + \frac{h_1}{2}$$

Substituting (5.7) we get

$$C_1 \sin(kl_1) = C_4 \left[\tan\left(k_2 \frac{l}{2} \right) \sin(k_2 l_1) - \cos(k_2 l_1) \right] + \frac{h_1}{2} \tag{5.9}$$

Using again the formulae of trigonometry for addition and subtraction of angles, we obtain

$$C_1 \sin(kl_1) = C_4 \frac{\cos\left(k_2 \frac{l_2}{2} \right)}{\cos\left(k_2 \frac{l}{2} \right)} + \frac{h_1}{2}$$

Combining (5.8) and (5.9) we can obtain C_4

$$C_4\left[\frac{k_2\sin\left(k_2\frac{l_2}{2}\right)\sin(kl_1)}{k\cos(kl_1)\cos\left(k_2\frac{l}{2}\right)}-\frac{\cos\left(k_2\frac{l_2}{2}\right)}{\cos\left(k_2\frac{l}{2}\right)}\right]=\frac{h_1}{2}$$

or

$$C_4\left[\frac{\frac{k_2}{k}\sin\left(k_2\frac{l_2}{2}\right)\tan(kl_1)-\cos\left(k_2\frac{l_2}{2}\right)}{\cos\left(k_2\frac{l}{2}\right)}\right]=\frac{h_1}{2}$$

This can be simplified with the formulae of trigonometry of addition and subtraction of angles into

$$C_4=\frac{h_1}{2}\frac{\cos\left(k_2\frac{l}{2}\right)}{\cos\left(k_2\frac{l_2}{2}\right)\cdot A} \tag{5.10}$$

where

$$A=\frac{k_2}{k}\tan\left(k_2\frac{l_2}{2}\right)\tan(kl_1)-1 \tag{5.11}$$

Using (5.7) and (5.8), we can find C_3 and C_1

$$C_3=\frac{h_1}{2}\frac{\sin\left(k_2\frac{l}{2}\right)}{\cos\left(k_2\frac{l_2}{2}\right)\cdot A} \tag{5.12}$$

$$C_1=\frac{h_1}{2}\frac{\frac{k_2}{k}\tan\left(k_2\frac{l_2}{2}\right)}{\cos(kl_1)\cdot A} \tag{5.13}$$

Now let us rewrite the coefficients and the deflections using non-dimensional terms. If we take into account that

$$\frac{k_2}{k} = \sqrt{\left(\frac{h}{h_2}\right)^3}$$

and that τ is the time of completely burning along the thickness h, and t is the time elapsed to burn the thickness $(h-h_2)=h_1$, k_2 will be

$$\frac{k_2}{k} = \left(\frac{h}{h_2}\right)^{\frac{3}{2}} = \left(\frac{\tau}{\tau - t}\right)^{\frac{3}{2}} = \left(\frac{1}{1-\bar{t}}\right)^{\frac{3}{2}} \tag{5.14}$$

where $\bar{t} = t/\tau$ is the non-dimensional time of burning.

Taking into account the Euler's load for instability of a non-damaged (by flame) column:

$$P_E = \frac{\pi^2 EI}{l^2}$$

we can write

$$k^2 = \frac{P}{EI} = \frac{\pi^2 P}{P_E l^2}$$

$$k = \frac{\pi}{l}\sqrt{\bar{P}} \tag{5.15}$$

where $\bar{P} = \frac{P}{P_E}$ is the non-dimensional applied load.

We suppose that the aspect ratio of the burning spot created by flame remains constant in time:

$$\frac{l_2}{h - h_2} = \frac{l_2}{h_1} = \mu = const \tag{5.16}$$

We can write also

$$\frac{h_1}{h} = \frac{t}{\tau} = \bar{t} \tag{5.17}$$

Considering also that

$$l = 2l_1 + l_2 \tag{5.18a}$$

$$\bar{h} = \frac{h}{l} \text{ (column aspect ratio)} \tag{5.18b}$$

combining (5.15), (5.16), (5.17), and (5.18a,b) we can write

$$k_2 \frac{l_2}{2} = k\left(\frac{1}{1-\bar{t}}\right)^{\frac{3}{2}} \cdot \frac{1}{2}\mu\bar{h}\bar{t} = \frac{\pi}{2}\sqrt{\bar{P}}\,\frac{\mu\bar{h}\bar{t}}{\left(1-\bar{t}\right)^{\frac{3}{2}}} \tag{5.19}$$

$$kl_1 = k\frac{1}{2}\left(l - l_2\right) = \frac{1}{2}kl\left(1-\mu\bar{h}\bar{t}\right) = \frac{\pi}{2}\sqrt{\bar{P}}\left(1-\mu\bar{h}\bar{t}\right) \tag{5.20}$$

$$k_2 \frac{l}{2} = k\left(\frac{1}{1-\bar{t}}\right)^{\frac{3}{2}} \frac{l}{2} = \frac{\pi}{2}\sqrt{\bar{P}}\,\frac{1}{\left(1-\bar{t}\right)^{\frac{3}{2}}} \tag{5.21}$$

Using (5.19), (5.20), and (5.21) we can rewrite the coefficient $C_{1,\,3,\,4}$ and A

$$C_1 = \frac{h_1}{2}\frac{\left(\frac{1}{1-\bar{t}}\right)^{\frac{3}{2}} \tan\left(\frac{\pi}{2}\sqrt{\bar{P}}\,\frac{\mu\bar{h}\bar{t}}{\left(1-\bar{t}\right)^{\frac{3}{2}}}\right)}{\cos\left(\frac{\pi}{2}\sqrt{\bar{P}}\left(1-\mu\bar{h}\bar{t}\right)\right)\cdot A} \tag{5.22}$$

$$C_3 = \frac{h_1}{2}\frac{\sin\left(\frac{\pi}{2}\sqrt{\bar{P}}\,\frac{1}{\left(1-\bar{t}\right)^{\frac{3}{2}}}\right)}{\cos\left(\frac{\pi}{2}\sqrt{\bar{P}}\,\frac{\mu\bar{h}\bar{t}}{\left(1-\bar{t}\right)^{\frac{3}{2}}}\right)\cdot A} \tag{5.23}$$

$$C_4 = \frac{h_1}{2}\frac{\cos\left(\frac{\pi}{2}\sqrt{\bar{P}}\,\frac{1}{\left(1-\bar{t}\right)^{\frac{3}{2}}}\right)}{\cos\left(\frac{\pi}{2}\sqrt{\bar{P}}\,\frac{\mu\bar{h}\bar{t}}{\left(1-\bar{t}\right)^{\frac{3}{2}}}\right)\cdot A} \tag{5.24}$$

$$A = \left(\frac{1}{1-\bar{t}}\right)^{\frac{3}{2}} \tan\left(\frac{\pi}{2}\sqrt{\bar{P}}\,\frac{\mu\bar{h}\bar{t}}{\left(1-\bar{t}\right)^{\frac{3}{2}}}\right)\tan\left(\frac{\pi}{2}\sqrt{\bar{P}}\left(1-\mu\bar{h}\bar{t}\right)\right) - 1 \tag{5.25}$$

Instability occurs when the deflections w_1 and w_2 go to infinity, and thus when the coefficients $C_{1,\,3,\,4}$ go to infinity. Every coefficient goes to infinity when A goes to zero. The other arguments at the denominator, i.e. $\cos(kl_1)$ and $\cos(k_2 l_2/2)$ can be disregarded, because the former cannot go to zero, since the argument is between 0 and never reach $\pi/2$ and the latter goes to 0 when the argument goes to $\pi/2$. However, for this case, A goes to infinity faster, because the same argument is now for the tangent. Thus, the coefficient goes to zero and not to infinity. This means that to study the instability, it is sufficient to calculate when A goes to zero. This can be solved numerically using commercially available programs.

$\bar{t}$ is the non-dimensional time elapsed, which varies from 0 to 1, i.e. between 0 and when $t = \tau$, which means that the column burned all materials along the thickness h and practically the column is separated in two parts. $\overline{P}$ is the load applied, which varies from 0 to 1, i.e. between 0 and when the load is equal to the Euler's load for instability without burning. At this particular load the column buckles immediately. μ is a parameter indicating the ratio of material burned in the longitudinal and through the thickness directions (x and z directions). μ varies from 0 to practically no limit, and when μ is equal to 1, we have isotropic burning, equal in all directions. If μ is large enough that the flame propagates all along l before going through the thickness h, the problem at this particular time frame becomes the problem of a beam burning uniformly along the span. This problem was previously analyzed. For this case the thickness is $h_2 = h - l/\mu$, and the theory for a column burning uniformly along the span can be used. Excluding this case we can say that μ varies from 0 to $1/\overline{h}$, which corresponds to the case of flame reaching the extremes of the column and burning all through the thickness at the exact same time frame. Finally we can say that for our purpose of analyzing column with classical beam theory $\overline{h}$ varies

from *0.01* to *0.2* (column aspect ratio), which means a column that have the length *5* to *100* times the thickness.

To find the roots of equation *A=0*, we need to plot the function on the right side of the equal sign and see when it intercepts the *x* axis. Using MathCAD for example, it is possible to find the value with very high precision. There are many points in which the function crosses the *x* axis, but we are interested only in the first one, corresponding to the first mode of buckling.

Using $\bar{t}$ as the independent variable and $\overline{P}$ as parameters we can plot the function as shown in figure 5.5. In this picture the load is considered 40% of the Euler's load, and the product $\mu \cdot \bar{h}$ between the burning ratio and the aspect ratio is a geometric parameter and it is imposed equal to *0.8*.

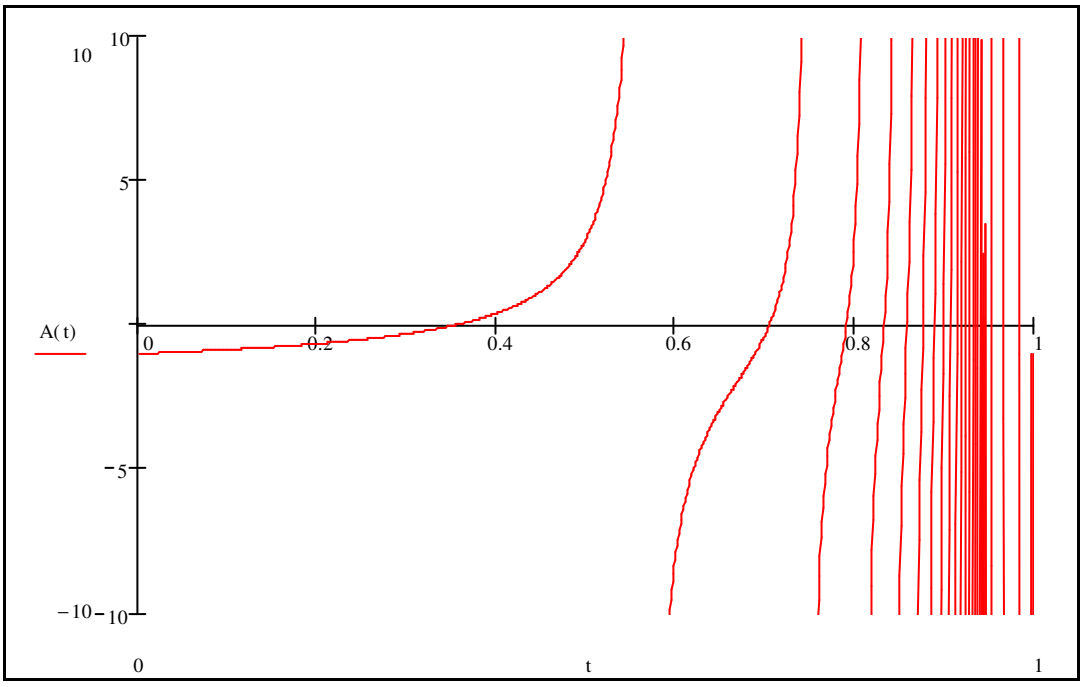

Figure 5.5: representation of the function *A(t)* for central burning spot with $P/P_E=0.4$ and $\mu h/l=0.8$

Now let's plot different function with different parameters P/P_E and $\mu h/l$ to see their effect. As we can observe in figure 5.6a,b,c,d, as the load increases, the time of instability decreases, as expected. In figure 5.7, the parameter $\mu h/l$ is varied. As $\mu h/l$ increases, situation that corresponds to increase of aspect ratio and/or increase of burning ratio (the column burns faster in the longitudinal direction), the time of instability decreases. This must not be misunderstood, because we are looking to different aspect ratios in some cases, so the Euler load changes. It is helpful anyway when we have as our input the burning ratio and the aspect ratio, the load applied and the initial Euler load of instability. For this case the non-dimensional time will be found easily with these graphs.

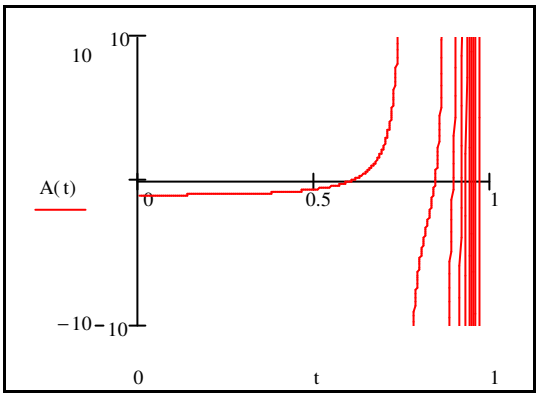

(a) P/P_E=0.1, $\mu h/l$=0.5

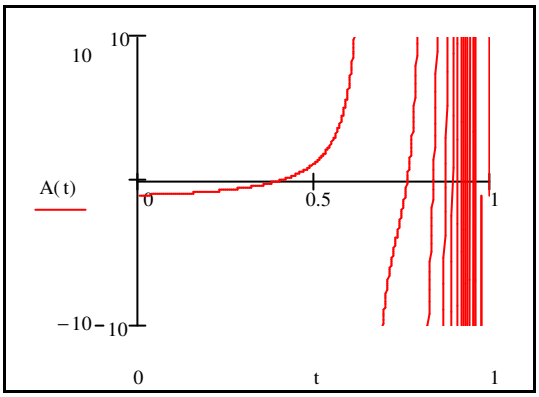

(b) P/P_E=0.4, $\mu h/l$=0.5

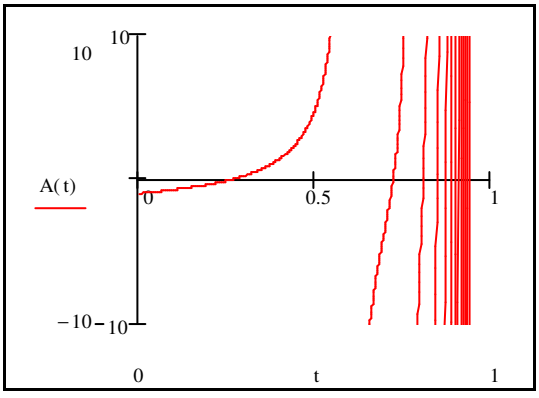

(c) P/P_E=0.7, $\mu h/l$=0.5

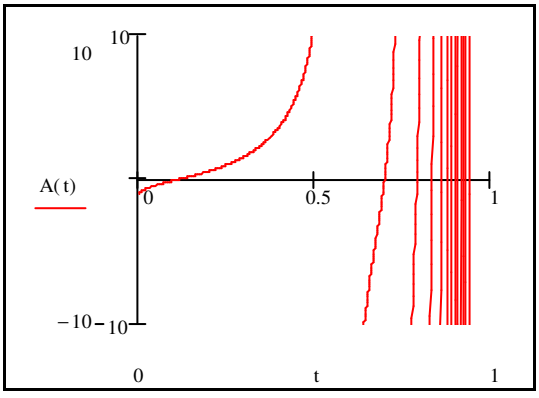

(d) P/P_E=0.95, $\mu h/l$=0.5

Figure 5.6: representation of the function for different values of non-dimensional load P/P_E

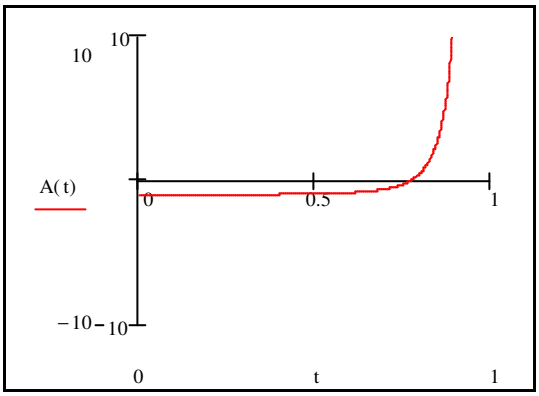

(a) ***P/P$_E$=0.4, μh/l=0.01***

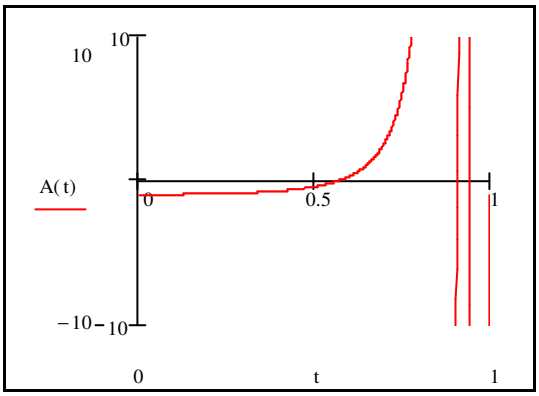

(b) ***P/P$_E$=0.4, μh/l=0.1***

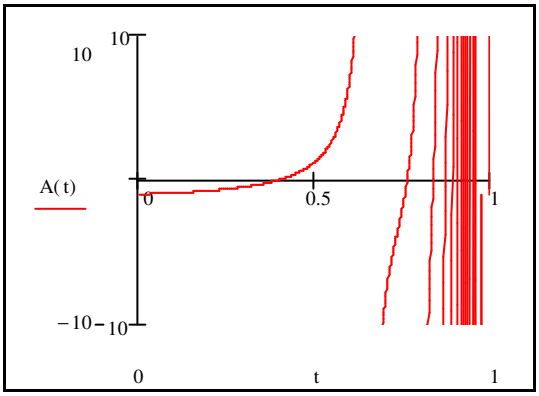

(a) ***P/P$_E$=0.4, μh/l=0.5***

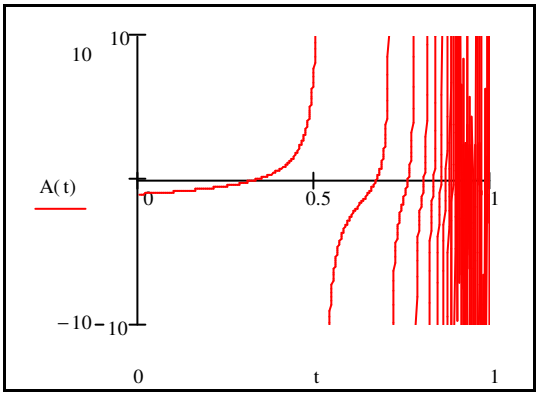

(b) ***P/P$_E$=0.4, μh/l=1***

Figure 5.7: representation of the function for different values of non dimensional load *μh/l*

Now let's plot the time of instability versus the applied load for different a parameter called *B* (figure 5.8), where

$$B = \frac{\mu h}{l}$$

As *B* decreases the non-dimensional time of buckling is in general higher for $0<P/P_E<1$. Lower values of *B* must be carefully interpreted, since *B* includes both aspect ratio and burning ratio. Comparing different aspect ratios means also a change in P_E, which means different Euler loads and different non-dimensional loads. Therefore, besides the non-dimensional load is the same, the actual applied load might sensibly vary, and consequently the time of buckling

corresponds to different actual loads. This need to be analyzed more in details, but before it is useful to compare the results for the same aspect ratio $\bar{h}$ (figure 5.9). No matter what the aspect ratio is, instability occurs first in the beam burning uniformly. This is explainable considering that the resistant thickness diminishes from the beginning for the beam burning uniformly, while for the other cases the upper and lower part still preserve the original thickness, increasing the resistance. Also in the plots of figure 5.9 and 5.10, the similar curves are plotted, but they correspond to different burning ratios and aspect ratio. This doesn't mean that the two columns behave the same way, since the Euler load changes for these two cases, and as a consequence the applied load P.

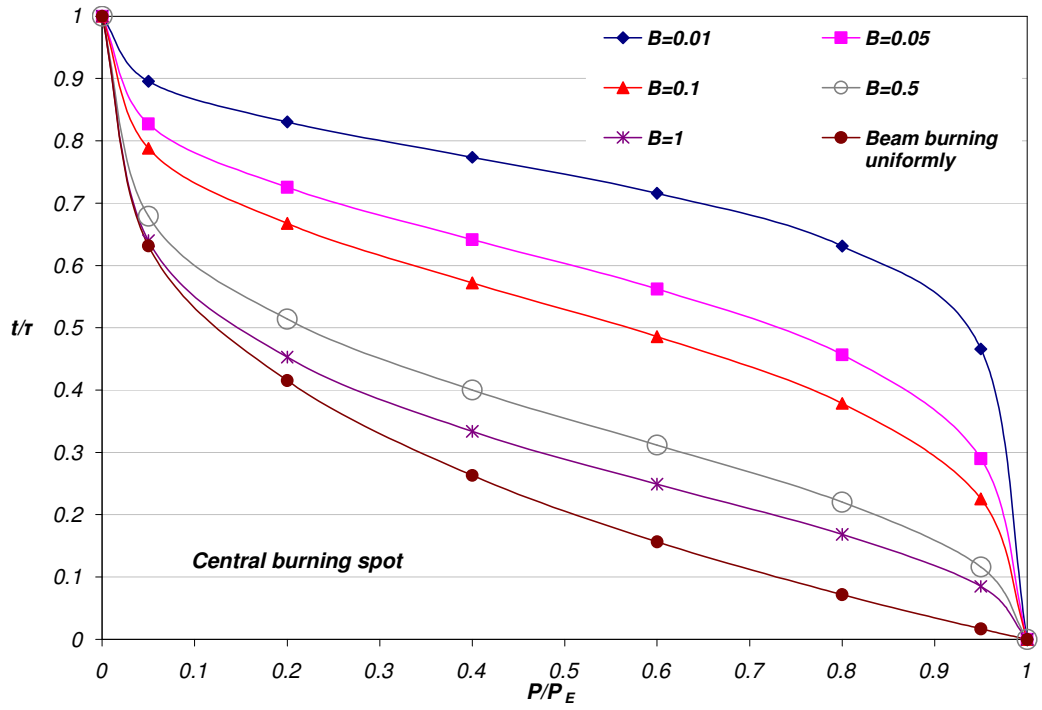

Figure 5.8: time of buckling versus applied load for different aspect ratios and burning ratio

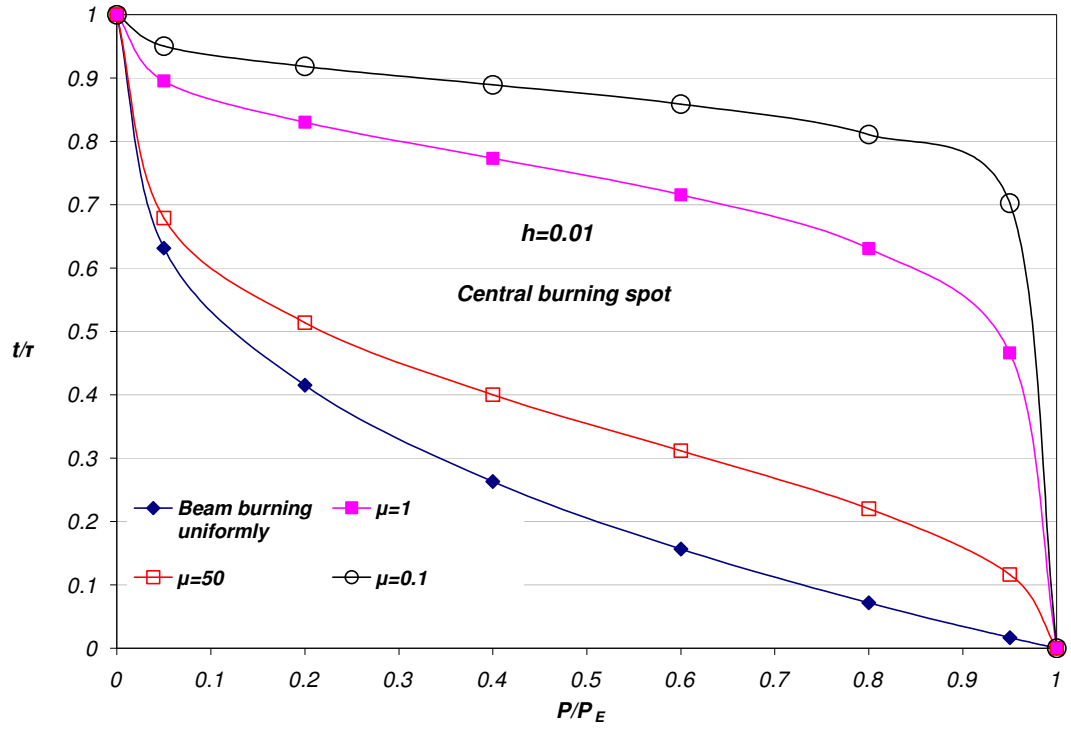

Figure 5.9: non dimensional time of buckling for different burning ratios and for aspect ratio 1/100

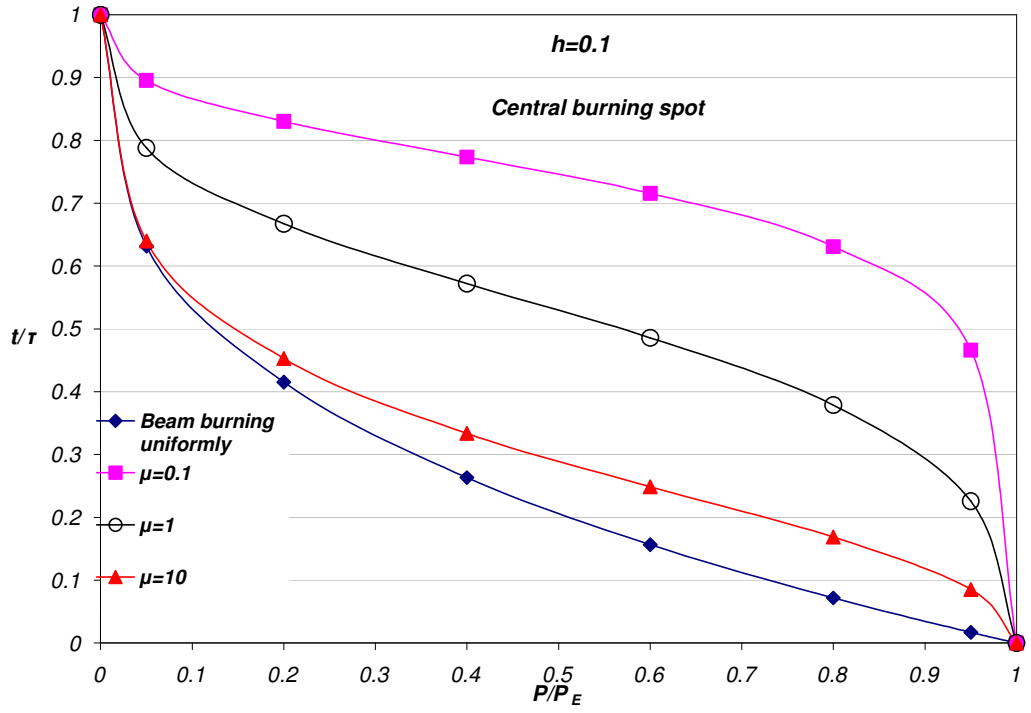

Figure 5.9: non dimensional time of buckling for different burning ratios and for aspect ratio 1/10

5.2.3 Stability of a column burning non-uniformly with burning spot at a corner

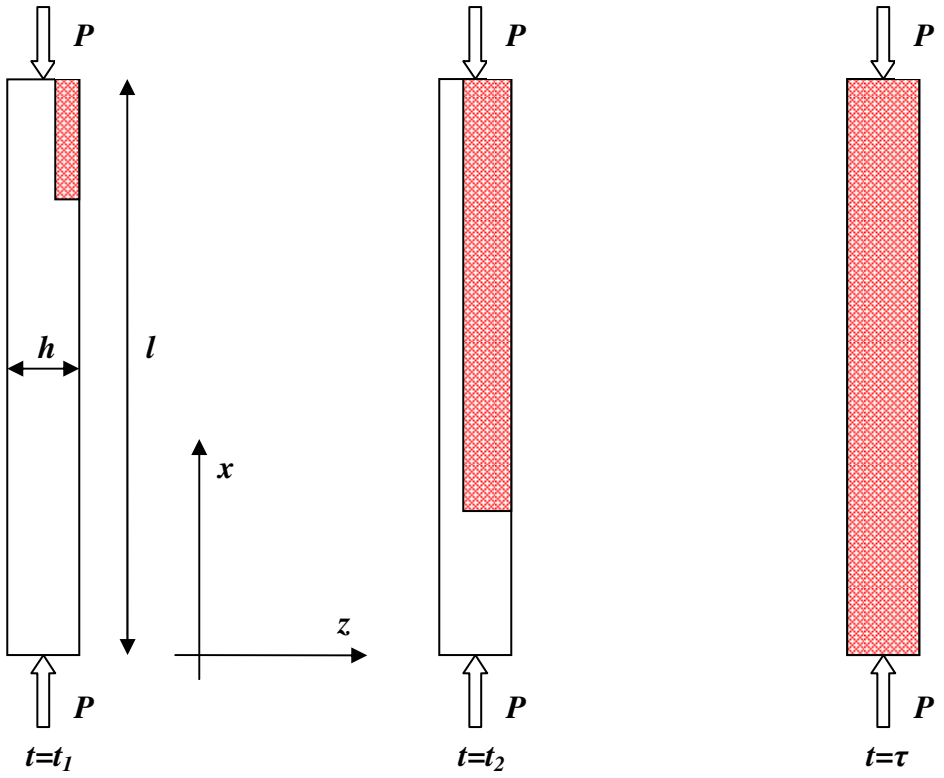

Figure 5.11: depiction of the column burning in the corner at different time frames

Figure 5.11 represents a column with a burning spot which starts from one of the corner, creating a non-symmetrical configuration. We can divide our model in two areas as depicted in figure 5.12.

For this case, equilibrium and governing equation will look differently than the case with burning spot at the middle of the beam. Since the upper part is burning and it is ablated, the applied load will be not anymore acting along the central longitudinal axis of the beam, but it will move along with the burning process. This will create a moment that is equilibrated with reaction forces ($V_{A,B}$) acting at the extremes of the beam, like depicted in figure 5.12.

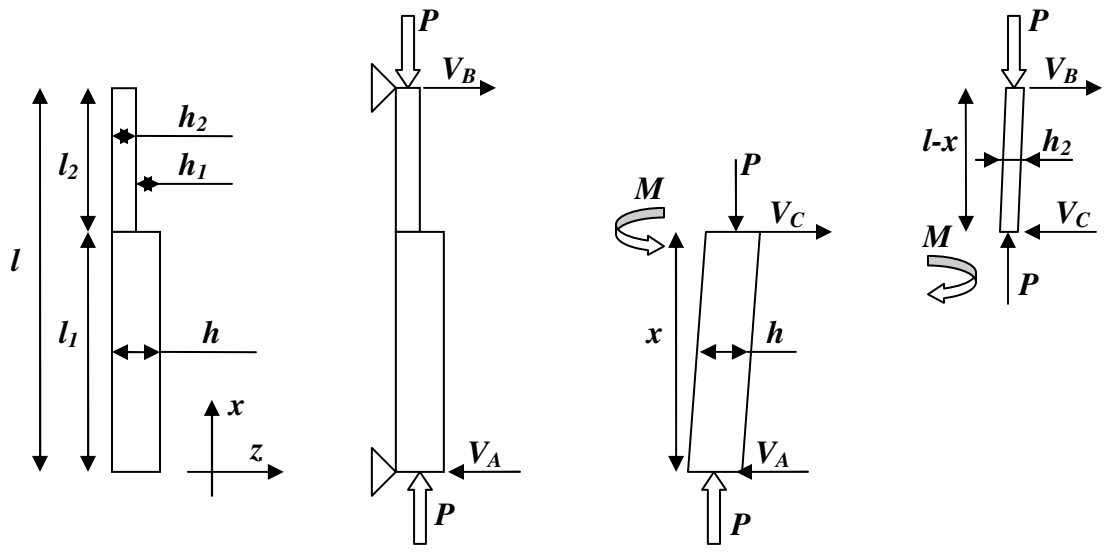

Figure 5.12: equilibrium of the different parts of the burning column

From static equilibrium

$$V_{A,B,C} \cdot l = P\frac{h-h_2}{2}$$

$$V_{A,B,C} = P\frac{h_1}{2l}$$

The governing equations for the part 1 and 2 are

$$EI\frac{d^2w}{dx^2} = M$$

$$M^{(1)} = -P \cdot w^{(1)} - V_A \cdot x = -P\left(w^{(1)} + \frac{h_1}{2}\frac{x}{l}\right)$$

$$M^{(2)} = P \cdot w^{(2)} - V_B \cdot (l-x) = P\left(w^{(2)} - \frac{h_1}{2}\frac{l-x}{l}\right)$$

$$\frac{d^2w^{(1)}}{dx^2} + k^2\left(w + \frac{h_1}{2}\frac{x}{l}\right) = 0$$

$$\frac{d^2w^{(2)}}{dx^2} + k_2^2\left(w - \frac{h_1}{2}\frac{l-x}{l}\right) = 0$$

with $k^2 = \frac{P}{EI}$ and $k_2^2 = \frac{P}{EI_2}$

$$I = \frac{bh^3}{12} \qquad I_2 = \frac{bh_2{}^3}{12}$$

The solutions are

$$w^{(1)} = C_1 \sin kx + C_2 \cos kx - \frac{h_1}{2}\frac{x}{l}$$
$$w^{(2)} = C_3 \sin k_2 x + C_4 \cos k_2 x + \frac{h_1}{2}\frac{l-x}{l}$$

We have four unknown ($C_{1,2,3,4}$) so we need four boundary/interface conditions:

$w^{(1)} = 0$, at $x = 0$ (5.25a)

$w^{(1)} = w^{(2)}$, at $x = l_1$ (5.25b)

$\frac{dw^{(1)}}{dx} = \frac{dw^{(2)}}{dx}$, at $x = l_1$ (5.25c)

$w^{(2)} = 0$, at $x = l$ (5.25d)

From the first boundary condition (5.25a) we can find that

$C_2 = 0$

From the boundary condition (5.25d) we can easily find that

$C_4 = -C_3 \tan(k_2 l)$ (5.26)

From boundary condition (5.25c) and (5.26) we obtain

$$C_1 = \frac{1}{k\cos(kl_1)} C_3 \left[k_2 \cos(k_2 l_1) + k_2 \tan(k_2 l)\sin(k_2 l_1)\right]$$

Multiplying the factor in square bracket by $\cos(k_2 l)$ and using the formulae of trigonometry for addition and subtraction of angles (knowing that $l = l_1 + l_2$), we obtain

$$C_1 = C_3 \frac{k_2 \cos(k_2 l_2)}{k \cos(k l_1) \cos(k_2 l)} \tag{5.27}$$

From boundary condition (5.25b) and the expression (5.26) and (5.27) we obtain the expression

$$C_3 \frac{k_2 \sin(k l_1) \cos(k_2 l_2)}{k \cos(k l_1) \cos(k_2 l)} - \frac{h_1 l_1}{2l} = C_3 \sin(k_2 l_1) - C_3 \tan(k_2 l) \cos(k_2 l_1) + \frac{h_1 (l - l_1)}{2l}$$

and using again the formulae of trigonometry for addition and subtraction of angles

$$C_3 \frac{k_2 \tan(k l_1) \cos(k_2 l_2)}{k \cos(k_2 l)} = C_3 \left[\frac{-\sin(k_2 l_2)}{\cos(k_2 l)} \right] + \frac{h_1 l}{2l}$$

Rearranging the above equation, and solving for C_3, we obtain

$$C_3 = \frac{h_1}{2} \frac{k \cos(k_2 l)}{k_2 \tan(k l_1) \cos(k_2 l_2) + k \sin(k_2 l_2)}$$

which can be rewritten as

$$C_3 = \frac{h_1}{2} \frac{\cos(k_2 l)}{\cos(k_2 l_2) \cdot A} \tag{5.28}$$

where

$$A = \frac{k_2}{k} \tan(k l_1) + \tan(k_2 l_2) \tag{5.29}$$

Combining (5.28) and (5.26), we obtain

$$C_4 = -\frac{h_1}{2} \frac{\sin(k_2 l)}{\cos(k_2 l_2) \cdot A} \tag{5.30}$$

Substituting (5.28) into (5.27), we obtain the last coefficient for the deflection of the burning beam

$$C_1 = \frac{h_1}{2} \frac{k_2 / k}{\cos(k l_1) \cdot A} \tag{5.31}$$

Like for the previous problem, when the burning spot was in the middle of the span of the column, we can write the deflection coefficient in terms of non-dimensional parameters:

$$\bar{h} = \frac{h}{l}$$
$$\mu = \frac{l_2}{h_1}$$
$$\bar{t} = \frac{t}{\tau}$$
$$\bar{P} = \frac{P}{P_E}$$

The arguments of the trigonometric functions in the coefficients will be the following:

$$\frac{k_2}{k} = \frac{1}{\left(1-\bar{t}\right)^{\frac{3}{2}}}$$
$$kl_1 = \pi\sqrt{\bar{P}}\left(1-\mu\bar{h}\bar{t}\right)$$
$$k_2 l_2 = \pi\sqrt{\bar{P}}\,\frac{\mu\bar{h}\bar{t}}{\left(1-\bar{t}\right)^{\frac{3}{2}}}$$
$$k_2 l = \pi\sqrt{\bar{P}}\,\frac{1}{\left(1-\bar{t}\right)^{\frac{3}{2}}}$$

The coefficients will assume the following expressions

$$C_1 = \frac{h_1}{2}\frac{1}{\left(1-\bar{t}\right)^{\frac{3}{2}}\cos\left(\pi\sqrt{\bar{P}}\left(1-\mu\bar{h}\bar{t}\right)\right)\cdot A} \tag{5.32}$$

$$C_3 = \frac{h_1}{2}\frac{\cos\left(\pi\sqrt{\bar{P}}\,\frac{1}{\left(1-\bar{t}\right)^{\frac{3}{2}}}\right)}{\cos\left(\pi\sqrt{\bar{P}}\,\frac{\mu\bar{h}\bar{t}}{\left(1-\bar{t}\right)^{\frac{3}{2}}}\right)\cdot A} \tag{5.33}$$

$$C_4 = -\frac{h_1}{2}\frac{\sin\left(\pi\sqrt{\bar{P}}\,\frac{1}{(1-\bar{t})^{\frac{3}{2}}}\right)}{\cos\left(\pi\sqrt{\bar{P}}\,\frac{\mu\bar{h}\bar{t}}{(1-\bar{t})^{\frac{3}{2}}}\right)\cdot A} \tag{5.34}$$

$$A = \frac{1}{(1-\bar{t})^{\frac{3}{2}}}\tan\left(\pi\sqrt{\bar{P}}\left(1-\mu\bar{h}\bar{t}\right)\right)+\tan\left(\pi\sqrt{\bar{P}}\,\frac{\mu\bar{h}\bar{t}}{(1-\bar{t})^{\frac{3}{2}}}\right) \tag{5.35}$$

Instability occurs when the deflection goes to infinity, thus when all coefficient goes to infinity. This takes place when *A* goes to zero. Like previously explained for the case of column burning not uniformly along the span in the center, the cosines at the denominator can be disregarded, and the only possibility that all coefficient go to infinity is for *A=0*. Solving numerically, we can plot the time of instability for different parameters.

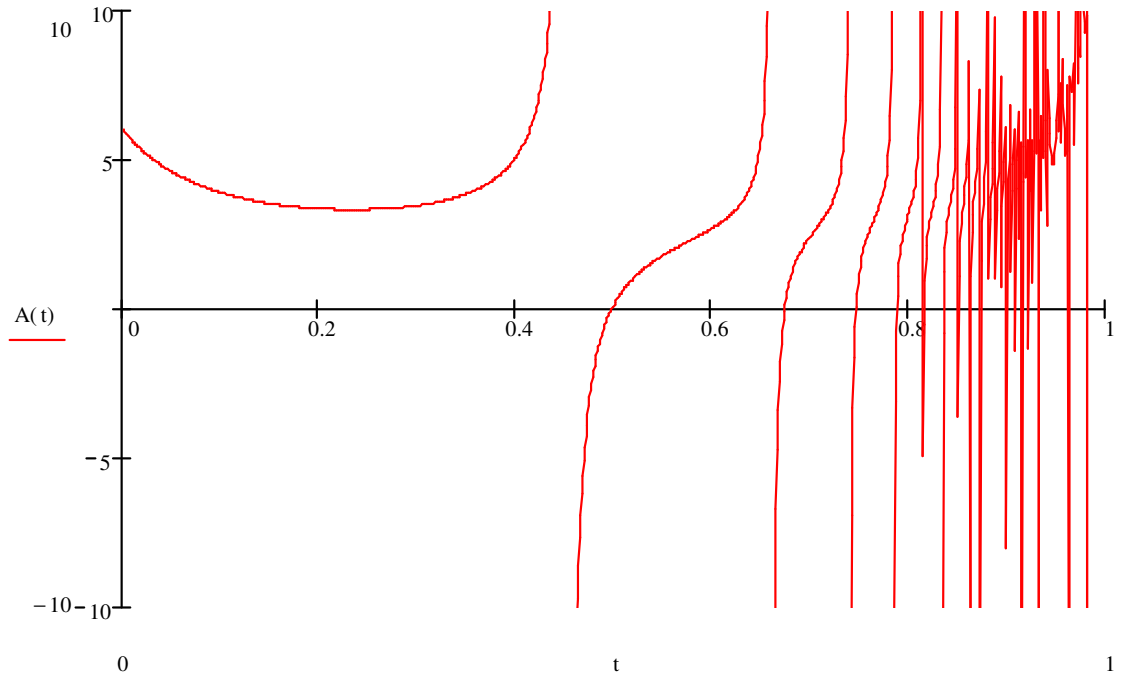

Figure 5.13: function *A(t)* for corner burning spot for $P/P_E=0.2$ and $\mu h/l=1$

Figures 5.14, 5.15, and 5.16 show the instability time for different values of burning ratio, aspect ratio, at different loads. The lowest time of instability is for column burning uniformly along the span. This is because more material is ablated due to burning for this case. In our model, we do not consider the stress concentration that can occur at the corner of the burning spot, because our model approximates a circular burning spot, where stress concentration does not occur. Moreover, we must consider the plots 5.14, 5.15, and 5.15 to understand the trend for these kind of phenomena, not to compare the different values. A comparison for different materials with the same burning condition will be done in the following section, where the different kind of nanocomposites tested in chapter 4 will be compared for isotropic burning.

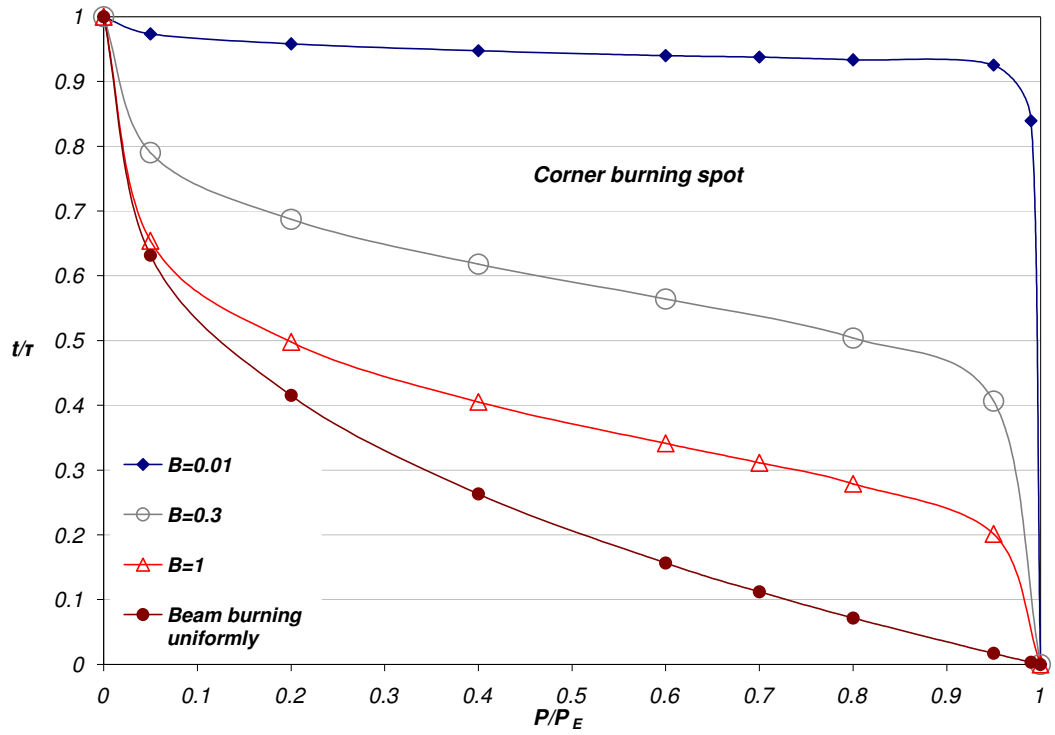

Figure 5.14: time of buckling versus applied load for different aspect ratios and burning ratio for burning spot on the corner of the column

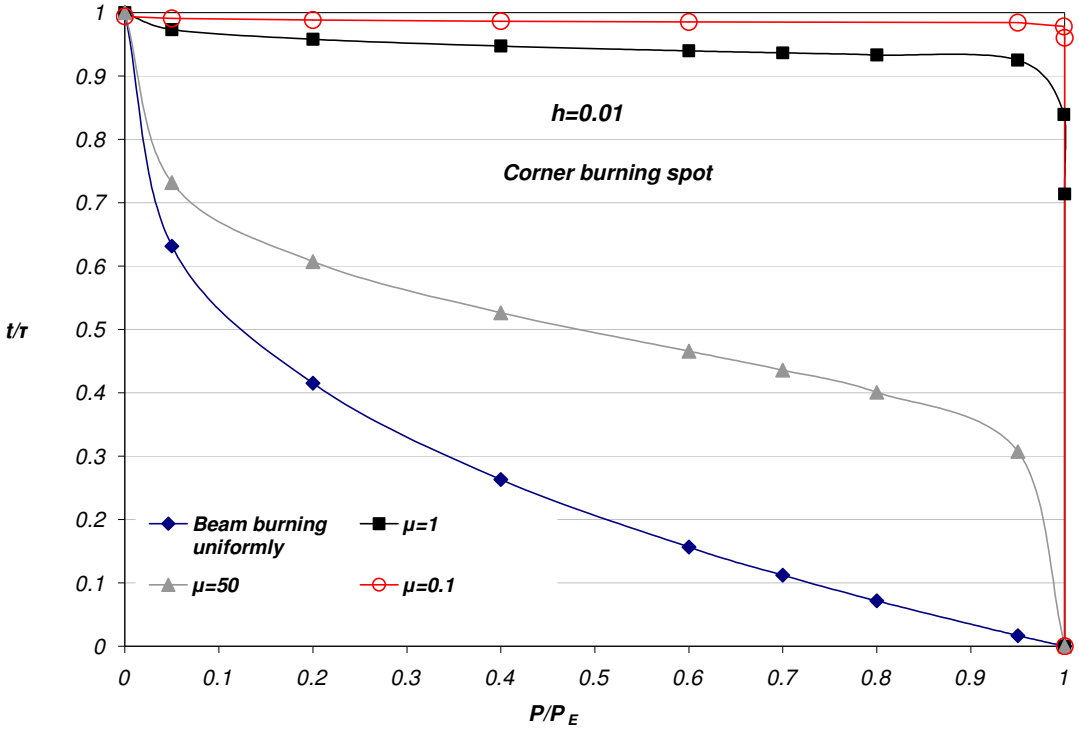

Figure 5.15: non-dimensional time of buckling for different burning ratios and for column aspect ratio 1/100

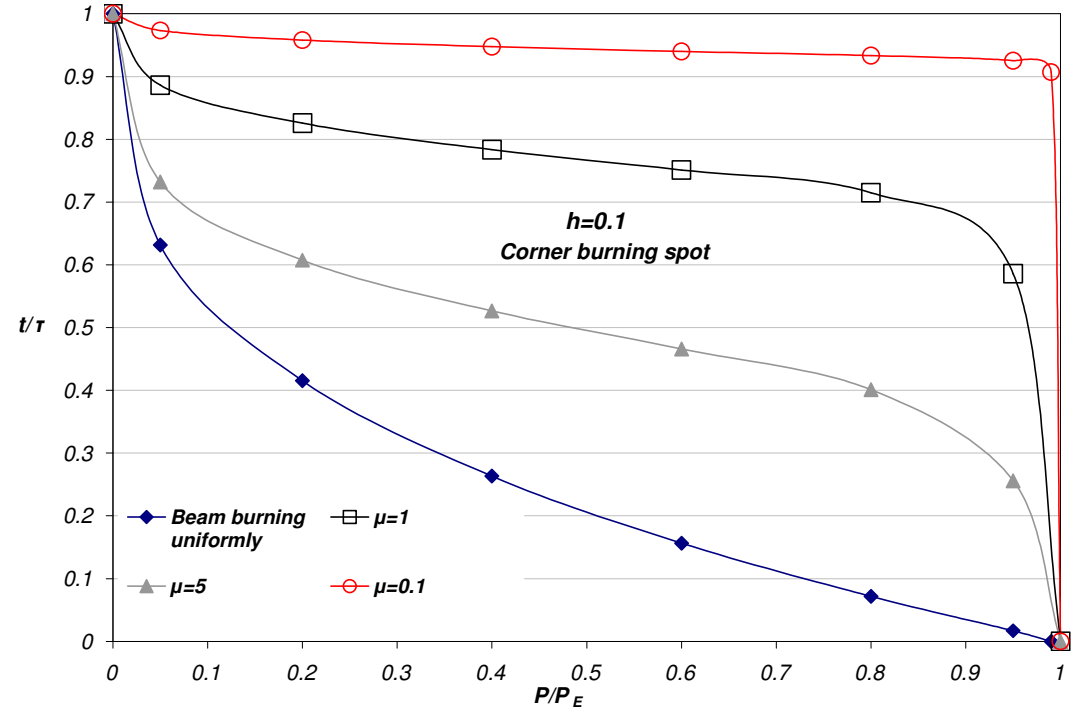

Figure 5.16: non-dimensional time of buckling for different burning ratios and for column aspect ratio 1/10

Let us now compared the results obtained for uniform burning, burning spot in the middle of the span, and burning pot at one corner of the column, for a column of aspect ratio of 0.01 and for burning ratio of 1 and 50 (figure 5.17).

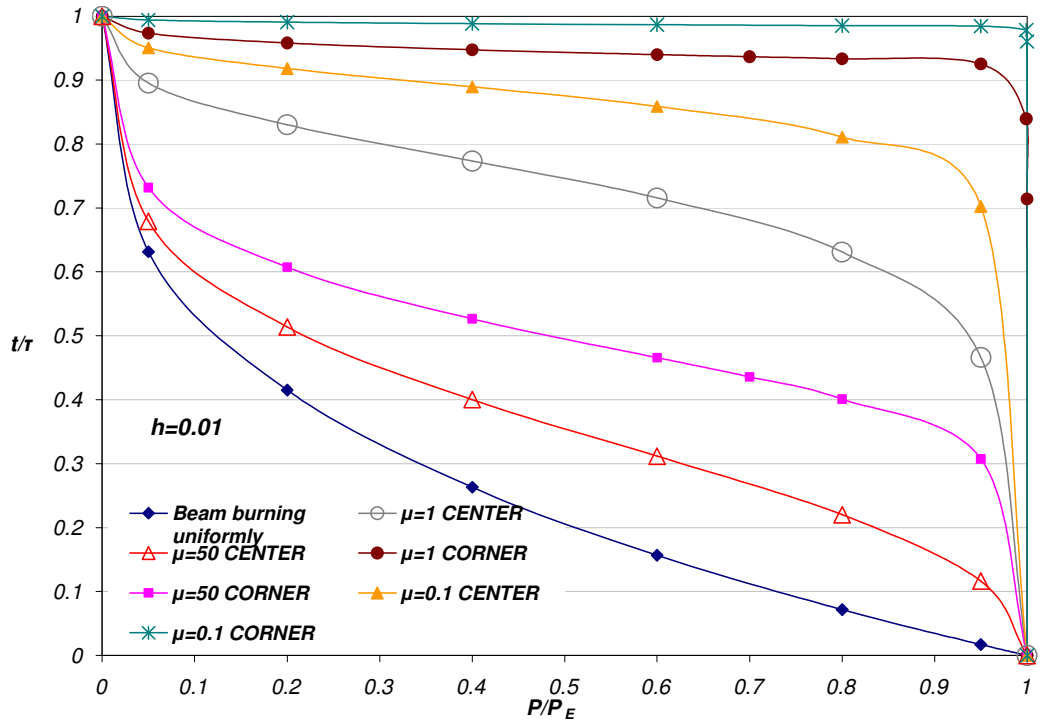

Figure 5.17: comparison of non-dimensional time of buckling for different burning ratios and for column aspect ratio 1/100, for column burning uniformly along the span, with a burning spot at the center and at the corner of the span

From figure 5.17, it is evident that the burning spot at the center of the beam is more critical than the burning spot at the corner. However, the lowest values of the time of instability are obtained for uniform burning along the span.

5.3 Stability of burning columns made of epoxy-clay-CNF nanocomposite

Let's now evaluate the time of instability for burning columns made of epoxy-clay-CNF nanocomposites. The model makes use of the mechanical and flammability properties found by testing and presented in chapter 4. To compute the time of burning, we will use the Peak of Heat Release Rate, since it was observed during the tests by cone calorimetry that shortly after the time of PHRR the resin was practically all burned out and only few small flames survived. The structure at this point is believed have lost all its resistance. The time to flameout will thus not be used as time of burning τ since it was recorded after all surviving flames extinguished, even the small ones when the resistance of the material was negligible since a long period of time already.

5.3.1 Calculated time of burning

The profile of the curve to calculate the time of burning τ will be assumed parabolic, as shown in figure 5.18, where the subscript 1 and 2 indicates two different virtual materials that behave similarly to the ones in chapter 4. The independent variable is the time of burning, and the ordinate is the Heat Release Rate. The area underneath the curve represents the total heat released per unit area expressed in kJ/m^2 and it is equal for all materials tested, since it depends only on the quantity of epoxy resin present and burned in every sample, which is approximately the same. This was observed also in the plots of the total heat release in (see chapter 4). Therefore, knowing the ratios for all PHRR it is possible to calculate the ratios of the time of burning τ. The parabolic equation assumed being the trend of the HRR is

$$HRR = -\frac{4 \cdot PHRR}{\tau^2} x^2 + \frac{4 \cdot PHRR}{\tau} x \tag{5.36}$$

If we integrate the HRR of equation 5.36 we obtain the area underneath the curve which represents the total heat released per unit area. The total heat released per unit area is equal for all cases studied:

$$1 = \frac{\int_0^{\tau_1} HRR_1 dt}{\int_0^{\tau_2} HRR_2 dt} \tag{5.37}$$

Equation 5.37 gives

$$1 = \frac{PHRR_1 \cdot \tau_1}{PHRR_2 \cdot \tau_2} \tag{5.38}$$

If we know the values for the PHRR of the different materials, it is now easy to find the ratios between the times of burning. From testing, we know when the PHRR occurs (see chapter 4). As expected, the time to PHRR occurs later for the nanocomposites than for pure-epoxy (see chapter 4 and figure 5.18). For simplicity, let us take as a reference the one for pure epoxy, and this will be half of the time of burning τ for pure epoxy.

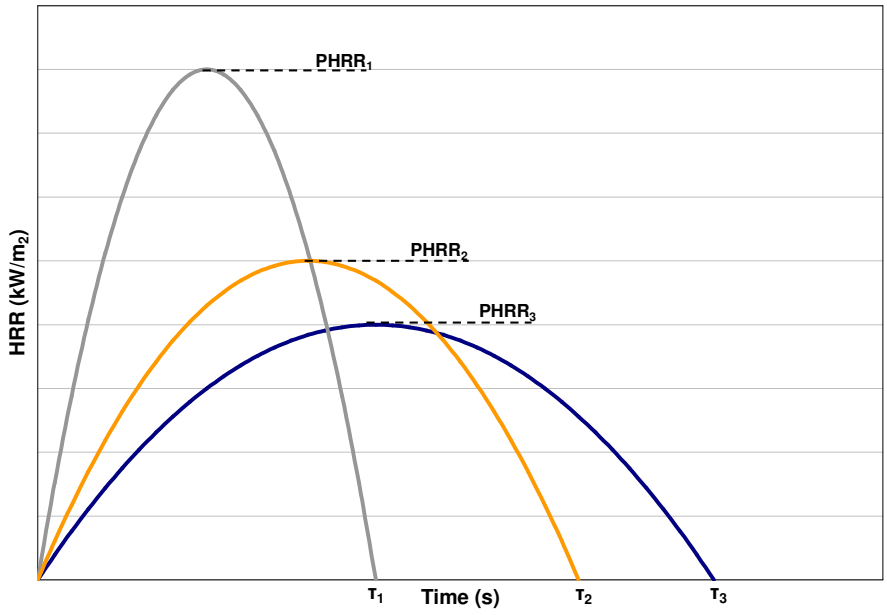

Figure 5.18: HRR vs time for three virtual materials with similar behavior of the ones tested

We can now calculate the time for all other nanocomposites using equation 5.38. Table 5.1 shows the PHRR, the calculated time of burning, and the Young's modulus, which will be used later, for the cases that will analyzed.

Material	PHRR (kW/m^2)	τ (s)	E (MPa)
Epoxy	1680	212	1908
EP-2%CL-S-I	1447	246	2428
EP-1%CL-1%CN-S-I	961	371	2377
EP-2%CL-2%CN-S-I	910	391	2342
EP-2%CN-S-I	911	391	2475

Table 5.1: PHRR, Young's modulus, and calculated time of burning for the nanocomposites analyzed

5.3.2 Stability of nanocomposites burning columns

Using the equations computed in section 5.2, let's now calculate the instability time for the different cases of uniform burning, burning spot in the middle and in the corner for the nanocomposites analyzed in chapter 4 and reported in table 5.1. The results will be expressed per unit of depth ($b=1\ mm$), and the thickness will be the one tested, i.e. $h=5\ mm$. We will consider an aspect ratios of 100, which means that the column is $500\ mm$ long. However, this can be applied to more cases, if the flammability properties are known for the new thicknesses. The PHRR depends in fact from the thickness, but it is believed that over a certain thickness it will be constant. This is because the PHRR depends on how deep the fire goes trough the material. Thin samples get hotter faster, so the flames go deeper. If the element is sufficiently thick, the depth of burning will be the same, no matter what is the thickness and the PHRR will be independent from the thickness. This topic is not investigated in this work.

5.3.2.1 Stability of nanocomposites column with uniform burning along the span

If we know the Young's modulus and the dimensions of the column, we can calculate the Euler's critical load using the following equation:

$$P_E = \frac{\pi \cdot E \cdot b \cdot h^3}{12 \cdot l^2}$$

Considering the different Young's moduli, the different aspect ratios *AR*, and that *b=1 mm* we can calculate the Euler's critical loads (table 5.2).

Material	τ (s)	E (MPa)	***AR=0.01*** $\mathbf{P_E}$ **(N)**
Epoxy	212	1908	0.2498
EP-2%CL-S-I	246	2428	0.3178
EP-1%CL-1%CN-S-I	371	2377	0.3111
EP-2%CL-2%CN-S-I	391	2342	0.3066
EP-2%CN-S-I	391	2475	0.3240

Table 5.2: Euler's critical loads for the nanocomposites studied and for different column aspect ratios

Using the time of burning of table 5.1, the critical load of table 5.2 and the following equation we can plot the time of instability versus the load applied for column aspect ratio of 0.01 (see figure 5.19).

$$t_{cr} = \tau \left(1 - \sqrt[3]{\frac{P}{P_{cr}}} \right)$$

The result shows that there is not much difference between the nanocomposites containing carbon nanofibers, i.e. 1%-1% Clay-CNF, 2% CNF, and 2%-2% Clay-CNF. Pristine epoxy has significant shorter time of instability than all other cases analyzed. The nanocomposite containing only nanoclays (2%CL) has time of instability slightly higher than pure epoxy for load loads, and it gets closer to nanocomposites containing CNFs for higher values. Overall it

has values intermediate between the pure epoxy and the nanocomposites containing CNFs. Instability occurs within 50 seconds for loads close to 0.1 N for pure epoxy, 0.17 N for 2%CL nanocomposites, and 0.2 N for nanocomposites containing CNFs.

These results shows that adding a percentage as small as 1% in weight of CNFs brings a big improvement in terms of instability time for columns burning uniformly along the span, due to the combined effect of longer time of burning and higher stiffness. The improvement given by adding 2% in weight of nanoclays is lower, but still not negligible. The nanocomposites containing 2% of CNFs more than double the time of instability.

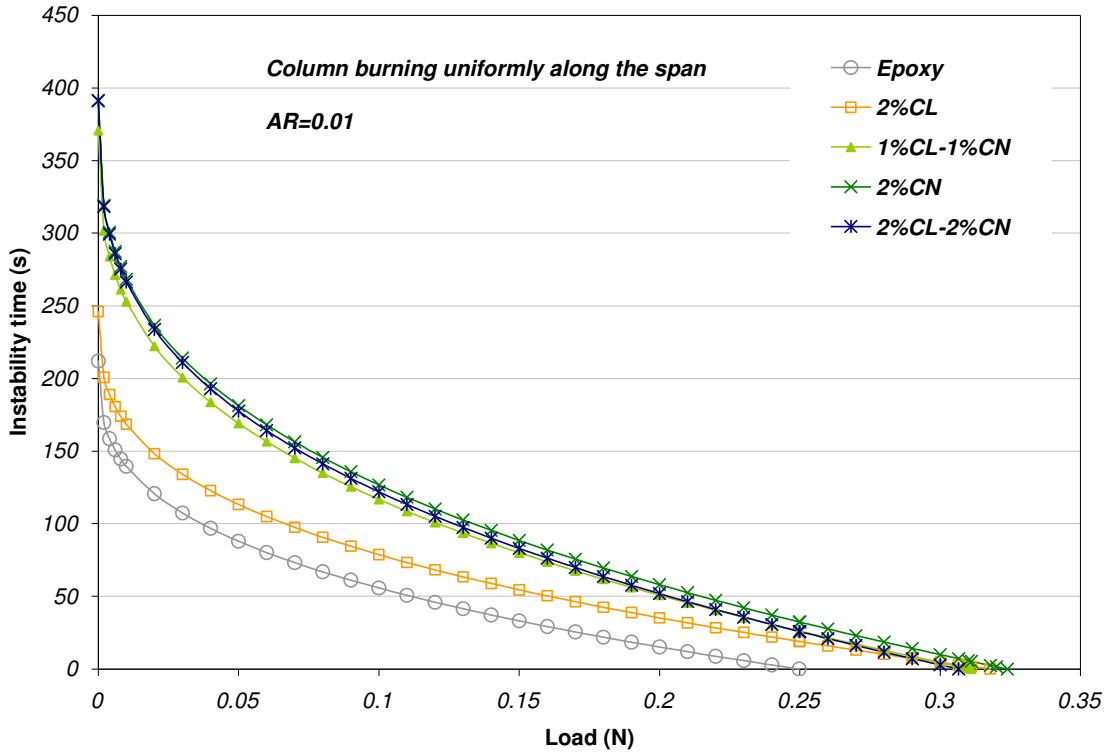

Figure 5.19: instability time for epoxy-clay-CNF nanocomposites column burning uniformly along the span

5.3.2.2 Stability of nanocomposites column with burning spot at the center

The time of instability of columns made of the same nanocomposites analyzed in chapter 4, with a burning spot in the middle of the span can be easily calculated using the data computed in section 5.2.2. To calculate the critical time of instability, we imposed equal to zero the term *A* in the denominator of the coefficient of the solution of the second order differential equation:

$$A = \left(\frac{1}{1-\bar{t}}\right)^{\frac{3}{2}} \tan\left(\frac{\pi}{2}\sqrt{\bar{P}}\,\frac{\mu\bar{h}\bar{t}}{(1-\bar{t})^{\frac{3}{2}}}\right)\tan\left(\frac{\pi}{2}\sqrt{\bar{P}}\left(1-\mu\bar{h}\bar{t}\right)\right)-1=0 \qquad (5.39)$$

In Equation 5.39, μ is the burning ratio between longitudinal and transversal direction and it is equal to 1, because our nanocomposites are isotropic. The aspect ratio $\bar{h}$ that we will analyze is 0.01, corresponding to a column wide 5 mm and long 500 mm. $\bar{P}$ is the ratio between the load and the Euler's load and $\bar{t}$ is the ratio between the critical time of instability and the calculated time of burning τ. Since we have the calculated time of burning and the critical Euler's load, we can easily calculate and plot the time of instability (figure 5.20).

In figure 5.20 it is evident the benefits that addition of nanoparticles such as nanoclay and CNFs gives in terms of instability time. The time of instability is much lower for pure epoxy columns, both at high and low loads. Nanocomposites containing only nanoclays (2%CL) have time of instability only slightly higher than the one of pure epoxy at low loads, but the beneficial effect become evident at high loads. The best results are for nanocomposites containing 2% weight content of CNFs. However, the effect of adding 2% clays and 2% CNFs, becomes less beneficial at high loads. The best results are again for 2%-CNF nanocomposites.

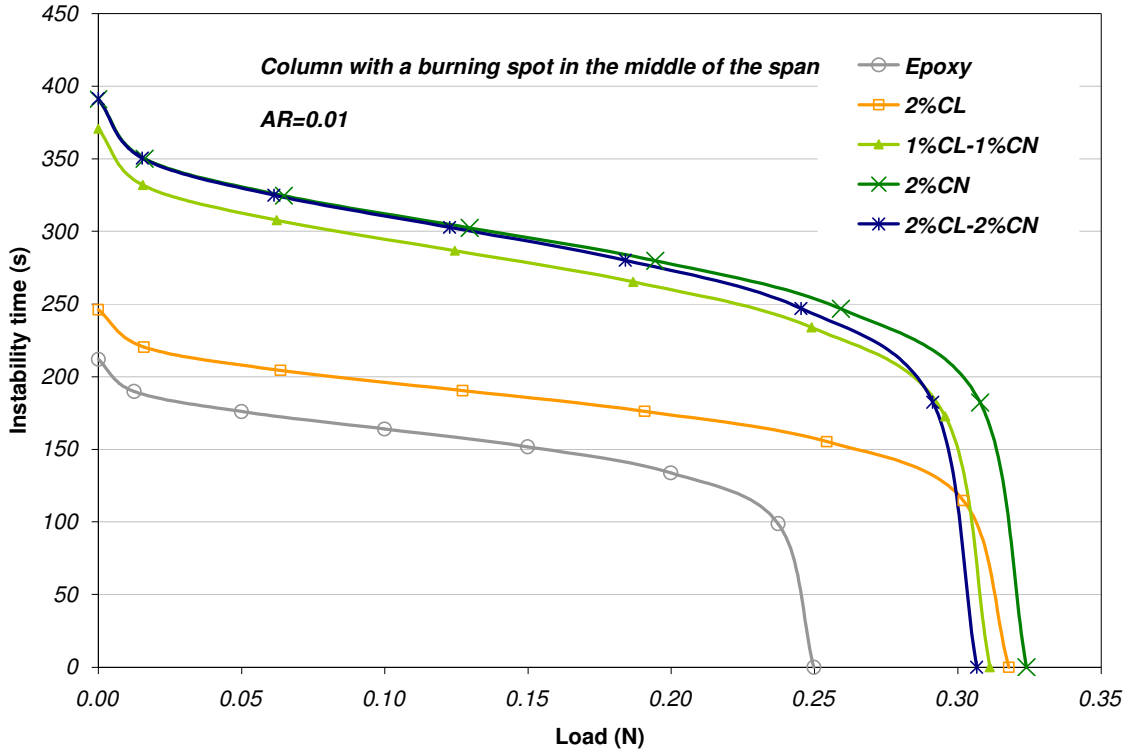

Figure 5.20: instability time for epoxy-clay-CNF columns with a burning spot in the middle of the span

5.3.2.3 Stability of nanocomposites column with burning spot at the corner

Like for columns with a burning spot at the middle of the span, to find the time of instability we maximize the coefficient of the solution of the second order differential equation of equilibrium imposing the term A at the denominator equal to zero:

$$A = \frac{1}{(1-\bar{t})^{\frac{3}{2}}}\tan\left(\pi\sqrt{\bar{P}}\left(1-\mu\bar{h}\bar{t}\right)\right)+\tan\left(\pi\sqrt{\bar{P}}\,\frac{\mu\bar{h}\bar{t}}{(1-\bar{t})^{\frac{3}{2}}}\right)=0 \qquad (5.40)$$

As explained before, μ is the burning ratio between longitudinal and transversal direction and it is equal to 1, because our nanocomposites are isotropic. The aspect ratio $\bar{h}$ that we will analyze is 0.01, corresponding to a column wide 5 mm and long 500 mm. $\bar{P}$ is the ratio between the load and the Euler's load and $\bar{t}$ is the ratio between the critical time of instability and the

calculated time of burning τ. Since we have the calculated time of burning and the critical Euler's load, we can easily calculate and plot the time of instability (figure 5.21).

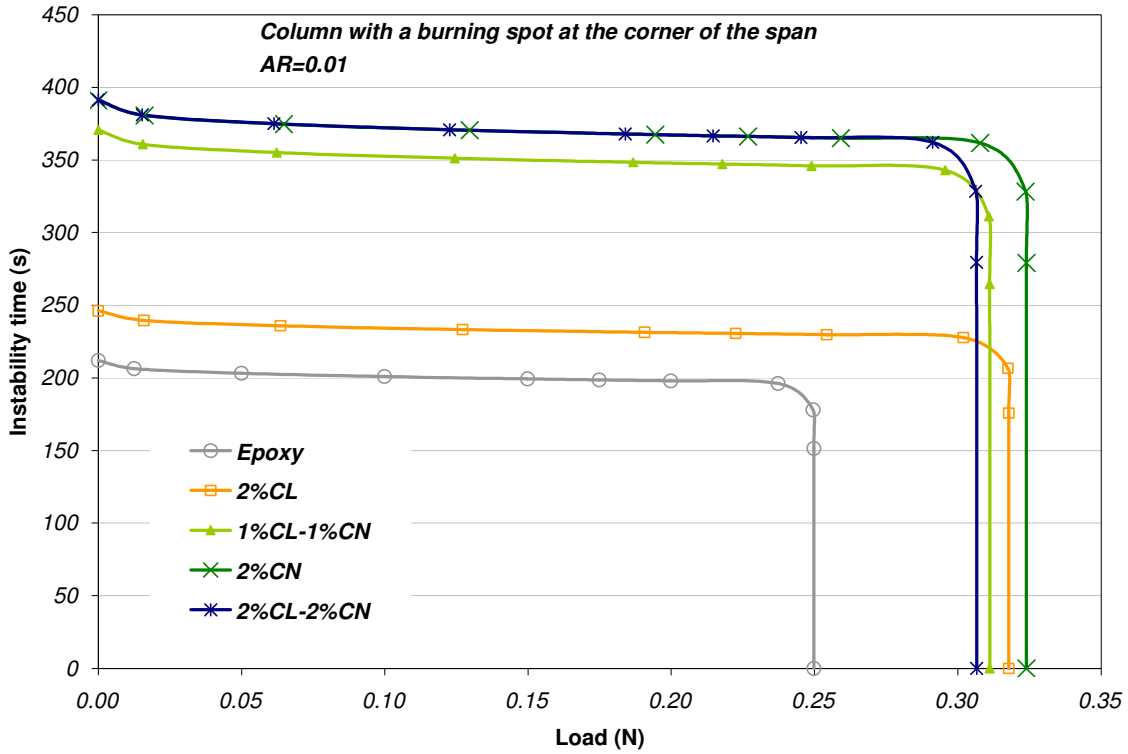

Figure 5.21: instability time for epoxy-clay-CNF columns with a burning spot at the corner of the span

Figure 5.21 shows interesting results. The time of instability remains constant for most of the loads, and then it drop suddenly for high loads. Pristine epoxy has lower instability time as expected. The highest values are for nanocomposites that contain 2% weight of CNFs. %-2% clay-CNF however has lower time of instability for high loads. Nanocomposites containing only nanoclays (2%CL) have (like observed before) time of instability slightly higher than epoxy for low and medium loads values, and time of instability comparable to nanocomposites containing CNFs for high loads. The effect on the time of instability for low and middle values is mainly due to the flammability properties of the material, while at high load values the mechanical properties (Young's modulus) play a key role.

5.4 Concluding remarks

The models analyzed in this chapter do not take into account the effect of the eccentricity of loading. The loading configuration, in fact, is not symmetric, since the burning occurs in one side of the column. The eccentricity produces the effect of changing the criteria of determining the time of instability. For loading without eccentricity, the column has no deflection until the critical load is reached. After that, the deflection becomes infinity instantaneously. The eccentricity instead produces a gradual deflection since the beginning of the loading. This deflection is finite, and in proximity of the critical load starts becoming bigger faster. If the eccentricity is small, which can be compared to the case of burning just initiated, the deflection is close to zero and the values are comparable to the case without any eccentricity. When the burning becomes more severe, i.e. it is going on for a non-negligible amount of time, the eccentricity becomes bigger, and the deflection is not close to zero anymore. The condition of instability can now be set for a known value of deflection, which will be considered as upper limit, after which the column will not perform its functions correctly. The deflection with eccentricity will go asymptotically to the trend of situation without eccentricity, for loads that go to infinity. For this reason, a correct model will take into account the eccentricity effect, and to determine instability a known value of deflection, over which the column is considered not serving its function anymore, must be set. As a first approximation, anyway, the model analyzed in this chapter can be considered valid.

Another remark that needs to be done is that it is unrealistic to imagine a column made only of pure resin mixed with nanoparticles. Most likely in a real world, a column will be manufactured of advanced composites, i.e. long reinforcing fibers in a matrix system. The stiffness calculated for our nanocomposites will be thus negligible, with respect to the stiffness

that the long fibers give to the material. For this reason, the effect of adding nanoparticles will be negligible for high load for figures 5.19, 5.20, and 5.21, where the effect of increasing the time of instability is mainly due to the increase of stiffness. Anyhow, adding nanoparticles, such as nanoclays and carbon nanofibers, to the matrix system to produce advanced composites become non-negligible for low level of loading (see figure 5.19, 5.20, and 5.21). In this condition, the flame retardation plays a big role. Advanced composites, in fact, loose their properties if the matrix system is burned out, since the matrix system is responsible of transferring the load to the reinforcing fibers. If the matrix burns slower, effect of adding nanoparticles as flame retardant, the advanced composites will be more resistant. For this reason, the calculation made in this chapter for low loading are very helpful and adding nanoparticles in the matrix system of an advanced composites can be very convenient.

Chapter 6

Conclusions and future work

6.1 Discussion on nano-filled epoxy test results

Two different nanoparticles, nanoclay and carbon nanofibers, are mixed into DGEBA epoxy by a combined mechanical and ultrasonication mixing procedure to produce three types of nanocomposites: epoxy-nanoclay, epoxy-carbon nanofiber, and epoxy-nanoclay-carbon nanofiber. Fracture, static mechanical and flammability tests are performed to evaluate their properties.

6.1.1 Discussion on epoxy-nanoclay test results

The addition of nanoclays into DGEBA epoxy results in a more mechanical resistant and stiffer, but more brittle, material, when compared to pristine epoxy. Modest improvements in flame retardation are also observed.

The net Izod impact resistance decreases proportionally with increasing clay content. Similar behavior is observed for the stress intensity factor and the energy release rate. The energy release rate in particular show a dramatic reduction of 80% with addition of 6% nanoclays.

The introduction of nanoclays produces lower ductility and reduction in tensile strain at break is proved. The tensile strength is significant higher only with addition of 2%wt of nanoclays, while for 4% and 6% the value is similar to the one for pure epoxy. This shows that 2% weight content of nanoclays is better dispersed in the matrix with the mixing techniques

adopted in this work, while higher percentages produces clusters of nanoparticles that lower the mechanical resistance. The Young's modulus increases for all percentages of clays of about 20%. In a similar manner, the flexural strength increase only with addition of 2% in weight of nanoclays. The strain at the peak flexural load decreases dramatically with addition of nanoclays, up to half of the value for pure epoxy. The tangent modulus of elasticity in bending modestly increases only for addition of 2% of nanoclays.

Epoxy resins are very flammable, while nanoclays themselves are not flammable. Addition of nanoclays into epoxy produces a flame retardation effect, when compared to the pure resin. Flammability tests show the reduction of the Peak of Heat Release Rate (PHRR) proportionally with the clay content. There is no significant change in the Mean of Heat Release Rate (MHRR). A similar behavior is observed for the Mass Loss Rate (MLR), with proportional reduction of the PMLR and no change for the MMLR. The time to ignition increases with addition of nanoclays, up to 100% increase for 6% weight content of nanoclays. The time to PHRR is retarded for nanoclay-nanocomposites, and increase in the time to flameout is observed only for 6%wt of nanoclay. No differences in the total smoke and total heat released of pure epoxy and epoxy-clay nanocomposites is detected.

Overall it seems that addition of 2% weight content of nanoclay maximizes the static mechanical properties, and minimizes the reduction in fracture characteristics. Better flame retardation is instead observed for high nanoparticles loading as 6% weight content of nanoclays.

6.1.2 Discussion on epoxy-carbon nanofibers test results

Addition of carbon nanofibers (CNFs) reinforcements produces overall better static mechanical properties, but with increase in brittleness. The flammability properties improve proportionally with the quantity of CNFs added.

The net Izod impact resistance decrease with addition of CNFs, but 2%wt of CNFs has the highest Izod impact strength among the CNF nanocomposites. Similar behavior is observed for the energy release rate. The stress intensity factor is higher than the one of pristine epoxy for 2%wt of CNFs, while the values for 1%wt and 3%wt are lower. Unless the energy release rate, the stress intensity factor does not account the stiffness that is added with addition of CNFs.

Epoxy containing CNFs is less ductile than virgin epoxy, as showed in the tensile strain at break results. The tensile strength is significant higher with addition of CNFs, and it shows a maximum in correspondence of 2% weight content, as observed for the fracture tests. The elastic modulus behaves similarly, with more than 30% higher value for 2%wt when compared to the one of virgin epoxy. The flexural strength has again a maximum in correspondence of 2% weight content of CNFs, with more than 50% higher value when compared to the one of pristine epoxy. The strain at the peak of flexural load decreases drastically with addition of CNFs. A behavior similar to the one observed for tensile strength, Young's modulus, and Flexural strength is observed for the tangent modulus of elasticity in bending.

The flammability properties greatly improve with addition of CNFs. The PHRR dramatically decreases proportionally with the content of CNFs. Similarly to what observed for epoxy-nanoclay nanocomposites, the MHRR does not change with addition of CNFs. A similar behavior is observed for the PMLR and the MMLR. The time to ignition does not vary significantly with addition of CNFs. The time to PHRR is slightly retarded, and the time to

flameout is in general longer with addition of CNFs. There is no difference between pure epoxy and epoxy with CNFs for the total smoke and heat released.

In conclusion, carbon nanofibers improve the static mechanical properties up to 50%, but they make epoxy more brittle and less ductile. The flammability characteristics seem to be improved too, with a dramatic reduction of PHRR and longer time to flameout.

6.1.3 Discussion on epoxy-clay-carbon nanofibers test results

Two types of nanocomposites produced with both nanoclay and CNF nanoparticles mixed in epoxy are manufactured and tested. Two weight concentrations are selected: 1%-1% epoxy-clay-CNF and 2%-2% epoxy-clay-CNF. The so produced nanocomposites are compared with pristine epoxy, 2% epoxy-clay and 2% epoxy-CNF nanocomposites.

The net Izod impact strength is lower for this class of nanocomposites when compared to the one of virgin epoxy and to the one of the nanocomposites produced with only one type of particle. The stress intensity factor for 1%-1% epoxy-clay-CNF has a value in between the values for 2% epoxy-clay and 2% epoxy-CNF nanocomposites. The value for 2%-2% epoxy-clay-CNF is sensibly lower. A similar behavior is observed for the energy release rate.

The nanocomposites produced are less ductile than pure epoxy, as showed in the strain at break. The tensile strength and the Young's modulus are higher for 1%-1% and 2%-2% epoxy-clay-CNF when compared to the one of pristine epoxy, but the value of 2%-2% epoxy-clay-CNF is lower than the one of 1%-1% epoxy-clay-CNF, showing that too many nano-reinforcements can decrease the strength because of the introduction of voids and the formation of clusters, due to poor dispersion. The flexural strength is higher than the one of pure epoxy, at the same level of 2% epoxy-clay, but sensibly lower than the one of 2% epoxy-CNF nanocomposites. The strain

at the peak flexural stress is dramatically lower for all nanocomposites tested when compared to the one of virgin epoxy. The tangent elastic modulus at bending is higher than the one of pristine epoxy, and lower than the one of 2% epoxy-CNF, for 1%-1% and 2%-2% epoxy-clay nanocomposites. The results show that the new nanocomposites produced with two different nanoparticles mixed together in epoxy have mechanical properties in between epoxy-clay and epoxy-CNF nanocomposites for 1%-1% epoxy-clay-CNF nanocomposites, but lower for 2%-2% epoxy-clay-CNF nanocomposites because of the too high nanoparticles weight content.

The PHRR decreases proportionally with the quantity of nanoparticles added and the type, with CNFs influencing the value more. For this reason the lowest value of PHRR is observed for 2%-2% epoxy-clay-CNF nanocomposites. The MHRR seems not to vary significantly. A similar behavior is observed for the MLR. The time to ignition is sensitive to the nanoclay presence, so it is higher for 2%-2% epoxy-clay-CNF. The time to the PHRR is retarded for all nanocomposites studied when compared to the one for pure epoxy. The time to flameout for both 1%-1% and 2%-2% epoxy-clay-CNF is higher than the one for pure epoxy, 2% epoxy-clay and 2% epoxy-CNF nanocomposites. As observed before (sections 6.1.1, 6.1.2) the total smoke and heat released are not dependent from the presence of nano-reinforcements.

After testing it is evident that the superposition principle applies to nanocomposites only when the reinforcement quantity is below certain limit, after which the mechanical properties seem to degrade. Flammability properties instead improve with increasing amount of nano-reinforcements added, and the influence of CNFs is more evident than the one of nanoclays.

6.2 Discussion on the stability of nanocomposite columns under fire

A modeling of stability of nanocomposites structural columns under fire is made considering three different configurations: uniform burning along the span, and burning spot at the center and at corner of the column. Different aspect ratios and ratios of burning in two perpendicular directions are considered. The results found after testing epoxy-clay-CNF nanocomposites were implemented in this model.

The non-dimensional time of instability for columns burning uniformly along the span diminishes with increasing load non-dimensionalized with critical Euler's load as a 1/3 power law. The trend does not depend on the aspect ratio of the column.

For burning spot in the middle of the span, the non-dimensional time of instability diminishes at a slower rate than for the uniform burning along the span. The results are dependent from the aspect ratio and the burning ratio. The same considerations can be done for burning spot at the corner of the column. When the two cases are compared (burning spot at the center and at the corner of the column), it is noticed that for the majority of the loading conditions, the non-dimensional time of instability is higher for burning spot at the corner of the column.

After substituting the values obtained from the mechanical and flammability tests of the epoxy-clay-CNF nanocomposites, it is shown that nanocomposites containing 1% and 2%wt of CNFs behave similarly and have higher time of instability than the one of pristine epoxy. The nanocomposites containing 2% of nanoclays have an intermediate value. It is also shown that the effect of the flammability properties influence mainly the low and medium portion of the loading spectrum, while the increased stiffness influences the higher portion of the loads. The overall highest time of instability was calculated for nanocomposites with 2% weight content of CNFs.

6.3 Future work

Despite the preliminary work done to optimize the mixing procedure of the nano-reinforcements into the epoxy, only a total 2% weight content of nano-reinforcements is effectively well dispersed. This is observed in the mechanical properties of the 2%CL, 2%CN, and 1%CL-1%CN nanocomposites. In the near future, a better way of mixing the nano-reinforcements need to be investigated, using different techniques, such as shear mixing. Shear mixing has the advantage to create a better separation between the nano-fillers breaking the clusters and producing a better wettability of resin inside area rich of nanofillers. Shear mixing also produced the effect to orientate the nanofillers, if the process is well controlled. The orientation can create a orthotropic nanocomposites, which will be desirable for many applications. It is also advisable to use Wide Angle X-Ray Diffraction and Atomic Force Microscope techniques to evaluate the dispersion, rather than just making consideration upon the mechanical properties. Another important work that needs to be carried out is mixing quantity of nano-reinforcements bigger than 10% in weight, to obtain more effective flame retardation properties and to understand the mechanical behavior at high nano-fillers loading.

The modeling of stability of columns under fire needs to be extended with the introduction of the effect of the load eccentricity produced by the burning process. Another element that needs to be introduced is the variation of the elastic modulus along the thickness due to the temperature gradient produced by the burning on one side. Finally, an experimental validation of the model is desirable. Columns can be loaded in fire condition and the deflection can be recorded by high definition imaging.

Vita

Stefano Bietto was born in Cuorgnè in the province of Torino, Italy, on May 16, 1976. Son of Pina and Gian Domenico, he attended the scientific high school "Liceo Scientifico Aldo Moro" in Rivarolo Canavese, but already in early age he showed interest and predisposition for mathematics and in general for scientific subjects. He graduated in 2002 in Aerospace Engineering at the Politecnico di Torino with a thesis on mechanical and non-destructive evaluation of laser welds on special aerospace aluminum alloys. Soon after, he moved to New Orleans to pursue his PhD in Engineering and Applied Sciences at the Mechanical Engineering Department of University of New Orleans. In September 2005, Stefano moved to Kansas as a consequence of the hurricane Katrina, which severely hit the city of New Orleans. Working for the Center for NanoComposites and Multifunctional Materials, he was able to complete his PhD research work. Stefano Bietto obtained his PhD in Engineering and Applied Sciences in 2007 from University of New Orleans.